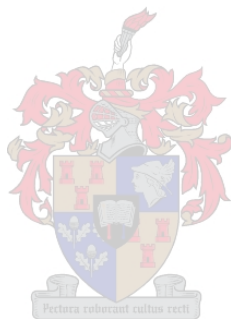# I-M-I···I-M-I interactions in transition metal complexes

by

Gamra Mohamed Elgadi

Thesis presented in partial fulfilment of the requirements for the degree Master of Science in Chemistry at the University of Stellenbosch

Faculty of Science

Department of Chemistry & Polymer Science

Supervisor: Prof. Catharine Esterhuysen

Co-supervisor: Prof. Jan Dillen

Stellenbosch

March 2016

Declaration

By submitting this thesis/dissertation electronically, I declare that the entirety of the work contained therein is my own original work, that I am the sole author thereof (save to the extent explicitly otherwise stated), that reproduction and publication thereof by Stellenbosch University will not infringe any third party rights and that I have not previously in its entirety or in part submitted it for obtaining any qualification.

GM Elgadi

Abstract

A theoretical study of iodine to iodine (I⋯I) interactions within dimers of transition metal-iodide complexes was performed utilizing the Cambridge Structural Database (CSD) and computational methods. A comprehensive analysis of the I⋯I interactions among previously published experimental crystal structures of metal-iodide complexes included in the CSD was first carried out. The CSD search initially identified all complexes containing the I–M–I moiety in the solid state, where M is a transition metal and I is an iodine atom, and then determined all complexes exhibiting I⋯I interactions to form dimers of I–M–I⋯I–M–I motifs. The analysis revealed that complexes containing copper (Cu), mercury (Hg), gallium (Ga), silver (Ag), platinum (Pt), palladium (Pd) or bismuth (Bi) are the most likely to undergo such I⋯I interactions. The complexes exhibited different types of I⋯I intermolecular contacts including single, double, multiple and bifurcated interactions. The crystal structures of these complexes were then visualized and analyzed to determine the most common orientations (i.e., conformations) of the two I–M–I moieties relative to each other. The most common conformations of these interactions in the solid state were found to be chair, boat, bent, >⋯<– shaped and zigzag forms. Shorter distances between I atoms (indicative of stronger interactions) are most likely to occur when the relative orientation of the two I–M–I moieties is in the chair form, with average distances ranging between 3.4 and 3.8 Å. The nature and strength of the I⋯I intermolecular interactions in dimers of some selected transition metal-iodide complexes (containing Cu, Hg, Ga, Ag, Pt, Pd or Bi) were also investigated by means of Density Functional Theory (DFT). Calculations were performed in the gas phase and in an implicit solvent model using different solvents with a wide range of dielectric constants (water, ethanol and chloroform). Various levels of DFT, namely PBEPBE/aug-cc-pVTZ-pp/6-31G(d), B3LYP/LANL2DZ and B3LYP/aug-cc-pVTZ-pp/6-31G(d) were used. Optimizations in different environments using an implicit polarizable continuum solvent model showed that there was a significant dependence of the I⋯I interaction energy (E_{INT}) and distance on the electrostatic environment in which the complex is found. As the dielectric constant increases the E_{INT} increases significantly, while the I⋯I intermolecular distance decreases considerably. The I⋯I interactions were also studied by the natural bond orbital (NBO) and the Atoms in Molecules (AIM) analyses to determine their nature and properties. NBO analysis does not

confirm the existence of an $I \cdots I$ bond within dimers of metal-iodide complexes in the gas phase or an implicit solvent model. There was no evidence of electron transfer between iodine atoms in the $I \cdots I$ moiety, indicating that the two fragments in the dimers are connected only via dispersion interactions. Since the transition metal-iodide complexes do not form stable dimers in the gas phase it was only possible to obtain AIM parameters (i.e., ρ_b, $L(\rho_b)$, and H_b) for the $I \cdots I$ interaction in a solvent. These were shown to depend on the electrostatic environment (i.e., dielectric constant of the solvent), such that, in general, an increase in the dielectric constant resulted in a significant increase in the calculated values of AIM parameters corresponding to stronger interactions.

Uittreksel

'n Teoretiese studie van jodium tot jodium (I ··· I) interaksies binne dimere van oorgangsmetaal-jodied komplekse is met behulp van die "Cambridge Structural Database" (CSD) en berekeningsmetodes uitgevoer. 'n Omvattende ontleding van die I ··· I interaksies tussen voorheen gepubliseerde eksperimentele kristalstrukture van metaal-jodied komplekse uit die CSD is vir die eerste keer uitgevoer. Die CSD soektog het aanvanklik alle komplekse met die I-M-I eenheid, waar M 'n oorgangsmetaal en I is 'n jodium atoom is, in die vaste toestand geïdentifiseer, waarna alle komplekse wat I ··· I interaksies ondergaan om dimere met die I-M-I··· I-M-I motief te vorm bepaal is. Hierdie ontleding het getoon dat komplekse met koper (Cu), kwik (Hg), gallium (Ga), silwer (Ag), platinum (Pt), palladium (Pd) en bismut (Bi) mees waarskynlik I ··· I interaksies vorm. Die komplekse het verskillende tipes I ··· I intermolekulêre kontakte getoon insluitende enkel-, dubbel-, veelvoudige- en vertakte-interaksies. Die kristalstrukture van hierdie komplekse is toe gevisualiseer en ontleed om die mees algemene oriëntasies (dws, konformasies) van die twee I-M-I eenhede relatief tot mekaar te bepaal. Dit is gevind dat die mees algemene konformasies van hierdie interaksies in die vaste toestand die stoel, boot, gebuigte, $> ··· <$ en sigsag vorme is. Korter afstande tussen I atome (aanduiding van sterker interaksies) is die meeste geneig om voor te kom wanneer die relatiewe oriëntasies van die twee I-M-I eenhede in die stoel vorm is, met gemiddelde afstande wat tussen 3,4 en 3,8 Å wissel. Die aard en sterkte van die I ··· I intermolekulêre interaksies in dimere van sommige gekose oorgangsmetaal-jodied komplekse (met Cu, Hg, Ga, Ag, Pt, Pd en Bi) is ook ondersoek deur middel van Digtheid Funksionele Teorie (DFT). Berekeninge is uitgevoer in die gasfase en in 'n implisiete oplosmiddelmodel met verskillende oplosmiddels met 'n wye verskeidenheid van diëlektriese konstantes (water, etanol en chloroform). Verskillende vlakke van DFT, naamlik PBEPBE/aug-cc-pVTZ-pp/6-31G(d), B3LYP/LANL2DZ en B3LYP/aug-cc-pVTZ-pp/6-31G(d) is gebruik. Optimisering in verskillende omgewings deur middel van 'n implisiete polariseerbare kontinuum oplosmiddelmodel het getoon dat daar 'n beduidende afhanklikheid van die I··· I interaksie energie (E_{INT}) en afstand op die elektrostatiese omgewing waarin die kompleks gevind is. Namate die diëlektriese konstante verhoog sal die E_{INT} ook aansienlik verhoog, terwyl die I ··· I intermolekulêre afstand gelyktydig verminder. Die I ··· I interaksies is ook deur die "Natural Bond Orbital" (NBO) en "Atoms in Molecules" (AIM) metodes geanaliseer om hulle aard en

eienskappe te bepaal. NBO ontleding kon die bestaan van 'n I ⋯ I binding binne dimere van metaal-jodied komplekse in die gasfase of 'n implisiete oplosmiddelmodel nie bevestig nie. Daar was geen bewyse van elektronoordrag tussen jodium atome in die I ⋯ I eenheid, wat daarop aandui dat die twee fragmente in die dimere slegs deur dispersie-interaksies verbind is. Omdat die oorgangsmetaal-jodied komplekse nie stabiele dimere in die gasfase gevorm het nie was dit slegs moontlik om AIM parameters (dws, ρ_b, $L(\rho_b)$, en H_b) vir die I ⋯ I interaksie in 'n oplosmiddel te bereken. Dit is aangetoon dat hierdie waardes afhanklik van die elektrostatiese omgewing (dit wil sê, diëlektriese konstante van die oplosmiddel) is, sodanig dat, oor die algemeen, 'n toename in die diëlektriese konstante tot 'n beduidende toename in die berekende waardes van AIM parameters gelei het wat met sterker interaksies ooreenstem.

Acknowledgements

I would like to gratefully thank my supervisors, Prof. Catharine Esterhuysen and Prof. Jan Dillen for their continuous guidance and limitless support during the course of this MSc study. Thank you so much for always being there to guide me and to answer all of my questions.

I would like also to extend my great appreciations to all my family. My husband, Hussein Etmimi is sincerely thanked for the countless support and encouragement during the last three years to make this study a success. My two daughters (Alla and Rawa) and son (Moaad) are specially thanked for their love and for being patient when I was not there for them. I would like also to say thank you so much to my mother, brothers and sisters in Libya for their support and prayers.

Furthermore, I want to show my gratitude towards the Supramolecular Materials Chemistry group at the University of Stellenbosch for the discussions we had about my work and the support they gave me during my study. My friend, Marike is specially thanked for her kind help and advice.

Finally, I would like to thank the University of Stellenbosch for providing the necessary facilities and the NRF for funding.

To my Father and Mother

Table of content

Conferences

This work was presented as a poster at the 23rd IUCr conference held 5-12 August 2014 in Montreal, Canada.

Esterhuysen, C., Groenewald, F., Elgadi, G., and Dillen, J., *Influence of the electrostatic environment on $I_3^-\cdots I_3^-$ and related I–M–I$\cdots$I–M–I interactions.* Acta Crystallographica Section A **(2014)**, A70, C652.

Glossary

AIM	Atoms in Molecules
AO	Atomic orbitals
BCP	Bond Critical Point
BSSE	Basis Set Superposition Error
C-PCM	Conductor-like PCM
CCP	Cage Critical Point
CP	Critical Point
CSD	Cambridge Structural Database
$d\,(\mathrm{I}\cdots\mathrm{I})$	$\mathrm{I}\cdots\mathrm{I}$ Intermolecular distance
D-PCM	Dielectric PCM
DFT	Density Functional Theory
E_{INT}	Interaction energies
HF	Hartree-Fock
LP	Lone pair
MO	Molecular orbitals
NAO	Natural Atomic Orbitals
NBO	Natural Bond Orbital
NCP	Nuclear Critical Point
NHO	Natural Hybrid Orbitals
NLMO	Natural Semi-Localized Molecular Orbitals
NMO	Natural Molecular Orbitals
PCM	Polarizable Continuum Model
RCP	Ring Critical Point
RY*	Rydberg orbitals
STO	Slater Type Orbitals
T_g	Glass transition temperature
vdW	van der Waals
ΔE_S	Stabilization Energy

Chapter 1

Introduction and objectives

1.1 Introduction

Iodine belongs to Group 17 of the periodic table (i.e., halogens), which consists of five similar elements that have high electronegativity. Like other halogens, iodine has seven valence electrons in its highest energy level, which makes it possible for iodine to react with atoms of other elements and gain an electron to satisfy the octet rule. The element usually exists as a layered structure of diatomic molecules (i.e., I_2), which have a relatively long I–I distance of 2.7 Å [1]. These I_2 molecules interact with each other through weak van der Waals forces, which results in higher melting points compared to other diatomic halogens [2]. Furthermore, because of its large atomic size and high electron affinity, iodine can form polyiodide compounds. In these hypervalent compounds, iodine is generally found with a wide range of oxidation states (I^- to I^{7+}). However, as a consequence of its high electronegativity it forms iodide compounds with other chemical elements, where iodine possesses the oxidation state of I^- [3].

The properties of iodine and its polyiodide compounds are unique, where the diatomic I_2 has characteristic donor-acceptor features [4]. For instance, iodine molecules (Lewis acid acceptors) have a strong affinity for iodide ions (I^-) (Lewis base donors), forming polyiodide compounds such as triiodide (I_3^-). For higher polyiodides, iodine could also interact with I^- and/or I_3^-, which can be considered as the essential "building blocks" of many other polyiodides. The $I_2 \cdots I^-$ interactions found in these polyiodides are very strong (~180 kJ/mol) compared to other relatively weak halogen$\cdots$halogen interactions such as $Cl \cdots Cl$ interactions between chlorocarbons (~5 kJ/mol) [5]. Thus, various polyiodides are formed where one polyiodide can contain up to 29 iodine atoms [6-8]. These polyiodides have different structures, which vary from simple discrete units to very complicated structures of two- and three-dimensional networks. The intermolecular or intramolecular iodine to iodine ($I \cdots I$) interaction distances in these polyiodides are usually shorter than the sum of the van der Waals radius of adjacent iodine

1

atoms (4.3 Å). However, the I–I bond distances in most polyiodides are shorter (~2.8 Å) [9] than a normal covalent bond in I_2, thus they are usually referred to as 'secondary bonds'. In a theoretical study, Kloo *et al.* [10] indicated that these I–I bonds in polyiodides such as triiodides are formed as intramolecular bonds which are associated with other dispersion interactions between the diatomic iodine (I_2) and the iodide ion (I^-).

The resultant polyiodides have numerous applications, such as the formation of blue starch-iodine complexes that are used as an analytical test for iodine. They also play a significant role in donor-acceptor interactions, leading to materials that exhibit high electrical conductivity. Recently, solid polyiodides have received much attention due to their unique electrical properties, which could range from the properties of an insulator to that of a metal depending on their structure and composition [11, 12]. These properties make it the material of choice for many applications including electronic and electrochemical devices, such as batteries, solar cells and displays [13, 14]. In 2000, Alan J. Heeger, Alan G. MacDiarmid and Hideki Shirakawa were awarded the Nobel prize in Chemistry for their novel preparation of conductive polymers using polyiodides [15]. For the formation of conducting polymers, the laureates used iodine to dope conjugated polyacetylene, where they prepared polyiodides using a charge transfer reaction [16].

In a recent theoretical investigation, Groenewald *et al.* [17] extensively studied the influence of the electrostatic environment on triiodide interactions in dimers of $I_3^-\cdots I_3^-$ using various levels of Density Functional Theory (DFT) in combination with a variety of basis sets. The authors clearly showed that the chemical environment is vital for the correct modelling of these types of interactions. Compared to the gas phase, optimizations performed in an implicit polarizable continuum solvent model with a variety of solvents indicated that there is a significant dependence of the $I_3^-\cdots I_3^-$ interaction energy on the dielectric constant of the solvent. $I_3^-\cdots I_3^-$ interactions are favored in the appropriate environment, where the strength of the $I_3^-\cdots I_3^-$ interaction energy converges as the dielectric constant increases. This implies that the attractive interaction energy reaches a maximum regardless of the stabilization provided by the surrounding environment. It was therefore shown that studying the strength of the $I\cdots I$ interactions within an environment with a high dielectric constant gives a reasonable description of the strength of the interaction within a crystalline environment.

2

Metal-iodide complexes show similar, although weaker, interactions with iodine. In particular, late transition metal iodides (which may or may not include stabilizing ligands) form the strongest interactions with I_2 [18]. The nature of this type of halogen···halogen interaction in organometallic compounds (i.e., those containing the M–I···I–M moiety, where M is a transition metal and I is an iodine atom) has been a matter of great interest. Westra *et al.* [19] showed that the formation of metal iodides by an oxidative addition reaction of I_2 to metal complexes can result in the formation of M–I···I–M structures via I···I interactions. The authors found that by adding I_2 to Pt(II) complexes of N-alkyl- N-benzoylthioureas and N,N-dialkyl-N-benzoylthioureas, metal iodides containing $Pt(II) - I \cdots I - Pt(II)$ chains were formed. Similar findings have been observed by other authors for Pt(IV) [20] and Pd(II) [21].

Similarly, attempts by Schneider *et al.* [22] to oxidize gold iodide (AuI) complexes with I_2 showed that no oxidative addition took place, but instead $Au–I^- \cdots I_2 \cdots I^- –Au$ chains were formed. The authors showed that the oxidative addition of I_2 depended strongly on the ligands in the AuI complex, and cases where the ligands did not sufficiently stabilize the oxidative addition product, $Au–I^- \cdots I_2$ interactions were present in the crystal structures. The authors suggested that the reason why this oxidative addition of I_2 to AuI complexes failed was because of the donor qualities of the ligands. However, the alternative formation of $Au–I^- \cdots I_2$ interactions may have also been improved by the electronic properties of the ligands.

Computational chemistry uses mathematical methods, combined into computer programs, which can be used to solve chemistry-related problems by calculations. These methods provide a good alternative to experimental work, where they provide accurate calculations to predict any observed chemical phenomena as well as unobserved ones. In recent years, theoretical investigations have been used to understand the interactions between the most common redox ions (I^- / I_3^-) in organometallic complexes used as sensitizing dyes utilizing computational methods [23-27]. Nazeeruddin *et al*. [27] undertook experimental and computational studies of various ruthenium (Ru)-polypyridyl complexes prepared from different Ru(II) compounds. The authors observed a good agreement between the theoretical and experimental findings, which resulted in a better understanding of the efficiency of dye-sensitized solar cell devices and factors affecting them. More recently, Lobello *et al.* [23] reported a computational investigation on the

interaction between Ru-based dyes and iodides employing DFT methods. The authors presented a theoretical method to study the electronic structure of the obtained dyes and their adducts with I^- and I_3^-, where they showed a good agreement between the computational calculations and the experimental absorption bands assigned to $[dye^+:I^-]$ complexes.

Aslanidis *et al.* [28] also reported on the reaction of various Cu(I) halides (chloride, bromide, and iodide) with different ligands including heterocyclic thiones and 1,3-propanebis(diphenylphosphine). Under the same reaction conditions, the authors isolated two different types of compounds depending on the structure of the copper halide used. For X = Cl or Br, monomeric structures with tetrahedrally coordinated Cu(I) were obtained whereas dimeric structures with bridging iodine atoms were formed for X = I. The authors indicated that DFT computational methods at the B3LYP level of theory provided a good description of the bonding structures as well as the electronic properties of the resultant complexes and their dimers. They showed that the interaction between the ligand and the central Cu(I) atom in these complexes is relatively weak, where the calculated interaction energies estimated at about 20 kcal/mol for all studied complexes.

The current study focuses on the use of computational chemistry to study $I \cdots I$ interactions, related to those found between triiodide anions, in transition metal-iodide complexes in order to determine the nature, type and strength of these interactions. Certain aspects of the study are aimed at opening the door to further investigations on the intermolecular and intramolecular interactions between iodine species in transition metal-iodide complexes. A deeper understanding of the nature of the interactions between iodide species and the role played by the central metal atom in the formation of metal-iodide complexes that form weak or strong I–M–I$\cdots$I–M–I interactions would allow the design of materials with tunable electronic properties analogous to the polyiodide materials currently used in electronics, solar cells and other electronic devices. In this study the calculations are performed in the gas phase and different environments described by a polarizable continuum solvent model to mimic the electrostatic environment of a crystal. The results will be compared to those observed experimentally in the solid state (obtained from Cambridge Structural Database, CSD [6]). The study also focuses on understanding the origin of these interactions as well as identifying factors affecting them. To

4

our knowledge, no theoretical studies have been conducted to date to model and investigate the I⋯I interactions in dimers of transition metal-iodide complexes in order to determine their nature and properties in the solid state and some selected environments.

1.2 Aim and objectives

The overall aim of the project is to investigate the prevalence and properties of I⋯I interactions in transition metal iodides. The main objectives of the study are threefold: The first objective was to perform a comprehensive analysis of previously published experimental crystal structures which contain transition metal iodides using the CSD. This was necessary in order to determine which complexes, containing the I–M–I moiety, form I⋯I interactions in the solid state. Metals most likely to form I–M–I⋯I–M–I interactions were identified based on results from the CSD searches. The second objective was to optimize and study the structures of some selected metal-iodide complexes and their dimers, using simplified ligands when necessary, with the aid of computational methods. This was using different protocols (e.g. various density functionals, basis sets and various solvents with the aid of the Polarizable Continuum Model). The role of other ligands in the complexes and/or cations was also be investigated. The aim was to provide an explanation of the origin of these interactions as well as factors affecting them. In the third objective, an analysis of the nature and properties of the I–M–I⋯I–M–I interactions were performed utilizing Natural Bonding Orbital (NBO) and Atoms in Molecules (AIM) analyses. NBO was utilized to determine the nature of the I⋯I interactions while AIM was used to study the topographical properties of these interactions. The calculated values for AIM parameters were compared to those values published for $I_3^- \cdots I_3^-$ interactions.

1.3 Thesis layout

The thesis consists of seven chapters, three of which describe the experimental results. Chapter 1 provides a general introduction to the study, followed by the objectives and thesis layout. Chapter 2 contains a historical background about iodine, polyiodides and iodine-iodine as well as metal-iodide interactions. It also describes, in detail, some aspects of the methods currently used in computational chemistry calculations. These include: DFT, basis sets, the implicit solvent

5

model, NBO analysis and AIM analysis. Chapter 3 gives detailed information and procedures about the CSD searches and the computational methods used for the study.

The results are presented in three chapters, namely Chapters 4, 5 and 6. Chapter 4 describes the CSD analysis, which was carried out on previously published crystal structures. Here, the CSD was used in order to establish which transition metal-iodide complexes containing the I–M–I moiety are able to form dimers involving I $\cdots$ I interactions in the solid state. This was done in order to obtain reasonable starting geometries for the calculations of the metal-iodide complexes calculations, which was carried out using DFT theory. Moreover, metal-iodides exhibiting these interactions were analyzed in order to describe the most common relative conformations observed at shorter I $\cdots$ I distances, which were indicative of stronger I $\cdots$ I interactions.

In Chapter 5 an investigation of the nature and strength of the I $\cdots$ I interactions in dimers of transition metal-iodides is discussed based on calculations of the minimum energy conformations at which I $\cdots$ I interactions occur. The intermolecular and intramolecular distances of these interactions in some selected metal-iodide complexes are determined employing various levels of DFT. These calculations were carried out in the gas phase as well as in an implicit solvent model using various solvents, which have a wide range of electrostatic constants. This allowed the determination of the effect of the surrounding environment on the I $\cdots$ I interaction distance and strength.

Chapter 6 describes a study of the nature and properties of the I $\cdots$ I interactions in dimers of two different transition metal-iodide complexes, containing copper (Cu) or platinum (Pt). Various interaction parameters with regards to the I $\cdots$ I interactions were investigated based on NBO and AIM calculations in the gas phase as well as in an implicit solvent model. The NBO and AIM parameters obtained were employed to aid in the understanding and classification (i.e., as van der Waals interactions or hydrogen bonding) of the I $\cdots$ I interactions existing in transition metal-iodide complexes in various environments (i.e., gas phase and in solution).

Chapter 7 summarizes the main conclusions drawn from the results and gives some recommendations for future work.

1.4 References

1. Wells, A.F., *Structural inorganic chemistry*. 5th ed: Clarendon Press, Oxford University Press, New York **1984**.

2. *The Halogens: Fluorine, Chlorine, Bromine, Iodine and Astatine*, in *Chemistry of the Elements (Second Edition)*, N.N. Greenwood and A. Earnshaw, **1997**, Butterworth-Heinemann: Oxford. p. 789-887.

3. Küpper, F.C., Feiters, M.C., Olofsson, B., Kaiho, T., Yanagida, S., Zimmermann, M.B., Carpenter, L.J., Luther, G.W., Lu, Z., Jonsson, M., and Kloo, L., *Commemorating Two Centuries of Iodine Research: An Interdisciplinary Overview of Current Research.* Angewandte Chemie International Edition **2011**, 50(49), 11598-11620.

4. Bent, H.A., *Structural chemistry of donor-acceptor interactions.* Chemical Reviews **1968**, 68(5), 587-648.

5. Metrangolo, P., Neukirch, H., Pilati, T., and Resnati, G., *Halogen Bonding Based Recognition Processes: A World Parallel to Hydrogen Bonding.* Accounts of Chemical Research **2005**, 38(5), 386-395.

6. Allen, F., *The Cambridge Structural Database: a quarter of a million crystal structures and rising.* Acta Crystallographica Section B **2002**, 58, 380-388.

7. Loos, K.R. and Jones, A.C., *Structure of triiodide ion in solution. Raman evidence for the existence of higher polyiodide species.* The Journal of Physical Chemistry **1974**, 78(22), 2306-2307.

8. Tebbe, K.-F. and Buchem, R., *The Most Iodine-Rich Polyiodide Yet: Fe_3I_{29}.* Angewandte Chemie International Edition in English **1997**, 36(12), 1345-1346.

9. Svensson, P.H., Bengtsson-Kloo, L., and Persson, P., *Metal iodides in polyiodide networks. The structural chemistry of CdI_2 with an excess of iodine.* Journal of the Chemical Society, Dalton Transactions **1998**(9), 1425-1429.

10. Kloo, L., Rosdahl, J., and Svensson, Per H., *On the Intra- and Intermolecular Bonding in Polyiodides.* European Journal of Inorganic Chemistry **2002**(5), 1203-1209.

11. Coppens, P., *Structural Aspects of Iodine-Containing Low-Dimensional Materials*, in *Extended Linear Chain Compounds*, J. Miller, Editor **1982**, Springer US. p. 333-356.

12.   Marks, T. and Kalina, D., *Highly Conductive Halogenated Low-Dimensional Materials*, in *Extended Linear Chain Compounds*, J. Miller, Editor **1982**, Springer US. p. 197-331.

13.   Stegemann, H., Jabs, G., Mittag, H., Schmidt, L., Fullbier, H., Cikmacs, P., Petrovskis, G., Lusis, A., and Orliukas, A.S., *N-alkylurotropiniumpolyiodides-preparation, investigation of the electrical and magnetic properties.* Zeitschrift Für Anorganische Und Allgemeine Chemie **1987**, 555(12), 183-191.

14.   Owens, B.B., Patel, B.K., Skarstad, P.M., and Warburton, D.L., *Performance of $Ag/RbAg_4I_5/I_2$ solid electrolyte batteries after ten years storage.* Solid State Ionics **1983**, 9–10, 1241-1245.

15.   "The Nobel Prize in Chemistry 2000". Nobel Media AB 2014. Web page: http://www.nobelprize.org/nobel_prizes/chemistry/laureates/2000/, accessed on 31 Aug 2015.

16.   Chiang, C.K., Fincher, C.R., Park, Y.W., Heeger, A.J., Shirakawa, H., Louis, E.J., Gau, S.C., and MacDiarmid, A.G., *Electrical Conductivity in Doped Polyacetylene.* Physical Review Letters **1977**, 39(17), 1098-1101.

17.   Groenewald, F., Esterhuysen, C., and Dillen, J., *Extensive theoretical investigation: influence of the electrostatic environment on the $I_3^-\cdots I_3^-$ anion–anion interaction.* Theoretical Chemistry Accounts **2012**, 131(10), 1-12.

18.   Svensson, P.H. and Kloo, L., *Synthesis, Structure, and Bonding in Polyiodide and Metal Iodide−Iodine Systems.* Chemical Reviews **2003**, 103(5), 1649-1684.

19.   Westra, A.N., Bourne, S.A., Esterhuysen, C., and Koch, K.R., *Reactions of halogens with Pt(II) complexes of N-alkyl- and N,N-dialkyl-N-benzoylthioureas: oxidative addition and formation of an I_2 inclusion compound.* Dalton Transactions **2005**(12), 2162-2172.

20.   Buse, K.D., Keller, H.J., and Pritzkow, H., *Reaction of molecular iodine with cis-dihalo(2,2'-bipyridyl)platinum(II) and cis-dihalo(1,10-phenanthroline)platinum(II). Oxidative addition and inclusion compounds.* Inorganic Chemistry **1977**, 16(5), 1072-1076.

21.   Gray, L.R., Gulliver, D.J., Levason, W., and Webster, M., *Coordination chemistry of higher oxidation states. 5. Reaction of palladium(II) iodo complexes with molecular iodine and crystal and molecular structure of diiodo(cis-1,2-*

bis(diphenylphosphino)ethene)palladium(II)-diiodine. Inorganic Chemistry **1983**, 22(17), 2362-2366.

22. Schneider, D., Schuster, O., and Schmidbaur, H., *Attempted Oxidative Addition of Halogens to (Isocyanide)gold(I) Complexes.* Organometallics **2005**, 24(14), 3547-3551.

23. Lobello, M.G., Fantacci, S., and De Angelis, F., *Computational Spectroscopy Characterization of the Species Involved in Dye Oxidation and Regeneration Processes in Dye-Sensitized Solar Cells.* The Journal of Physical Chemistry C **2011**, 115(38), 18863-18872.

24. Privalov, T., Boschloo, G., Hagfeldt, A., Svensson, P.H., and Kloo, L., *A Study of the Interactions between I^-/I_3^- Redox Mediators and Organometallic Sensitizing Dyes in Solar Cells.* The Journal of Physical Chemistry C **2009**, 113(2), 783-790.

25. Hu, C.-H., Asaduzzaman, A.M., and Schreckenbach, G., *Computational Studies of the Interaction between Ruthenium Dyes and X^- and X_2^-, X = Br, I, At. Implications for Dye-Sensitized Solar Cells.* The Journal of Physical Chemistry C **2010**, 114(35), 15165-15173.

26. Schiffmann, F., VandeVondele, J., Hutter, J., Urakawa, A., Wirz, R., and Baiker, A., *An atomistic picture of the regeneration process in dye sensitized solar cells.* Proceedings of the National Academy of Sciences **2010**, 107(11), 4830-4833.

27. Nazeeruddin, M.K., De Angelis, F., Fantacci, S., Selloni, A., Viscardi, G., Liska, P., Ito, S., Takeru, B., and Grätzel, M., *Combined Experimental and DFT-TDDFT Computational Study of Photoelectrochemical Cell Ruthenium Sensitizers.* Journal of the American Chemical Society **2005**, 127(48), 16835-16847.

28. Aslanidis, P., Cox, P.J., Divanidis, S., and Tsipis, A.C., *Copper(I) Halide Complexes with 1,3-Propanebis(diphenylphosphine) and Heterocyclic Thione Ligands: Crystal and Electronic Structures (DFT) of [CuCl(pymtH)(dppp)], [CuBr(pymtH)(dppp)], and [Cu(μ-I)(dppp)]2.* Inorganic Chemistry **2002**, 41(25), 6875-6886.

Chapter 2

Historical and theoretical background

2.1 Iodine-iodine and Metal-iodine interactions

2.1.1 Iodine

Iodine is a halogen with a relatively high atomic number of 53 compared to other chemical elements found in the same group (i.e., halogens). At room temperature, the nonmetallic crystalline material has a dark gray color that has a shiny appearance (see Figure 2.1). Due to its high vapor pressure, iodine can easily sublime to its vapor state which has a distinct violet color at moderate temperatures. In fact, the word iodine originates from the word *ioeidēs*, which means violet or purple in the Greek language. Like the other halogens, free iodine exists mostly as diatomic molecules of I_2, however the element can be also found in nature as a highly water-soluble iodide ions of I^-. Iodine is also found in the outer layer of the Earth in very small quantities with abundance of 5.0×10^{-5} % [1]. Due to the combination of these unique properties such as a high atomic number, low toxicity, high electronegativity and high reactivity with other organic compounds, iodine can be used in many applications including disinfectants [2], chemical analysis and many other medical uses [3].

Figure 2.1: Digital photograph showing solid iodine with the nonmetallic crystalline appearance [4].

Solid iodine has a layered lattice structure, containing separate diatomic molecules of I_2, which have been observed in the molten and the vapor states [5]. These layers form a two-dimensional network of I_2 molecules with an I–I bond distance of 2.7 Å [6]. However, compared to other halogens (which are also diatomic) solid crystals of iodine have a higher melting point [7]. This can be attributed to the van der Waals forces acting between diatomic I_2 molecules. The I–I bond has a relatively weak bond dissociation energy of 36.1 kcal/mol, and iodine also forms weaker bonds with other molecules compared to other lighter halides [8]. Another significant consequence of this weak bonding is that the diatomic I_2 molecules have the tendency to dissociate into iodide ions (i.e., I^-), which plays a significant role in donor-acceptor interactions. Thus, iodine is considered a Lewis acid acceptor, which forms charge-transfer complexes with electron donors such as pyridine. Similarly, with the Lewis base donors such as iodide and triiodide ions, it forms polyiodides [9]. The structure of iodine at 110 K is shown in Figure 2.2, with intramolecular distances of 2.72 Å [10]. From Figure 2.2, one can see that the intermolecular distances within the layers and between adjacent layers are found to be 3.50 and 4.27 Å, respectively. Similar values of intermolecular distances within the layers (3.50 and 3.97 Å) and between adjacent layers (4.27 Å) of iodine have been reported elsewhere [11].
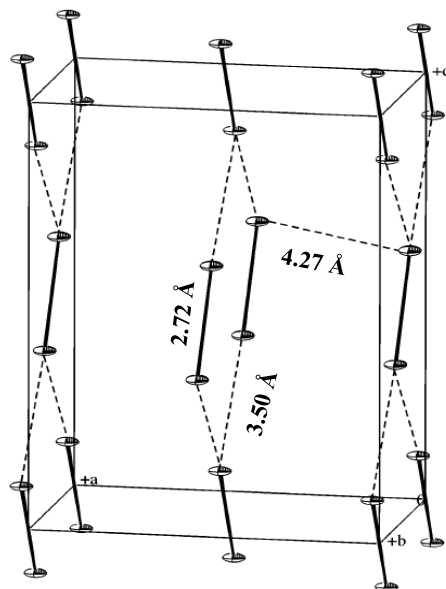

Figure 2.2: The crystalline structure of iodine at 110 K [10].

2.1.2 Iodine-iodine interactions and the formation of polyiodides

Iodine···iodine interactions are a type of intermolecular or intramolecular interaction that are associated with distances shorter than the sum of the van der Waals radii of contacting atoms. In recent years, the nature of this type of halogen···halogen bonding (i.e., I···I interaction) on metal containing inorganic compounds has been a matter of great interest [12-15]. This type of interaction has, in the past, been referred to as a donor-acceptor interaction, a secondary interaction, a charge-transfer interaction or incipient electrophilic and nucleophilic attack [16]. Furthermore, it has been noticed that there is a directional preference with which the contacting groups position themselves relative to each other in these interactions.

As mentioned, iodine molecules (I_2) can interact with iodide and triiodide ions and form polyiodide species where one polyiodide can consist of up to 29 iodine atoms [17, 18]. This is often achieved through donor-acceptor interactions, which can be influenced by the counter ions, leading to a variety of possible polyiodide structures. The resultant polyiodides have the common formula of $(I_{2m+n})^{n-}$, where m is the number of diatomic I_2 molecules and n is the number of iodide anions (I^-) (m and n must be > 0). Although these polyiodides contain simple distinct one-dimensional units of I_2 molecules they may also contain more complex network structures such as two-dimensional or even three-dimensional structures. These structures may also exist as small separate polyiodides or even larger network structures of intercalated polyiodide ions. Examples of these polyiodides range from simple I_3^- anions through linear I_4^{2-}, V-shaped I_5^- and branched structures of higher polyiodides such as I_7^- or I_9^- [19-21].

The ability of iodide ions to associate with iodine molecules to form polyiodide ionic complexes has been recognized since the early days of modern chemistry. It was shown that among the dihalogens, iodine has the highest tendency to link into polycoordinated anions, which could form a wide range of structures and motifs [10]. In fact, it was shortly after the discovery of iodine that scientists reported the preparation of triiodide compounds using iodine [22]. Others also claimed to have isolated large blue crystals (which they identified as potassium triiodide) by the evaporation of a concentrated iodine-potassium iodide solution [23]. It was observed that the solubility of iodine in polar solvents such water and ethanol is enhanced considerably by adding

a small quantity of iodide ions. The reason for the increased solubility of iodine was in fact explained by the formation of the triiodide ion in solution. In recent years, polyiodides have earned much attention due to their unique electric conduction properties, ranging from that of insulators to conductive metals [24]. Such properties, which may depend on the structure and composition of the polyiodide, find many applications in electronic and electrochemical devices such as fuel cells and batteries [25, 26].

Stenzel *et al*. [27] studied iodine-iodine interactions in various compounds, namely dialkyldiiodophosphonium iodides and triiodides. It was shown before that in these iodophosphonium cations, each iodine atom is attached to four phosphorus atoms, which could act as an electrophile [28]. To meet these requirements, Stenzel *et al*. indicated that each two cations of these dialkyldiiodophosphonium iodides will be bridged by iodide anions that act as the nucleophile. The authors showed that a rapid iodine transfer reaction occurs between compounds containing phosphonium (V) triiodides (R_2PI_3, where R is t-Bu, i-Pr or Et) and iodophosphanes. They also observed that the interactions between cations of $R_2PI_2^+$ and iodide anions of I^- and I^{3-} decrease significantly with increasing the amount of iodine added to the systems (i.e., R_2PI_3/I_2).

The type of bonds in polyiodides cannot often be explained by simple covalent bonding, which has been the subject of many theoretical studies in recent years [10, 29]. These bonds are usually characterized by their highly complex and variable arrangements, which exhibit an interesting structural chemistry. In polyiodides, iodine mainly adopts a wide range of formal oxidation states (ranging from I^{7+} to I^-), which can be found in different iodide salts. However, due to its relatively high electronegativity iodine usually forms polyiodides where iodine possesses the oxidation state of I^- [9]. Furthermore, it has been shown that the $I \cdots I$ intramolecular interaction distances found in polyiodides is longer than the normal covalent I–I bond distance (3–4 Å) while the intermolecular interactions are shorter than the sum of van der Waals radii of iodine (4.3 Å) [29]. This great range of $I \cdots I$ interaction distances makes it very difficult to define the I to I bonds found in polyiodide structures, which are usually referred to as "secondary bonds". In 1972 the term "secondary bonding" was introduced by Alcock to explain a wide range of interactions found in nonmetallic elements, including charge-transfer bonding [30].

13

Different preparative methods for the synthesis of various polyiodides have been reported in the literature. The most commonly used method involves the *in situ* addition of equivalent amounts of I_2 to an iodide salt containing a suitable cation [18]. The simplest form of polyiodides is the triiodide ion (I_3^-), where the $I_2 \cdots I^-$ interaction is very strong (~180 kJ/mol) [31]. Similar to other polyiodides, triiodides can generally be formed by mixing an iodide salt (e.g. CsI) with iodine crystals (I_2) forming triodides that can exist in the solid state and in solution as linear molecules. In a study by Kloo *et al*., the authors showed that the formation of these bonds can be described by the presence of intramolecular bonding as well as other dispersion interactions between the I_2 and I^- units [29]. For the synthesis of other higher polyiodides, an exchange reaction, where I_3^- anions are reacted with the appropriate salt of the desired cation, can be also used. This leads to the formation of other known, larger polyiodides such as I_4^{2-}, I_5^-, I_7^-, I_8^{2-}, I_9^-, I_{10}^{2-}, I_{10}^{4-}, I_{11}^-, I_{12}^{2-}, I_{13}^{3-}, I_{16}^{2-}, I_{22}^{4-}, I_{26}^{3-}, I_{26}^{4-}, I_{28}^{4-} and I_{29}^{3-} [32]. Here, the structure and physical properties of these higher polyiodides can be described by the interaction between three simple building units of I^-, I_2, and I_3^-. In such interactions, the diatomic iodine molecules I_2 act as the Lewis acid acceptor while I^- and I_3^- anions work as the Lewis base donors.

Although numerous examples of small polyiodides, such as I_3^- , I_4^{2-} and I_5^-, are available nowadays the formation of higher polyiodides containing discrete diatomic molecules of I_2 becomes more difficult [10, 33]. According to Deplano *et al*. [34] all higher polyiodides from I_4^{2-} cannot be easily isolated as separate units, which are obtained by various donor–acceptor interactions between I^- and/or I_3^- anions with the diatomic I_2 molecules. The authors indicated that the iodine molecules act as a link between other higher polyiodides, which exist as distinct I^- and I_3^- units. They described these crossover links by the presence of a covalent bond which can be described by the formation of $I_2 \cdot I^-$ and/or $I_2 \cdot I_3^-$ adducts via donor–acceptor interactions. Generally speaking, all known polyiodides from I_7^- and larger can be regarded as the product weak or medium strength interactions, which can be mainly obtained via donor-acceptor interactions between I^- and I_3^- anions with I_2 molecules, that have relatively longer I–I bond distances [13].

2.1.3 Characterization of iodine and polyiodides

In the past, several techniques have been used for the characterization of polyiodides. These include X-ray based methods, vibrational spectroscopy, absorption spectroscopy and electrochemical methods [10]. Vibrational spectroscopy methods are considered as powerful techniques for the analysis of polyiodides in the solid and liquid state. However, they can be mainly used when the polyiodides under investigation are amorphous or noncrystalline, which limits their applications. When the polyiodides are crystalline, their structural characterization can be obtained from other X-ray based methods such as liquid X-ray scattering (LXS). Conductivity measurements can also be used for the characterization of iodine and polyiodides, where they play an important role in the conduction process.

It is well known that when iodine is dissolved in different solvents, it gives a wide range of colors depending on the solvent used. For instance, in aliphatic solvents iodine gives a violet color, while in alcohols, ethers, and aromatic solvents such as benzene it is brown or reddish-brown [35]. This broad range of colors makes it possible to use absorption spectroscopy methods in the ultraviolet-visible (UV-Vis) spectral region for the analysis and characterization of iodine and polyiodides. In the early 1970, Gabes *et al.* [36, 37] investigated the use of UV-Vis spectroscopy for the analysis of different polyhalides including triiodides (I_3^-) in the solid state and in CCl_4 solvent. The authors reported that the I_3^- anion has two characteristic absorption bands at 290 and 367 nm. Other polyiodides have been also investigated, where authors reported an absorption band of 600 nm which was assigned to the pentaiodide (I_5^-) anion [34, 38]. Mizuno *et al.* [39] also invistgated the UV-Vis spectroscopy of polyiodides and reported that the absorption band of pentaiodides could occur at about 700 nm. Other higher polyiodides, such as I_7^- and I_9^-, were also studied which showed similar absorption bands as the triiodide and pentaiodide anions [40].

Other methods such as Raman and Infrared spectroscopy have been also successfully used for the characterization of polyiodides. In 2012, Reiss *et al.* [41] reported the synthesis and characterization of a new polyiodide compound in the α,ω-Diazaniumalkane iodide/iodine

15

system using spectroscopic techniques. The authors showed that structural parameters of the tetraiodide anion derived from X-ray crystallographic data are in excellent agreement with the results obtained from Raman spectroscopy. Other thermal analysis techniques such as thermogravimetry and Differential Scanning Calorimetry have been used for the characterisation of polyiodides [42].

Different investigations showed that iodine can be used to enhance the electrical conductivity of some compounds such as cyclic or aromatic hydrocarbons, graphite and polymers [43-45]. Kusabayashi *et al*. [46] showed that when higher I_2 content is used, the electrical conductivity of triiodides, namely $(Me_3PhN)I_3$ and $(MePy)I_3$ increases significantly. Forsyth *et al*. [47] also showed that the addition of I_2 to polymers such as poly(propylene oxide) in the presence of metal iodide salts (i.e., NaI or LiI) may result in ohmic conductivity. The authors also observed that even in the absence of the metal iodide salt, the polymer/I_2 complexes still exhibit high conductivity compared to the pristine polymer. In such electrolyte polymers, the conductivity depends significantly on the glass transition temperature (T_g) defined as the temperature at when the polymer chains start to move leading to a significant change in its mechanical properties. However, in polymer/I_2 complexes a small change in the conductivity around the T_g was observed with a relatively high conductivity below that temperature [47].

2.1.4 Metal-iodide complexes

Similar to other halogens (i.e., fluorine, chlorine and bromine), iodine can react with metals forming metal halides, which can be described by the following equation:

$$2M + nX_2 \rightarrow 2MX_n$$
$$2.1$$

where M is the metal, X is the halogen and MX_n is the metal halide.

The resultant complexes which can be formed from different halide ions such as fluoride, chloride, bromide, and iodide ions are among the most widely known complexes

16

containing anionic ligands [48, 49]. Some of these metal halides are formed by ionic bonds, such as sodium chloride, while others contain covalence bonded structures. Examples of the latter structures include discrete molecules such as uranium hexafluoride or even polymeric metal halides (e.g., palladium chloride) [50]. In principle, most metal halides can be obtained by a direct reaction of their constituent elements. However, this type of reaction can be very exothermic, which limits its application as a practical preparation technique for some metal halides. In addition, some halogens could act as strong oxidizers, leading to the formation of the highly oxidized metal halide only. It was shown, however, that heating higher halides results in their thermal decomposition, which leads to the formation of other lower halides by a disproportionation reaction [50].

Metal halides such as transition metal iodides could act as electron-pair acceptors in which the iodine acceptor atom is attached to another iodine via a covalent I–I bond or through weak I $\cdots$ I interactions. This results in the formation of transition metal-iodide$\cdots$iodide complexes, in which iodine atoms can have a variety of formal oxidation states similar to those found in pure polyiodides, ranging from I^- to I^{7+}. In addition, transition metals could have various oxidation states, resulting in the formation of a wide range of transition metal-iodide$\cdots$iodide complexes with different properties. However, these metal-iodide$\cdots$iodide structures show a common characteristic feature, which is the presence of bridging iodide ions or units. It was shown that in pure polyiodide networks, the interaction between iodide ions mainly involves the formation of some distinct polyiodide structural units of I^-, I_2, I_3^- only [34]. The number of diatomic I_2 molecules was shown to determine the length of the polyiodide network [10]. However, in metal-iodide$\cdots$iodide complexes, the I^- and I_3^- anions found in pure polyiodides are replaced by the M-I unit, which can be considered as the new building units for higher polyiodides of metal iodides. In the case where metal-iodide complexes are obtained from the interaction between the metal-iodide (M-I) and diatomic I_2, late transition metal-iodides form the strongest interactions with I_2 [10].

Different studies have shown that the formation of metal-iodides can be carried out by the reaction between diatomic iodine (I_2) and metal complexes, which can result in the preparation of an I_2-rich compound. Similar to other donor species, the reaction of metal-iodides with

17

polyiodide compounds occurs via a special mechanism, where the metal-iodide causes the iodine atom to compete for the iodide ions. In a recent investigation, Westra *et al.* [51] studied the reaction of different halogens with two different Pt(II) complexes of N-alkyl-N-benzoylthioureas and N,N-dialkyl-N-benzoylthioureas. The authors showed that the addition of diatomic I_2 molecules to Pt(II) complexes resulted in the formation of metal-iodides containing $Pt(II) - I \cdots I - Pt(II)$ chains. The authors indicated that this could happen under moderate conditions, where the I_2 molecules undergo facile oxidative addition to the Pt(II) complexes. Similar results have been observed for Pt(IV) [52] and Pd(II) [53].

The interactions between the Ru(II)-based complexes and iodide anions (I^-) and their applications in the regeneration process of dyes have been the subject of many experimental and theoretical studies in recent years [54-56]. In 2011, Tuikka *et al.* [54] investigated the halogen interactions between Ru-based dye containing the thiocyanate (SCN^-) ligand (i.e., $(Ru(dcbpy)_2(SCN)_2)$) (dcbpy = dicarboxy-bipyridine) and iodine (I_2) molecules and provided experimental evidence for the formation of stable Ru-based dye-…I_2 adducts. The authors showed that a stable Ru complex adduct of $[Ru(dcbpy)_2(SCN)_2]I_{24}(CH_3OH)$ is formed via an $S \cdots I$ interaction between the SCN^- ligand and the I_2 molecule.

Rogachev *et al.* [57] also investigated the bonding in I_3^- anion adducts with metal complexes containing two different transition metals, namely $[Cr(CO)_5]$ and $[Mn(CO)_5]^+$. The authors showed that the "end-on coordination is favored by $5-13$ kcal/mol over side-on to the central I of I_3^-, with a ~10 kcal/mol barrier for isomerization". They also observed that "the stabilizing effect of I_3^- with $[Cr(CO)_5]$ and $[Mn(CO)_5]^+$ for both end-on and side-on through central I of I_3^- coordination, with the end-on bonded isomer being slightly more stable".

In another study, Blake *et al.* [13] studied the structure of different polyiodides containing transition metals, which include $[Co([9]aneS_3)_2]I_{11}$, $[Ni([9]aneS_3)_2]I_6$, $[Ni([9]aneS_3)_2]I_{10}$, $[Pd([12]aneS_4)]I_6$ and $[Pd([14]aneS_4)]I_{10}.MeCN$ ($[9]aneS_3$ = 1,4,7-trithiacyclononane, $[12]aneS_4$ = 1,4,7,10 tetrathiacyclo-dodecane and $[14]aneS4$ = 1,4,8,11-tetrathiacyclotetradecane). The authors indicated that the best procedure for preparing polyiodides is to react a boron fluoride salt of the metal complex in the presence of an excess amount of I_2, where the favored polyiodide

compound is formed via a self-assembly mechanism. The authors also showed that reactions using preformed I_3^- or I_5^- anions generally result in the formation of compounds containing triiodides units only, which can be easily isolated. The latter can be also extended further to form other structures through short $I \cdots I$ contacts, which results in the formation of metal-iodide$\cdots$iodide complexes containing higher polyiodides.

In general, interactions found in metal-iodide$\cdots$iodide complexes can be divided into binary and nonbinary interactions [10]. The $I \cdots I$ interactions in the binary metal-iodide$\cdots$iodide complexes containing metals such as gold, cadmium, or mercury are usually described as being similar to the interactions in pure polyiodides. However, based on $I \cdots I$ distances found in these systems, the interaction between the donor and acceptor species is usually weaker than that found in normal polyiodides [34, 38]. Thus, the metal-iodide complexes can be regarded as species with less donor features than those of I^- and I_3^- ions. On the other hand, the nonbinary metal-iodide$\cdots$iodide structures can be considered as metal-iodide$\cdots$iodide complexes with stabilizing ligands. Consequently, the $I \cdots I$ interaction in these nonbinary metal-iodide$\cdots$iodide systems is found to be stronger than those in the binary structures.

2.2 Theoretical methods used in computational chemistry

Computational chemistry is a subfield of chemistry, which uses theoretical and mathematical calculations to solve chemical and physical problems. These theoretical calculations are often achieved utilizing powerful computer modeling systems to study the structures of various molecules and complex compounds. Today, several computational software packages are available in order to determine the structures and properties for these complexes and their solid crystals in a wide range of chemical surroundings. Properties such as molecular structures, bonding distances as well as interaction and conformation energies of atoms and molecules can now be simulated and predicted using various computational methods [58]. These methods include Hartree-Fock (HF) theory, Density Functional Theory (DFT), Natural Bond Orbital (NBO) analysis and Atoms in Molecules (AIM) analysis, which were used in this study. These methods along with the concepts of basis sets and the implicit solvent model are now discussed in the following sections.

19

2.2.1 Hartree-Fock Theory

The Hartree-Fock (HF) theory is a method of estimation which can be used to determine the N-electron wave functions and energies of atoms in quantum chemical calculations [59]. It approximates the N-electron wave functions by using the antisymmetrized product of one-electron wave functions, $\vec{\chi}_i$. The method is based on a iterative process known as the self-consistent field procedure to determine the wave functions and energies of a set of orbitals. The basis of the HF method goes back to the end of the 1920s, following the description of the time dependent Schrödinger equation, which is a partial differential equation that defines how the quantum state of a physical system varies with time [60]. The Schrödinger equation exists in two terms. These are the time-dependent and time-independent Schrödinger equations. The time-dependent Schrödinger equation is the most general form, which can be described as:

$$i\hbar \frac{\partial}{\partial t} \Psi = \hat{H}\Psi \qquad\qquad 2.2$$

Where i is an imaginary component, $\hbar$ is obtained by dividing the Planck constant by 2π, Ψ is the wave function of the quantum system and $\hat{H}$ is the Hamiltonian operator.

The Hamiltonian operator ($\hat{H}$) describes the total energy of any assumed wave function, which accepts various forms depending on the physical state. However, when the $\hat{H}$ is applied to a certain wave function of Ψ where the resultant product is proportional to the same Ψ, then Ψ will be considered as a stationary function state. Hence, the proportionality constant, E will be equal to the energy of the wave function, Ψ:

$$E\Psi = \hat{H}\Psi \qquad\qquad 2.3$$

HF theory always gives the exact N-body wave function of a physical system as a particular Slater determinant, Φ_{SD}. Thus, the Φ_{SD} can be described as follows:

20

$$\varphi_{SD} \approx \Psi_o \;=\; \frac{1}{\sqrt{N!}} \begin{vmatrix} \chi_1(\vec{x}_1) & \chi_2(\vec{x}_1) & \dots & \chi_N(\vec{x}_1) \\ \chi_1(\vec{x}_2) & \chi_2(\vec{x}_2) & \dots & \chi_N(\vec{x}_2) \\ \vdots & \vdots & \ddots & \vdots \\ \chi_1(\vec{x}_N) & \chi_2(\vec{x}_N) & & \chi_N(\vec{x}_N) \end{vmatrix} \qquad 2.4$$

This equation can then be simplified to give the product of the diagonal elements as follows:

$$\varphi_{SD} \;=\; \frac{1}{\sqrt{N!}} \, det \, \{\chi_1(\vec{x}_1) \, \chi_2(\vec{x}_2) \, \dots \, \chi_N(\vec{x}_N)\} \qquad 2.5$$

In the HF method, the one-electron functions $\chi_i(\vec{x}_i)$ (also called spin orbitals) must be orthonormal in order to obtain a minimum energy from the corresponding Slater determinant, which can be shown as:

$$E_{\text{HF}} \;=\; min_{\varphi_{SD} \to N} \, E[\varphi_{SD}] \qquad 2.6$$

$\hat{H}$ applied to Φ_{SD} gives the HF energy as:

$$E_{\text{HF}} \;=\; \langle \varphi_{SD} | \hat{H} | \varphi_{SD} \rangle = \sum_i^N \langle i | \hbar | i \rangle + \frac{1}{2} \sum_i^N \sum_j^N \langle ii | jj \rangle - \langle ij | ji \rangle \qquad 2.7$$

2.2.2 Density Functional Theory

Density Functional Theory (DFT) is a quantum mechanics method that uses the electron density to estimate the electronic structure and energy of atoms. Today, this method is widely used to perform various computational chemistry calculations for molecules and ions. The origin of this method dates back to 1964 and relates to the work done by Hohenberg and Kohn, who proposed that the electronic energy of a ground state can be obtained by the electron density, ρ [61]. In concept, DFT is similar to HF with one basic difference, which is that DFT calculates the energy

21

as a function of the electron density while HF calculates the energy from orbitals. Since DFT provides better results than HF it has consequently become a very popular method. However, in order to obtain the minimum energy, different approximations have to be made for each method. With DFT, the atoms and molecules can be characterized by using functionals to determine their properties, where functionals are defined as functions of another function. A number (E_{trial}) is then assigned to a function (Ψ_{trial}), which then represents the functional. Hence, the DFT can be used to predict the functional to obtain the energy from the electron density.

The electron density of a system is related to its energy as a one-to-one correspondence. The aim of DFT is to obtain functionals that best describe the physical situation where the electron density is connected with the energy of a system. In other words, DFT uses a functional to obtain a figure or value from a function (i.e., a set of variables), which itself depends on other coordinates. For instance, the electron density is considered as a function, while the energy depending on an electron density is regarded as a functional. The functional then uses a function, $f(x)$ as input, which yields a number (a) as output as shown in the following equation:

$$F\left[f(x)\right] \rightarrow a \qquad\qquad 2.8$$

The functional E[Ψ] can then be minimized by finding all possible N-electron wave functions that are acceptable and get as close as possible to the true energy, E_0. Although DFT has its original concepts in the Thomas–Fermi model, the first theorems that made it possible for modern DFT to exist are the first and second Hohenberg-Kohn theorems [61]. The first Hohenberg-Kohn theorem shows that the physical properties of the ground state for atoms and molecules can be successfully obtained by the electron density, which only depends on three-dimensional variables or coordinates. The second Hohenberg-Kohn theorem defines the functional of the energy for a system and shows that the correct electron density of the ground state minimizes this functional of energy. It is worth mentioning here that in 1965 Kohn and Sham [62] suggested that the kinetic energy of electrons should be calculated from an additional set of orbitals, which represents the electron density. This in fact contributed to the success of modern DFT significantly.

2.2.3 Basis sets

Basis sets are a group of functions that can be incorporated in linear arrangements, which are used to perform various physical and chemical quantum calculations [63]. They are approximations that can basically be used in all *ab initio* methods, where solutions are generated without reference to experimental data. In computational chemistry, basis sets are used to describe the orbitals that coincide with atoms, which contribute to the molecular orbitals resulting in the creation of the appropriate wave function. It is worth mentioning here that the smaller the basis set, the poorer the representation of orbitals and vice versa. Therefore, large basis sets are required for a better representation of all the orbitals in a molecule, which can provide an accurate description of the system. However, a perfect basis set requires that an infinite number of basis sets or functions have to be used to describe each atom. This becomes difficult as very large basis sets and functions dramatically increase the resources required to perform calculations, making it almost impossible in practical cases.

On the other hand, a minimal basis set normally requires that a single basis function is used for each orbital on the free atom, which should apply for each atom in the molecule. Furthermore, the type of basis sets used influences the accuracy significantly. This means that if the basis sets are well selected, fewer sets of functions are therefore needed to achieve a given level of accuracy. In other words, a better single basis set is required to reproduce the unknown function, so that fewer sets of functions are necessary to yield an accurate result.

Nowadays, different types of basis sets and functions are used to describe orbitals in modern computational chemistry. The most common basis functions are known as Atomic Orbitals (AO), which are widely used in theoretical calculations of electronic structures. These include the Gaussian Type Orbitals (GTO), which are derived from Slater type orbitals (STO):

$$\eta^{STO} = N \, r^{n-1} \exp[-\zeta r] \, Y_{lm} \, (\Theta, \, \varphi) \qquad\qquad 2.9$$

Where N is a normalization constant, n is the principal quantum number, ζ represents the orbital exponent and Y_{lm} corresponds to the spherical harmonics describing the angular part of the function.

The GTO can be then described as:

$$\eta^{GTO} = N\, x^l\, y^m\, z^n\, \exp[-\alpha r^2] \qquad\qquad 2.10$$

where N is a normalization factor, α determines how compact (i.e., α is large) or diffuse (i.e., α is small) the resulting function is, which represents the orbital exponent. The exponents l, m and n are used to define the GTO as s functions ($L = l + m + n = 0$), p functions ($L = l + m + n = 1$), d functions ($L = l + m + n = 2$), etc.

As mentioned, the smallest number of functions required to describe the electrons of each atom in a molecule is defined as the minimal basis set. This usually consists of a single basis function for each orbital, such as a hydrogen atom which can be described by one s-function. In general, STOs are mostly required for atomic and molecular systems where high accuracy must be obtained. In addition, many GTOs (about three times) are usually required to reach the same level of accuracy obtained by STO functions [64]. This is illustrated in Figure 2.3, which indicates that a 1s-STO is successfully modelled by a linear combination of three GTOs basis functions. However, the increased number of GTO basis functions can be still favored because the required integrals are easily calculated compared to STOs functions. Therefore, GTOs are favored and are widely used as basis functions to determine the electronic structure of atoms with great computational efficiency.

There are other basis sets that contain several basis functions that correspond to every orbital in the atom. These are known as extended basis sets, which include double-zeta, triple-zeta, and quadruple-zeta basis sets as well as split-valence basis sets. The double-zeta basis sets have two basis functions representing each orbital, e.g. the hydrogen atom would now be represented by two s functions (1s and 1s'). The triple-zeta and quadruple-zeta basis sets are basically similar but they contain three and four times the number of basis functions than the minimal basis set

24

required. On the other hand, the split-valence basis sets are simplified by using multiple functions for each valence orbital only, instead of every orbital. Other extended basis sets, which are commonly added to minimal basis sets, include polarized basis sets and diffuse basis sets [63].
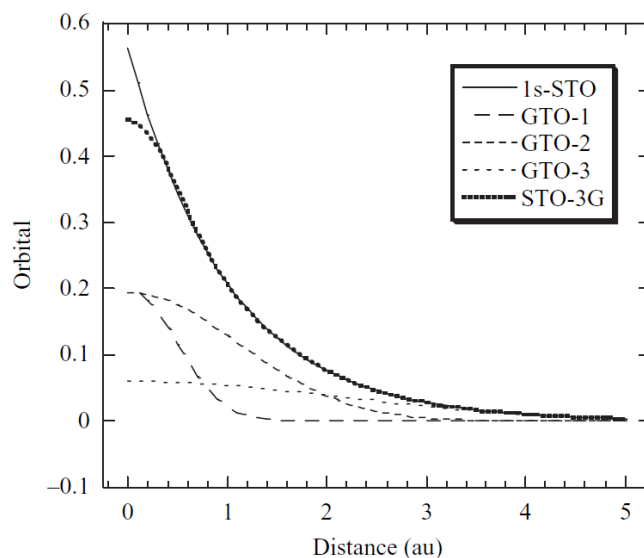

Figure 2.3: A linear combination of three GTOs basis functions (STO-3G) modelling one 1s-STO function [64].

2.2.4 Implicit solvent model

Solvation models are important aspects of computational chemistry that evaluate the effect of the surrounding environment, namely the solvent. Generally speaking, solvents can result in various interaction effects, which can be divided into two main groups including specific and non-specific solvation effects. The non-specific effects, which can be considered as long-range solvation effects include polarization and dipole orientation of the solvent. On the other hand, other interactions result in short-range solvation effects, which are more specific. These include hydrogen bonding, van der Waals interactions, solvent structure, solute solubility and donor-acceptor interactions. In computational chemistry, solvation models can be mainly divided into two types, including methods that observe the solvent molecules separately and those that consider the solvent as a continuous medium [65, 66]. Combinations are also possible, for example a continuum solvent model and a discrete solvent model can be used in computational

25

calculations. The polarizable continuum solvent model considers the solvent as a consistent and identical medium and places the solute in a suitable cavity that is surrounded by the solvent. The polarizability of the solvent is measured by the dielectric constant (ε, i.e., relative permittivity), which is a unique macroscopic property of the solvent. The dispersion interactions occurring between the solute and solvent results in a stabilization effect, which is equal to the van der Waals energy acting between the solute and solvent. The solvation free energy may be then written as:

$$\Delta G_{solvation} = \Delta G_{cavity} + \Delta G_{dispersion} + \Delta G_{electrostatic} \qquad 2.11$$

To make the *ab initio* calculations more meaningful, a Polarizable Continuum Model (PCM) was used in this study, where the solvent is modelled as a polarizable continuum medium and not as discrete individual molecules. The cavity is generated by overlapping spheres, where a suitable cavity is formed by a set of interlocking atomic van der Waals radii, which can be fitted by empirical parameters. Depending on the model used, there are several variables that could affect the calculation, namely the size, shape and reaction field of the cavity. There are two types of PCMs which are widely used, including dielectric PCM (D-PCM) and conductor-like PCM (C-PCM) [58, 67]. D-PCM describes the continuum as polarizable dielectric effects while C-PCM considers the continuum as a conductor-like effect. The molecular free energy of solvation (G_{sol}) is then calculated as the sum of the electrostatic energy (G_{es}), the dispersion-repulsion energy (G_{dr}) and the energy of cavitation (G_{cav}):

$$G_{sol} = G_{es} + G_{dr} + G_{cav}. \qquad 2.12$$

2.2.5 Natural Bond Orbital analysis

Natural Bond Orbital (NBO) analysis was initially designed by Löwdin in 1955 [68]. The theory of NBO was later developed by Weinhold in 1997 [69]. In computational chemistry, NBO uses one-electron density calculations to determine and describe the nature of orbitals. Thus, NBO can be used to calculate the distribution of electron density in atoms and in bonds between atoms, and used to define molecular bond structures. The NBO concept is part of a series of

Natural Localized Orbitals (NMOs), which are transitional between Atomic Orbitals (AOs) and Molecular Orbitals (MOs). Other combinations of NMOs also include Natural Atomic Orbitals (NAOs), Natural Hybrid Orbitals (NHOs) and Natural semi-Localized Molecular Orbitals (NLMOs). When NBOs are identified in a molecule, they can be given as linear combinations of the NAOs of its constituent atoms. This results in a localized position in which the atomic orbitals are involved in the bonding (i.e., NBOs). For instance, the NHO on atom A can be obtained as:

$$h_A = \sum_k a_k \, \Lambda_k^{(A)} \qquad\qquad 2.13$$

where $\Lambda_k^{(A)}$ is the maximum occupancy orbital. NBO is then used to describe the NHO in molecules, where each bonding NBO σ_{AB} can be written using two valence NHOs (h_A and h_B) on atoms A and B:

$$\sigma_{AB} = c_A \, h_A + c_B h_B \qquad\qquad 2.14$$

where c_A and c_B are the corresponding polarization coefficients.

The corresponding antibonding NBO can be also written as:

$$\sigma_{AB}^* = c_A \, h_A - c_B h_B \qquad\qquad 2.15$$

In the current study, NBOs are mainly used to calculate the distribution of electron density in atomic and molecular orbitals. This includes the maximum electron density, which can provide the most accurate possible Lewis structure, that is very close to the ideal structure. This ideal Lewis structure can be then defined as the structure with the highest electronic charge in its Lewis orbitals, which can be obtained by a computer program that can calculate the correct NBOs. The bonding NBOs will be considered as Lewis orbitals (orbital occupancies close to 2) while the antibonding NBOs will be given as the non-Lewis orbitals (orbital occupancies close to 0).

2.2.6 Atoms in Molecules analysis

Atoms in Molecules (AIM) analysis can generally be used for the description of quantum observables, which are localized in 3D space such as the electron density ρ(r) and energy densities of a system. The analysis is based on the theory of AIM, which is a quantum concept that is used to model electronic systems to successfully define atoms within molecules and crystals. This can be obtained by a quantum mechanical state function, which provides the energy of atomic and molecular structures. The development of chemistry has shown that some functional properties of atoms can be transferred from one molecule to another in a chemical reaction. AIM relies on observables such as electron density ρ(r), and energy densities to model and explain the electronic changes of these experimental observations. In addition, AIM can be used to clearly define chemical bonding of atoms in a molecule based on the topological properties of ρ(r).

The method used in AIM was first published in 1985 by Richard Bader [70]. The theory was later developed by Bader and other researchers at the University of McMaster [71], and is now widely used for computational modelling of atoms found in molecules. Bader initially proposed that the distribution of electron density of an atom in a molecule is a probability distribution. This can be used to describe the average state in which the electronic charge is dispersed within the actual physical space of the attractive force applied by the nuclei. This means that the approximate quantum mechanical state function not only provides the energy of a given molecular structure, it can also contain the required information to describe the atoms and their properties in that particular molecule. Bader indicated that the value of a physical quantity can be obtained by a matching operator acting on the state function. This means that quantum mechanics is concerned with observables as a result of operators relating to physical properties. It was also shown that some observables may result in sharp values while others could lead to average values, which depend on the nature of the state function.

The attractive field of the nuclei, which gives the molecule its basic geometrical and spatial properties dominates the topology of the electron density. The electron density can be then defined as the substantial local maximum at the position of each nucleus. It will have a critical

point (CP), which is described as a spatial point at which the first derivatives of the electron density disappear [72], i.e.:

$$\nabla_\rho = i\,\frac{d\rho}{dx} + j\,\frac{d\rho}{dy} + k\,\frac{d\rho}{dz} \rightarrow \begin{cases} = \vec{0} & \text{(at critical points and at } \infty) \\ \\ \neq \vec{0} & \text{(at all other points)} \end{cases} \qquad\qquad 2.16$$

This implies that every derivative in the gradient vector ($\nabla\rho$) is zero and not only the sum of each individual derivative. The gradient vectors of ρ ($\nabla\rho$) can be defined as the first derivatives of the charge density and describe the change in charge density. Thus, the gradient vectors of ρ provide both qualitative and quantitative information on the topological properties of ρ. The gradient of a scalar quantity function such as $\rho(r)$ at a given point in space is a gradient vector, which points in the direction where a large increase in the $\rho(r)$ occurs. The magnitude of this increase should be equal to the rate of increase in that direction.

Furthermore, a zero flux surface is defined as a surface where the scalar product of a gradient vector and a unit vector perpendicular to the surface equals zero. Therefore, the zero flux surface partitions the charge distribution of the system (molecules) into subsystems (atoms). CPs can be then described by two values namely the rank (i.e., dimension) and the signature, denoted as (r, s). The rank gives the non-zero curvatures of ρ at the CP and the signature is the sum of the signs of the curvatures. There are four three-dimensional (3D) CPs with three non-zero curvature values that are stable [73]. These are:

(3, -3)   Three curvatures of the electron density having negative values implying ρ is a local maximum, i.e. a nuclear attractor (an atom);

(3, -1)   Two curvatures have negative values, implying that ρ is a 2-dimensional (2D)-maximum in the direction defined by the negative curvatures, while one curvature is positive showing a 1-dimensional (1D)-minimum in the third direction that is perpendicular to this direction;

29

(3, +1)   Two curvatures with positive values, indicating that ρ is a 2D-minimum in the direction defined by the positive curvatures, while one is positive showing a 1D-maximum in the third direction which is perpendicular to this direction;

(3, +3)   Three curvatures having positive values indicating that ρ is a local 3D-minimum.

This means, for instance, that any point on the zero flux surface where ∇ρ = 0 is defined as a critical point that have two negative curvatures (i.e., (3, -1)). The 3 indicates the rank or the dimension of the critical point (i.e. 3D) and -1 indicates that the point is at a 2D-maximum and 1D-minimum. Each critical point mentioned above represents a specific chemical entity as follows: (3, -3) nuclear critical point (NCP); (3, -1) bond critical point (BCP); (3, +1) ring critical point (RCP); (3, +3) cage critical point (CCP) [73]. In the case of an NCP there is only one attractor per mononuclear area (known as an atomic basin) which defines the atoms in 3D space. Since the electron density decreases as one moves away from the position of the nucleus in any direction, the nucleus of an atom is defined by a local 3D maximum. This means that all the nearby gradient paths terminate at the nucleus. On the other hand, a molecular bond is defined by a pathway of maximum electron density between nuclei (two attractors), which is called *bond path*, where the local minimum on that line between the bonded nuclei is described as a BCP. As mentioned above, RCP and CCP points also exist but will not be discussed since they are not relevant to this study.

It is worth mentioning that a CP with r < 3 is considered as mathematically unstable, which will split or disappear under small changes in the density as a result of a nuclear motion. The existence of such a CP (i.e., where r < 3) indicates a change in the topology of the density, which implies a change in the molecular structure. Therefore, CPs with r < 3 do not usually exist in charge distributions at equilibrium. In our study, the AIM theory was used to define the nature of three different properties namely electron density $[\rho_b(r)]$, Laplacian of the electron density $[L(\rho_b(r))]$, and the total energy density $[H_b(r)]$. This was done at the intra- and intermolecular bond critical points (BCPs) for the I⋯I moiety in the gas phase and in various solvents. The latter was carried out utilizing an implicit solvent model with a wide range of dielectric constants to study the effect of the electrostatic environment on the I⋯I interactions.

2.3 References

1. *http://www.periodictable.com/Elements/053/index.html,* accessed on April 2015.

2. Gottardi, W., *Iodine as Disinfectant*, in *Iodine Chemistry and Applications* **2014**, John Wiley & Sons, Inc. p. 375-410.

3. Krause, W., *Iodinated X-Ray Contrast Agents*, in *Iodine Chemistry and Applications* **2014**, John Wiley & Sons, Inc. p. 353-374.

4. *http://www.britannica.com/science/iodine,* accessed on April 2015.

5. Kaiho, T., *Physical Properties of Iodine*, in *Iodine Chemistry and Applications* **2014**, John Wiley & Sons, Inc. p. 7-14.

6. Wells, A.F., *Structural inorganic chemistry*. 5th ed: Clarendon Press, Oxford University Press, New York **1984**.

7. *The Halogens: Fluorine, Chlorine, Bromine, Iodine and Astatine*, in *Chemistry of the Elements (Second Edition)*, N.N. Greenwood and A. Earnshaw, Editors. **1997**, Butterworth-Heinemann: Oxford. p. 789-887.

8. Sharpe, A.G., *The Physical Inorganic Chemistry of the Halogens*, in *Halgen Chemistry*, V. Gutmann, Editor **1967**, Academic Press Inc: London. p. 1-39.

9. Küpper, F.C., Feiters, M.C., Olofsson, B., Kaiho, T., Yanagida, S., Zimmermann, M.B., Carpenter, L.J., Luther, G.W., Lu, Z., Jonsson, M., and Kloo, L., *Commemorating Two Centuries of Iodine Research: An Interdisciplinary Overview of Current Research.* Angewandte Chemie International Edition **2011**, 50(49), 11598-11620.

10. Svensson, P.H. and Kloo, L., *Synthesis, Structure, and Bonding in Polyiodide and Metal Iodide−Iodine Systems.* Chemical Reviews **2003**, 103(5), 1649-1684.

11. van Bolhuis, F., Koster, P.B., and Migchelsen, T., *Refinement of the crystal structure of iodine at 110 degrees K.* Acta Crystallographica **1967**, 23(1), 90-91.

12. Brammer, L., Minguez Espallargas, G., and Libri, S., *Combining metals with halogen bonds.* CrystEngComm **2008**, 10(12), 1712-1727.

13. Blake, A.J., Li, W.-S., Lippolis, V., Parsons, S., and Schröder, M., *Extended structures of polyiodide salts of transition metal macrocyclic complexes.* Acta Crystallographica Section B **2007**, 63(1), 81-92.

14. Titi, H.M., Patra, R., and Goldberg, I., *Intermolecular iodine–iodine interactions in bis(pyridine-3-carboxylato)[tetrakis(4-iodophenyl)porphyrinato]tin(IV) and bis(pyrimidine-5-carboxylato)[tetrakis(4-iodophenyl)porphyrinato]tin(IV).* Acta Crystallographica Section C **2013**, 69(9), 1013-1016.

15. Lydia C. Gilday, Sean W. Robinson, Timothy A. Barendt, Matthew J. Langton, Benjamin R. Mullaney, and Paul D. Beer., *Halogen Bonding in Supramolecular Chemistry*. Chemical Reviews **2015**, *115* (15), 7118–7195.

16. Desiraju, G.R. and Parthasarathy, R., *The nature of halogen...halogen interactions: are short halogen contacts due to specific attractive forces or due to close packing of nonspherical atoms?* Journal of the American Chemical Society **1989**, 111(23), 8725-8726.

17. Loos, K.R. and Jones, A.C., *Structure of triiodide ion in solution. Raman evidence for the existence of higher polyiodide species.* The Journal of Physical Chemistry **1974**, 78(22), 2306-2307.

18. Tebbe, K.-F. and Buchem, R., *The Most Iodine-Rich Polyiodide Yet: Fe_3I_{29}.* Angewandte Chemie International Edition in English **1997**, 36(12), 1345-1346.

19. Abate, A., Brischetto, M., Cavallo, G., Lahtinen, M., Metrangolo, P., Pilati, T., Radice, S., Resnati, G., Rissanen, K., and Terraneo, G., *Dimensional encapsulation of $I^-...I_2...I^-$ in an organic salt crystal matrix.* Chemical Communications **2010**, 46(16), 2724-2726.

20. Poli, R., Gordon, J.C., Khanna, R.K., and Fanwick, P.E., *The first discrete structure for the heptaiodide ion.* Inorganic Chemistry **1992**, 31(14), 3165-3167.

21. Blake, A.J., Gould, R.O., Li, W.-S., Lippolis, V., Parsons, S., Radek, C., and Schröder, M., *Template Assembly of Polyiodide Networks at Complexed Metal Cations: Synthesis and Structures of $[Pd_2Cl_2([18]aneN_2S_4)]_{1.5}I_5(I_3)_2$ and $[K([15]aneO_5)_2]I_9$.* Angewandte Chemie International Edition **1998**, 37(3), 293-296.

22. Pelletier, B. and Caventou, J.B., Annales de Chimie et de Physique **1819**, 10, 164.

23. Johnson, G.S., *On potassium triiodide.* Journal of the Chemical Society **1877**, 31, 249-253.

24. Coppens, P., *Structural Aspects of Iodine-Containing Low-Dimensional Materials*, in *Extended Linear Chain Compounds*, J. Miller, Editor **1982**, Springer US. p. 333-356.

25.   Owens, B.B., Patel, B.K., Skarstad, P.M., and Warburton, D.L., *Performance of Ag/RbAg₄I₅/I₂ solid electrolyte batteries after ten years storage.* Solid State Ionics **1983**, 9–10, 1241-1245.

26.   Stegemann, H., Jabs, G., Mittag, H., Schmidt, L., Fullbier, H., Cikmacs, P., Petrovskis, G., Lusis, A., and Orliukas, A.S., *N-alkylurotropiniumpolyiodides-preparation, investigation of the electrical and magnetic properties.* Zeitschrift Für Anorganische Und Allgemeine Chemie **1987**, 555(12), 183-191.

27.   Stenzel, V., Jeske, J., du Mont, W.-W., and Jones, P.G., *Iodine-Iodine Interactions in Dialkyldiiodophosphonium Iodides and Triiodides.* Inorganic Chemistry **1995**, 34(21), 5166-5170.

28.   du Mont, W.-W. and Ruthe, F., *Iodophosphonium salt structures: homonuclear cation– anion interactions leading to supramolecular assemblies.* Coordination Chemistry Reviews **1999**, 189(1), 101-133.

29.   Kloo, L., Rosdahl, J., and Svensson, Per H., *On the Intra- and Intermolecular Bonding in Polyiodides.* European Journal of Inorganic Chemistry **2002**, 2002(5), 1203-1209.

30.   Alcock, N.W., *Secondary Bonding to Nonmetallic Elements.* Advances in Inorganic Chemistry and Radiochemistry **1972**, Volume 15, 1-58.

31.   Metrangolo, P., Neukirch, H., Pilati, T., and Resnati, G., *Halogen Bonding Based Recognition Processes: A World Parallel to Hydrogen Bonding.* Accounts of Chemical Research **2005**, 38(5), 386-395.

32.   Housecroft, C.E. and Sharpe, A.G., *Inorganic Chemistry*. 3th ed: Pearson Prentice Hall, Harlow, England **2008**.

33.   J. Blake, A., Li, W.-S., Lippolis, V., Schroder, M., A. Devillanova, F., O. Gould, R., Parsons, S., and Radek, C., *Template self-assembly of polyiodide networks.* Chemical Society Reviews **1998**, 27(3), 195-206.

34.   Deplano, P., Ferraro, J.R., Mercuri, M.L., and Trogu, E.F., *Structural and Raman spectroscopic studies as complementary tools in elucidating the nature of the bonding in polyiodides and in donor-I₂ adducts.* Coordination Chemistry Reviews **1999**, 188(1), 71-95.

35.   Benesi, H.A. and Hildebrand, J., *A spectrophotometric investigation of the interaction of iodine with aromatic hydrocarbons.* Journal of the American Chemical Society **1949**, 71(8), 2703-2707.

36.   Miertuš, S., Scrocco, E., and Tomasi, J., *Electrostatic interaction of a solute with a continuum. A direct utilizaion of AB initio molecular potentials for the prevision of solvent effects.* Chemical Physics **1981**, 55(1), 117-129.

37.   Xu, X. and Goddard, W.A., *The X3LYP extended density functional for accurate descriptions of nonbond interactions, spin states, and thermochemical properties.* Proceedings of the National Academy of Sciences of the United States of America **2004**, 101(9), 2673-2677.

38.   Bigoli, F., Deplano, P., Ienco, A., Mealli, C., Mercuri, M.L., Pellinghelli, M.A., Pintus, G., Saba, G., and Trogu, E.F., *Structure and Bonding of Diiodine Adducts of the Sulfur-Rich Donors 1,3-Dithiacyclohexane-2-thione (ptc) and 4,5-Ethylenedithio-1,3-dithiole-2-thione (ttb).* Inorganic Chemistry **1999**, 38(21), 4626-4636.

39.   Mizuno, M., Tanaka, J., and Harada, I., *Electronic spectra and structures of polyiodide chain complexes.* The Journal of Physical Chemistry **1981**, 85(13), 1789-1794.

40.   Becke, A.D., *Density-functional thermochemistry. V. Systematic optimization of exchange-correlation functionals.* The Journal of Chemical Physics **1997**, 107(20), 8554-8560.

41.   Reiss, G.J. and van Megen, M., *Synthesis, Structure and Spectroscopy of a New Polyiodide in the α, ω-Diazaniumalkane Iodide/Iodine System.* Zeitschrift für Naturforschung **2012**, 67, 447-451.

42.   Wang, Y., Xue, Y., Wang, X., Cui, Z., and Wang, L., *The stable polyiodides: Experimental and theoretical studies of formation mechanism.* Journal of Molecular Structure **2014**, 1074(0), 231-239.

43.   Uchida, T. and Akamatu, H., *Electrical Conduction in the Violanthrene-Iodine System.* Bulletin of the Chemical Society of Japan **1962**, 35(6), 981-985.

44.   Chiang, C.K., Fincher, C.R., Park, Y.W., Heeger, A.J., Shirakawa, H., Louis, E.J., Gau, S.C., and MacDiarmid, A.G., *Electrical Conductivity in Doped Polyacetylene.* Physical Review Letters **1977**, 39(17), 1098-1101.

45.   Audenaert, M., Gusman, G., Mehbod, M., Deltour, R., Noirhomme, B., and Vander Donckt, E., *Electrical properties of poly(2-vinylpyridine)-iodine films.* Solid State Communications **1979**, 30(12), 791-793.

46.   Kusabayashi, S., Mikawa, H., Kawai, S., Uchida, M., Kiriyama, R., *Semiconducting Properties of Organic Polyiodides.* Bulletin of the Chemical Society of Japan **1964**, 37(6), 811-817.

47.   Forsyth, M., Loye, H.C.Z., Lerner, M., Tipton, A., Degroot, D.C., Kannewurf, C.R., Ratner, M., and Shriver, D.F., *Characterization of Polyiodide-Polymer Complexes by Resonance Raman Spectroscopy.* MRS Online Proceedings Library **1990**, 210.

48.   Windolph, R.R. and Leffler, A.J., *Transition metal-bromine reactions in dimethylformamide.* Inorganic Chemistry **1972**, 11(3), 594-597.

49.   Clark, R.J.H. and Williams, C.S., *The Far-Infrared Spectra of Metal-Halide Complexes of Pyridine and Related Ligands.* Inorganic Chemistry **1965**, 4(3), 350-357.

50.   Earnshaw, A. and Greenwood, N., *Chemistry of the Elements*. 2th ed: Butterworth-Heinemann, Oxford, Vol. 17. **1997**. 789-887.

51.   Westra, A.N., Bourne, S.A., Esterhuysen, C., and Koch, K.R., *Reactions of halogens with Pt(II) complexes of N-alkyl- and N,N-dialkyl-N-benzoylthioureas: oxidative addition and formation of an I_2 inclusion compound.* Dalton Transactions **2005**(12), 2162-2172.

52.   Buse, K.D., Keller, H.J., and Pritzkow, H., *Reaction of molecular iodine with cis-dihalo(2,2'-bipyridyl)platinum(II) and cis-dihalo(1,10-phenanthroline)platinum(II). Oxidative addition and inclusion compounds.* Inorganic Chemistry **1977**, 16(5), 1072-1076.

53.   Gray, L.R., Gulliver, D.J., Levason, W., and Webster, M., *Coordination chemistry of higher oxidation states. 5. Reaction of palladium(II) iodo complexes with molecular iodine and crystal and molecular structure of diiodo(cis-1,2-bis(diphenylphosphino)ethene)palladium(II)-diiodine.* Inorganic Chemistry **1983**, 22(17), 2362-2366.

54.   Tuikka, M., Hirva, P., Rissanen, K., Korppi-Tommola, J., and Haukka, M., *Halogen bonding-a key step in charge recombination of the dye-sensitized solar cell.* Chemical Communications **2011**, 47(15), 4499-4501.

55.   Nazeeruddin, M.K., De Angelis, F., Fantacci, S., Selloni, A., Viscardi, G., Liska, P., Ito, S., Takeru, B., and Grätzel, M., *Combined Experimental and DFT-TDDFT Computational Study of Photoelectrochemical Cell Ruthenium Sensitizers.* Journal of the American Chemical Society **2005**, 127(48), 16835-16847.

56.   Grätzel, M., *Conversion of sunlight to electric power by nanocrystalline dye-sensitized solar cells.* Journal of Photochemistry and Photobiology A: Chemistry **2004**, 164(1–3), 3-14.

57.   Rogachev, A.Y. and Hoffmann, R., *Hypervalent Compounds as Ligands: I3-Anion Adducts with Transition Metal Pentacarbonyls.* Inorganic Chemistry **2013**, 52(12), 7161-7171.

58.   Cossi, M., Rega, N., Scalmani, G., and Barone, V., *Energies, structures, and electronic properties of molecules in solution with the C-PCM solvation model.* Journal of Computational Chemistry **2003**, 24(6), 669-681.

59.   Szabo, A. and Ostlund, N.S., *Modern Quantum Chemistry: Introduction to Advanced Electronic Structure Theory*: MacMillan Publishing Co., New York **1982**. 108-230.

60.   Schrödinger, E., *An Undulatory Theory of the Mechanics of Atoms and Molecules.* Physical Review **1926**, 28(6), 1049-1070.

61.   Hohenberg, P. and Kohn, W., *Inhomogeneous Electron Gas.* Physical Review **1964**, 136(3B), 864-871.

62.   Kohn, W. and Sham, L.J., *Self-Consistent Equations Including Exchange and Correlation Effects.* Physical Review **1965**, 140(4A), A1133-A1138.

63.   Koch, W. and Holthausen, M.C., *A Chemist's Guide to Density Functional Theory*. 2th ed: Wiley-VCH Verlag GmbH, Weinheim **2001** 92-116.

64.   Jensen, F., *Introduction to Computational Chemistry*. 2th ed: John Wiley & Sons Ltd, West Sussex, England **2007**. 192-231.

65.   Smith, P.E. and Pettitt, B.M., *Modeling Solvent in Biomolecular Systems.* The Journal of Physical Chemistry **1994**, 98(39), 9700-9711.

66.   Cramer, C.J. and Truhlar, D.G., *Implicit Solvation Models: Equilibria, Structure, Spectra, and Dynamics.* Chemical Reviews **1999**, 99(8), 2161-2200.

67.   Tomasi, J., Mennucci, B., and Cammi, R., *Quantum Mechanical Continuum Solvation Models.* Chemical Reviews **2005**, 105(8), 2999-3094.

68.   Löwdin, P.-O., *Quantum Theory of Many-Particle Systems. I. Physical Interpretations by Means of Density Matrices, Natural Spin-Orbitals, and Convergence Problems in the Method of Configurational Interaction.* Physical Review **1955**, 97(6), 1474-1489.

69.   Weinhold, F., *Nature of H-bonding in clusters, liquids, and enzymes: an ab initio, natural bond orbital perspective.* Journal of Molecular Structure: THEOCHEM **1997**, 398–399, 181-197.

70.   Bader, R.F.W., *Atoms in molecules.* Accounts of Chemical Research **1985**, 18(1), 9-15.

71.   Bader, R.F.W., *Atoms in Molecules: A Quantum Theory*: Oxford University Press, Oxford, U.K **1990**.

72.   Matta, C.F. and Boyd, R.J., *An Introduction to the Quantum Theory of Atoms in Molecules*, in *The Quantum Theory of Atoms in Molecules*, C.F. Matta and R.J. Boyd, Editors. **2007**, WILEY-VCH Verlag GmbH & Co.: Weinheim. p. 1-34.

73.   Blinder, S.M., *Atoms and Photons: Origins of the Quantum Theory*, in *Introduction to Quantum Mechanics*, S.M. Blinder, Editor **2004**, Academic Press: San Diego. p. 1-15.

Chapter 3

Methodology

3.1 Introduction

In this chapter an overview of the experimental and computational methods used in this study will be given. Before any further investigation could be performed, it was necessary to carry out a comprehensive analysis of previously published crystal structures of metal-iodide complexes using the Cambridge Structural Database (CSD) [1] in order to identify all the different metal-iodide complexes that contain the M–I and I–M–I moieties. Among all identified metal-iodide complexes containing the I–M–I moiety, all structures that have I $\cdots$ I interactions (i.e., in a dimer form) were selected. This was done to establish all metal complexes that are most likely to form I $\cdots$ I interactions in the dimer form (i.e., I–M–I $\cdots$ I–M–I). The obtained dimer structures were carefully analyzed to determine the most common I–M–I conformations found in the previously documented metal-iodide complexes in the CSD.

Gaussian 09 is a software package used to predict the energies, molecular structure and molecular properties of different metal-iodide complexes in a wide variety of chemical environments. All calculations were performed using the Gaussian 09 rev. B.01 and D.01 packages, which were the latest available versions of the Gaussian series of programs [2]. The character of the I $\cdots$ I intermolecular interactions in all identified metal-iodide complexes was investigated by means of DFT calculations. The other ligands in the complexes and/or cations as well as their effects on the I $\cdots$ I interactions were simplified in order to reduce the amount of computational power and time required.

The nature and structural properties of the I–M–I $\cdots$ I–M–I interactions were analyzed utilizing the NBO and AIM analyses. NBO is used to study the electronic structure by calculating the distribution of electron density in atoms and bonds between atoms, while AIM analysis is used to determine the presence of bonding, by identifying BCPs. The effect of substituents was

investigated by comparing the electron density (ρ) values at the BCPs in the substituted compounds.

3.2 Cambridge Structural Database analysis

The Cambridge Structural Database (CSD) is one of the major sources for published literature on crystal structures of compounds and complexes, including those that contain organic and organometallic compounds [1]. The database was established in 1965, and now contains the results of hundreds of thousands of X-ray and neutron diffraction analyses of crystals and their accurate 3D structures. Each crystal structure undergoes extensive examination and validation process by professional chemists and crystallographers, which makes it an essential and reliable resource to scientists around the world. All crystal structures in the CSD can be identified by a six letter refcode, which is a unique identifier assigned to every new entry in the CSD.

In addition to raw 3D structural data, the CSD also contains other bibliographic information (such as chemical and physical properties) about thousands of crystal and complex structures. Today, various software programs that are associated with the CSD are available and can be used to access the database. These include ConQuest, Mercury, Vista, PreQuest, Isostar and Mogul. The software and interfaces used to access the CSD are ConQuest, which can be used to perform searches for all previously published crystal structures [3], and Mercury, which is usually used to do the visualization and analysis of all crystal structures [3, 4].

3.2.1 CSD searches of metal-iodide complexes

A complete search of previously published crystal structures containing metal-iodide complexes was carried out. All CSD searches were performed on CSD V3.34 (2013 release with Nov 2012 update) and V5.35 (2014 release with Nov 2013 update). The searches were carried out utilizing the ConQuest V1.15 and V1.16 search program. Before performing the search, the I⋯I interaction distance was set at the sum of the van der Waals radii of iodine (4.3 Å) plus 0.3 Å to ensure that all interactions were studied (i.e., even weak interactions were identified). This means that metal-iodide complexes were identified by searching for fragments containing the I–

M–I moiety with an intermolecular I⋯I contact less than 4.6 Å. This resulted in a number of complexes for each metal, which contain the I⋯I interactions. Excel sheets showing all the identified complexes for each metal are given in the digital supplementary information (see page 126 for details).

3.2.2 Structure visualization of metal-iodide complexes

All structural data obtained from the CSD searches were analyzed with the Mercury V3.3 (2013) and V3.4 (2014) suite. The structural coordinates of compounds containing I⋯I interactions were converted to Cartesian coordinates and saved in xyz format using the Mercury suite. All output files were visualized and rendered with the Chemcraft visualization suite [5]. This was carried out to obtain the internal coordinates such as specific bond distances, angles, torsion angles and I⋯I distances. These parameters were converted to z-matrix file using the Chemcraft program, which was then used for structure optimization using Gaussian 09.

3.3 Building the dimer

One of the aims of this study was to investigate the interaction between iodine atoms in dimers of transition metal-iodide complexes (i.e., exhibiting the I–M–I⋯I–M–I moiety). Therefore, based on the CSD results, some metal complexes which are most likely to have this form of interaction were identified. The ConQuest program was set to search for I–M–I fragments, which have a close contact that is less than 4.6 Å. A dimer form was then built for each complex utilizing the Chemcraft visualization program and saved in z-matrix format. Schemes 3.1 and 3.2 show schematic representations of the parameters that were measured, including bond distances, angles, torsion angles and the I⋯I interaction distance. The dimer was then used for the optimization study using the Gaussian 09 package as given in Section 3.4.1.
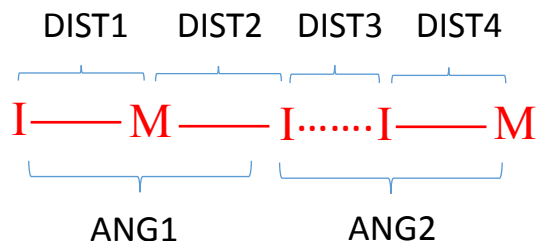
Scheme 3.1: A schematic representation of a dimer containing the I–M–I⋯I–M moieties, DIST is a distance and ANG is an angle.
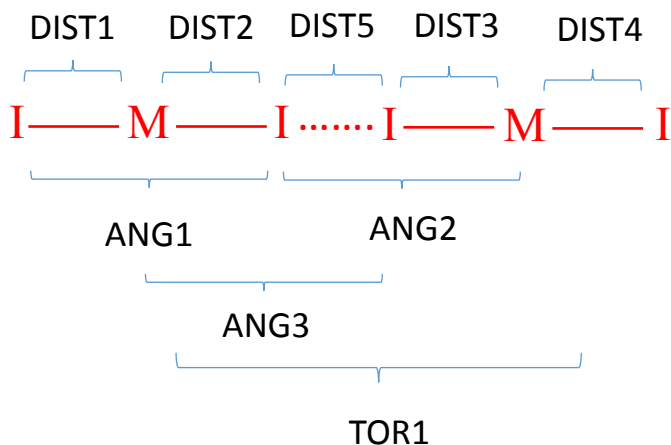
Scheme 3.2: A schematic representation of a dimer containing the I–M–I⋯I–M–I moieties, DIST is a distance, ANG is an angle and TOR is a torsion angle.

3.4 Computational Methods

To study the molecular structure and topological properties of all identified metal-iodide complexes, different computational methods were used. Calculations were carried out at the DFT level of theory in the gas phase and various solvents. Geometry optimizations of these metal- iodide complexes were performed using simplified ligands when necessary. This allowed us to predict the interaction energies, molecular structures and molecular properties of all studied metal-iodide complexes in a wide variety of chemical environments (gas phase and solvent model). The electronic structures of all the identified metal-iodide complexes were studied using NBO analysis (V3.1 program) [6, 7]. Furthermore, the nature and topological properties of all

identified metal-iodide complexes were examined by AIM analysis (V.14.06.12) [8]. All these computations were performed with the aid of the Gaussian suite of programs (Gaussian 09) [2].

3.4.1 Geometry optimization

The structures of the resultant complexes containing simplified ligands were investigated with the aid of the software package Gaussian 09 using different protocols (i.e., DFT functionals, basis sets and solvent model) [9]. Gaussian 09 is a program that provides advanced electronic structure modeling. Geometry optimizations were performed for all complexes (single and dimer) using DFT in combination with different basis sets. The basis set superposition error (BSSE) correction was applied in Gaussian by implementing the counterpoise = 2 keyword [10, 12]. It should also be mentioned that frequency calculations were performed for all structure optimization calculations in order to confirm that the structures were at minimum energy conformations. All calculations were performed in the gas phase and in an implicit polarizable continuum solvent model [13] in a variety of solvents, i.e., water ($\mathcal{E}$=78.3553), ethanol ($\mathcal{E}$=24.852), and chloroform ($\mathcal{E}$ = 4.7113).

Various DFT methods, namely PBEPBE [13] and B3LYP [15, 16] were used primarily with aug-cc-pVTZ-pp [17] as the basis set for the transition metal, while 6-31G(d) was used as the basis set for the rest of the atoms in the complex. These methods were chosen as they were found to give sensible results for the interactions between triiodide ions [9]. LANL2DZ was also used for difficult cases. Grimme's D3 correction [10] was added to all methods to correctly model dispersion interactions, as this was shown to be important for weak $I \cdots I$ interactions between triiodide units [9]. Table 3.1 summarizes all the DFT methods and the basis sets that were used for each metal complexs in the single form (I–M–I) and the dimer form (I–M–I $\cdots$I–M–I). For the gas phase calculations, the minimum interaction energy between iodine atoms in the $I \cdots I$ moiety was obtained by using the keyword counterpoise=2 for all different metal-iodide complexes. Similarly, the keyword SCRF = (solvent name) was used to obtain the minimum energy of interaction in the implicit solvent model at the PBEPBE/aug-cc-pVTZ-pp level of theory. It should be mentioned also that a single point energy calculations were performed for both the

42

single form for the complex (I–M–I) as well as its dimer form (I–M–I···I–M–I). The I···I interaction energies were calculated by using the following equation:

E_{INT} = Energy (dimer of complex (I–M–I···I–M–I)) – 2 × Energy (single complex (I–M–I))   3.1

3.4.2 Natural Bond Orbital analysis

Natural Bond Orbital (NBO) analysis was used to determine the nature and properties of the intermolecular interactions in dimers of complexes (I–M–I···I–M–I). NBO analysis was performed by the NBO 3.1 program to calculate the distribution of electron density iodine atoms in the I···I moiety by analyzing two different types of orbitals. These are: the lone pair (LP) which is regarded as the donor orbital and Rydberg orbitals (RY*) that is considered as the acceptor orbital. The keyword Pop = nboRead was added to the input file and the calculations were requested by including the line: $nbo bndidx $end at the end of the file. The estimation of the stabilization energy for these orbitals is given by:

$$E(2) = \Delta E_{ij} = q_i \frac{F(i,j)^2}{\varepsilon_j - \varepsilon_i}$$ 3.2

where q_i is the donor orbital occupancy, ε_i and ε_j are the orbital energy and F(i, j) is the off-diagonal NBO Fock matrix element.

3.4.3 Atoms in Molecules analysis

The topological properties of the electron density have been characterized using the Atoms in Molecules (AIM) methodology analysis. AIM calculations were performed utilizing the AIMALL (v.14.06.12) software package [8]. The BPEBPE/aug-cc-pVTZ–pp basis set was used to optimize the structures utilizing Gaussian 09 rev.B.01 package [2]. The wave function files (*.wfx files) used for AIM analysis were generated from fully optimized structure with option Output = WFX of the Gaussian program. The calculated values of the electron density $\rho_b(r)$, Laplacian of the electron density $L(\rho_b(r))$ and the total energy density $H_b(r)$ of I···I interactions at BCP was performed in the gas phase and in an implicit solvent model, including the figures of two-dimensional contour plots for these parameters.

Table 3.1: A summary of different DFT level of theory and basis sets used for geometry optimizations.

Metal	CSD Refcode	Formula	Shape	Basis set	Methods used for (I–M–I)	Methods used for (I–M–I···I–M–I)
Pt	NUKCAY	$(2(0.5(C_{10}H_2I_2N_2Pt).$ $0.5(C_{10}H_{22}I_2N_2Pt))$	bent	6-31G(d) (aug-cc-pVTZ-pp)	PBEPBE	PBEPBE
Cu	DEHKACO2	$(2(C_{24}H_{20}P^+). Cu_2I_4{}^{2-})$	>···<	(aug-cc-pVTZ-pp)	PBEPBE	PBEPBE
Ga	OJAVIE	$(C_8H_{22}Ga_2I_4N_2)$	chair	6-31G(d) (aug-cc-pVTZ-pp)	PBEPBE	B3LYP
Ag	PAWXOB	$((Ag_2I_5{}^{3-})_n.$ $2n(C_{11}H_{20}N_2{}^{2+}). n(I^-).$ $2n(H_2O))$	linear	(aug-cc-pVTZ-pp) LANL2DZ	PBEPBE B3LYP/LANL2DZ	–
Hg	JAHCOK01	$(C_{36}H_{30}Hg_2I_4P_2)$	bent	LANL2DZ 6-31G(d) (aug-cc-pVTZ-pp)	PBEPBE B3LYP/LANL2DZ	B3LYP/LANL2DZ
Bi	ZUCKIR	$(C_{40}H_{37}BiI_2N_3O_2P_2{}^+.$ $C_{10}H_{10}BiI_4N_2{}^-. C_5H_5N)$	bent	6-31G(d) (aug-cc-pVTZ-pp) LANL2DZ	PBEPBE B3LYP/LANL2DZ	B3LYP/LANL2DZ
Pd	HOVMAH	$(C_{20}H_{22}I_4N_2Pd_2S_2.$ $C_2H_4Cl_2)$	linear	(aug-cc-pVTZ-pp) LANL2DZ	PBEPBE B3LYP/LANL2DZ	–
Pd	AGAHOF	$(2(C_{12}H_{28}N^+), Pd_2I_6{}^{2-})$	chair	(aug-cc-pVTZ-pp) LANL2DZ	PBEPBE B3LYP B3LYP/LANL2DZ	B3LYP/LANL2DZ

3.5 References

1. Allen, F., *The Cambridge Structural Database: a quarter of a million crystal structures and rising.* Acta Crystallographica Section B **2002**, 58, 380-388.

2. Frisch, M.J., Trucks, G.W., Schlegel, H.B., Scuseria, G.E., Robb, M.A., Cheeseman, J.R., Scalmani, G., Barone, V., Mennucci, B., Petersson, G.A., Nakatsuji, H., Caricato, M., Li, X., Hratchian, H.P., Izmaylov, A.F., Bloino, J., Zheng, G., Sonnenberg, J.L., Hada, M., Ehara, M., Toyota, K., Fukuda, R., Hasegawa, J., Ishida, M., Nakajima, T., Honda, Y., Kitao, O., Nakai, H., Vreven, T., Montgomery Jr., J.A., Peralta, J.E., Ogliaro, F., Bearpark, M.J., Heyd, J., Brothers, E.N., Kudin, K.N., Staroverov, V.N., Kobayashi, R., Normand, J., Raghavachari, K., Rendell, A.P., Burant, J.C., Iyengar, S.S., Tomasi, J., Cossi, M., Rega, N., Millam, N.J., Klene, M., Knox, J.E., Cross, J.B., Bakken, V., Adamo, C., Jaramillo, J., Gomperts, R., Stratmann, R.E., Yazyev, O., Austin, A.J., Cammi, R., Pomelli, C., Ochterski, J.W., Martin, R.L., Morokuma, K., Zakrzewski, V.G., Voth, G.A., Salvador, P., Dannenberg, J.J., Dapprich, S., Daniels, A.D., Farkas, Ö., Foresman, J.B., Ortiz, J.V., Cioslowski, J., and Fox, D.J., *Gaussian 09, Revision B.01*, Gaussian, Inc., **2009**: Wallingford, CT, USA.

3. Bruno, I.J., Cole, J.C., Edgington, P.R., Kessler, M., Macrae, C.F., McCabe, P., Pearson, J., and Taylor, R., *New software for searching the Cambridge Structural Database and visualizing crystal structures.* Acta Crystallographica Section B **2002**, 58(3 Part 1), 389-397.

4. Macrae, C.F., Edgington, P.R., McCabe, P., Pidcock, E., Shields, G.P., Taylor, R., Towler, M., and van de Streek, J., *Mercury: visualization and analysis of crystal structures.* Journal of Applied Crystallography **2006**, 39(3), 453-457.

5. http://www.chemcraftprog.com, accessed on 20 March 2014.

6. *NBO version 3.1, E. D. Glendening, A. E. Reed, J. E. Carpenter, F. Weinhold.* **1998**.

7. Reed, A.E., Curtiss, L.A., and Weinhold, F., *Intermolecular interactions from a natural bond orbital, donor-acceptor viewpoint.* Chemical Reviews **1988**, 88, 899-926**.**

8. AIMAll (Version 15.09.12), Todd A. Keith, TK Gristmill Software, Overland Park KS, USA, 2015 (aim.tkgristmill.com).

9.   Groenewald, F., Esterhuysen, C., and Dillen, J., *Extensive theoretical investigation: influence of the electrostatic environment on the $I_3^- \cdots I_3^-$ anion–anion interaction.* Theoretical Chemistry Accounts **2012**, 131(10), 1-12.

10.   Grimme, S., Antony, J., Ehrlich, S., Krieg, H., *A consistent and accurate ab intio dispersion correction (DFT-D) for the 94 elements H-Pt.* Journal of Chemical Physics **2010**, 132, 154104.

11.   Boys, S.F. and Bernardi, F., *The calculation of small molecular interactions by the differences of separate total energies. Some procedures with reduced errors.* Molecular Physics **1970**, 19(4), 553-566.

12.   Simon, S., Duran, M., and Dannenberg, J., *How does basis set superposition error change the potential surfaces for hydrogen‑bonded dimers?* The Journal of Chemical Physics **1996**, 105(24), 11024-11031.

13.   Tomasi, J., Mennucci, B., and Cammi, R., *Quantum Mechanical Continuum Solvation Models.* Chemical Reviews **2005**, 105(8), 2999-3094.

14.   Perdew, J.P., Burke, K., and Ernzerhof, M., *Generalized Gradient Approximation Made Simple.* Physical Review Letters **1996**, 77(18), 3865-3868.

15.   Xu, X. and Goddard, W.A., *The X3LYP extended density functional for accurate descriptions of nonbond interactions, spin states, and thermochemical properties.* Proceedings of the National Academy of Sciences of the United States of America **2004**, 101(9), 2673-2677.

16.   Becke, A.D., *Density-functional thermochemistry. V. Systematic optimization of exchange-correlation functionals.* The Journal of Chemical Physics **1997**, 107(20), 8554-8560.

17.   Dunning, T.H., *Gaussian basis sets for use in correlated molecular calculations. I. The atoms boron through neon and hydrogen.* The Journal of Chemical Physics **1989**, 90(2), 1007-1023.

46

Chapter 4

Analysis of crystal structures

4.1 Introduction

In this chapter an extensive analysis of previously published experimental crystal structures of metal-iodide complexes taken from the Cambridge Structural Database (CSD) is described. The CSD search was used to establish which complexes contain the I–M–I moiety in the solid state, where M is a transition metal and I is an iodine atom. Complexes containing other p-block elements (main group metals) were also studied. All metal-iodide complexes containing the I–M–I moiety that are most likely to have I···I interactions forming dimers of I–M–I···I–M–I were identified. Furthermore, the crystal structures of these identified dimers were visualized and analyzed to determine the most common orientations (i.e., conformations) of the two I–M–I moieties forming I···I interactions relative to each other. Moreover, the most common relative conformations in which these metal-iodide complexes are most likely to have shorter interaction distances (which indicative of stronger I···I interactions) were also determined.

4.2 Cambridge Structural Database analysis

In the current study, an analysis of the Cambridge Structural Database (CSD) [1] was important to fully examine all previously published experimental crystal structures. A comprehensive analysis of different complexes containing metal-iodide compounds was therefore carried out. This allowed us to establish which complexes containing an I–M–I moiety are able to form I$\cdots$I interactions in the solid state. It was shown that the strength of the interaction in halogens depend greatly on the relative sizes of the attractive atoms where the halogen bond strength is in the following order: Cl > Br > I [2]. The structural data analyses were obtained from CSD V5.33 and V5.34 utilizing the ConQuest V1.16 search program [3] and Mercury V3.3 [4]. In all searches, an intermolecular interaction contact, which is less than the sum van der Waals distance of iodine (4.3 Å) plus 0.3Å between the terminal I atoms on the I–M–I$\cdots$I–M–I, was used to ensure that even weak interactions were identified. In other words, all metal-iodide complexes were identified by searching for fragments containing the I–M–I moiety with an intermolecular contact between iodide atoms of less than 4.6 Å. Schematic representations of the searches are shown in Schemes 3.1 and 3.2 (see Section 3.3). It should be mentioned that other types of multiple I$\cdots$I interactions were also present. However, our interest was only on the single I$\cdots$I interactions that resulted in the formation of dimers.

4.2.1 ConQuest search

Initially, all complexes containing an I–M–I moiety, irrespective of whether they formed a close contact between the iodine atoms or not, were identified. The ConQuest program was set to search for I–M–I fragments, where iodine atoms are covalently bounded via a single bond to the central metal atom. The next step was to find which of these complexes contain an I–M–I$\cdots$I–M and/or I–M–I$\cdots$I–M–I unit, where the two segments contact via an iodine to iodine interaction. All the ConQuest search results are tabulated in Tables 4.1 and 4.2, which show all metals that are most likely to form complexes containing the I–M–I moiety and which of these then form I–M–I$\cdots$I–M–I dimers, respectively. The percentage (%) of metal-iodide complexes exhibiting I$\cdots$I close contacts out of the total number of complexes is indicated in parenthesis in Table 4.2.

Table 4.1: ConQuest search results for transition metal-iodide complexes that contain the I–M–I moiety.

M	Sc	Ti	V	Cr	Mn	Fe	Co	Ni	Cu	Zn	Ga	Ge	As	Se
No. of complexes	3	16	10	13	45	66	102	82	868	266	127	32	27	6
M	Y	Zr	Nb	Mo	Tc	Ru	Rh	Pd	Ag	Cd	In	Sn	Sb	Te
No. of complexes	8	39	8	122	1	60	115	357	189	320	80	144	91	168
M	La	Hf	Ta	W	Re	Os	Ir	Pt	Au	Hg	Tl	Pb	Bi	Po
No. of complexes	34	9	2	112	55	30	90	335	73	467	22	303	197	-

Table 4.2: ConQuest search results for transition metal-iodide complexes where a dimer of I–M–I⋯I–M–I forms via an I⋯I interaction. Percentage of I–M–I⋯I–M–I dimers is indicated in parenthesis.

M	Sc	Ti	V	Cr	Mn	Fe	Co	Ni	Cu	Zn	Ga	Ge	As	Se
No. of complexes	1	2	-	-	1	1	6	-	50	5	31	3	13	1
(%)	(33)	(13)	(0)	(0)	(2)	(2)	(6)	(0)	(6)	(2)	(24)	(9)	(48)	(17)
M	Y	Zr	Nb	Mo	Tc	Ru	Rh	Pd	Ag	Cd	In	Sn	Sb	Te
No. of complexes	-	3	3	11	-	1	1	9	8	19	11	13	27	19
(%)	(0)	(8)	(38)	(9)	(0)	(2)	(1)	(3)	(4)	(6)	(14)	(9)	(30)	(11)
M	La	Hf	Ta	W	Re	Os	Ir	Pt	Au	Hg	Tl	Pb	Bi	Po
No. of complexes	7	1	-	6	5	3	5	22	6	99	1	23	79	-
(%)	(21)	(11)	(0)	(5)	(9)	(10)	(6)	(7)	(8)	(21)	(5)	(8)	(40)	(0)

From Table 4.1, one can see that most transition metals have a large number of complexes that contain the I–M–I moiety (i.e., more than 100 complexes). However, as shown in Table 4.2 the number of metal complexes that contain an I⋯I interaction is significantly lower. For instance, there are 60, 66 and 115 I–Ru–I, I–Fe–I and I–Rh–I complexes respectively, however only one of each exhibits an I⋯I interaction, while for complexes of V, Cr, Ni, Y, Tc, Ta and Po there are no I⋯I interactions present (i.e., no dimer formation). On the other hand, transition metals such as Sc, As, Nb, Sb and Bi have a relatively high percentage of

49

complexes that form $I \cdots I$ contacts. Interestingly, the metal-iodide complexes that most commonly exhibit $I \cdots I$ interactions are those of the main group elements As, Sb and Bi, with 48, 30 and 40% of all complexes exhibiting these close contacts.

4.2.2 Structure analysis of dimers

All crystal structures containing the dimeric fragments (i.e., with a I–M–I···I–M–I close contact) which were identified using ConQuest (given in Table 4.2) were visually analyzed with the aid of the program Mercury V3.3. This was done in order to establish which complexes exhibit $I \cdots I$ interactions which are less than the sum of van der Waals radii plus 0.3 Å between the terminal I atoms on the two I–M–I fragments. This also gave us an indication of the strength of the $I \cdots I$ interaction in all analyzed models (assuming that the bond strength-length relationship where shorter distances indicate stronger interactions holds for such interactions), in order to identify all metals that provide an environment that results in a strong $I \cdots I$ interaction. This was done by rotating the structure to look at each identified close contact to determine whether it was a true intermolecular or intramolecular interaction rather than a coincidental contact. This decision was based on whether the two I–M–I fragments were pointing towards each other, i.e. chemical intuition. Table 4.3 gives a summary of the results obtained, which shows the number of metal complexes containing inter- and/or intramolecular I–M–I···I–M–I interactions. The percentage (%) of metal-iodide complexes exhibiting I–M–I···I–M–I interactions out of the total number of complexes is indicated in parenthesis in Table 4.3.

Table 4.3 shows that some metals such as Cr, V, Sc, Ni, Mn, Y, Tc, Po and Ta do not provide a good environment to exhibit the desired interaction between I–M–I moieties. This is in good agreement with other reports in the literature [5, 6]. Hitchcock *et al*. [6] investigated the synthesis of various vanadium(II) iodides by reacting $VCl_3(MeCN)_3$ with $SiMe_3I$ in acetonitrile under reflux. The reaction resulted in the formation of a new compound containing the vanadium(II) cation (i.e., $(V(MeCN)_6)^{2+}$) and a counterion of I_4^{2-}. The authors observed that there was no $I \cdots I$ interaction in the obtained complex, which was attributed to the polyiodide conformation not being symmetrical. Similarity, in the structure of the polyiodide salts containing Ni, namely $[Ni([9]aneS_3)_2]I_6$ and $[Ni([9]aneS_3)_2]I_{10}$ ([9]aneS$_3$ = 1,4,7-trithiacyclononane, [12]aneS$_4$ = 1,4,7,10 tetrathiacyclo-dodecane and [14]aneS4 =

1,4,8,11-tetrathiacyclotetradecane) the polyiodide anions are linked by $S \cdots I$ interactions, forming well-separated sheets of cations and anions, rather than $I \cdots I$ interactions [5].

Table 4.3: Analysis of metal-iodide complexes containing inter- and intramolecular I–M–I···I–M–I interactions. Percentage of I–M–I···I–M–I dimers is indicated in parenthesis.

M	Sc	Ti	V	Cr	Mn	Fe	Co	Ni	Cu	Zn	Ga	Ge	As	Se
No. of complexes	-	4	-	-	-	1	11	-	36	7	53	6	33	1
(%)	(0)	(25)	(0)	(0)	(0)	(2)	(11)	(0)	(4)	(3)	(42)	(19)	-	(17)
M	Y	Zr	Nb	Mo	Tc	Ru	Rh	Pd	Ag	Cd	In	Sn	Sb	Te
No. of complexes	-	6	3	18	-	2	4	10	9	29	21	23	59	25
(%)	(0)	(15)	(37)	(15)	(0)	(3)	(3)	(3)	(5)	(9)	(26)	(16)	(65)	(15)
M	La	Hf	Ta	W	Re	Os	Ir	Pt	Au	Hg	Tl	Pb	Bi	Po
No. of complexes	7	1	-	6	5	3	5	36	15	99	1	23	79	-
(%)	(21)	(11)	(0)	(5)	(9)	(10)	(7)	(11)	(21)	(21)	(5)	(8)	(40)	(0)

On the other hand, our results show that metals such as Ti, Ga, Nb, Sb, Au, Hg, In and Bi have large numbers of complexes which exhibit $I \cdots I$ interactions. There are a wide variety of complexes that exhibit these types of interaction, for instance Blake *et al*. [5] investigated the structure of two polyiodides containing Co and Pd complexes. They observed that in the crystal structures of $[Co([9]aneS_3)_2]I_{11}$, $[Pd([12]aneS_4)]I_6$ and $[Pd([14]aneS_4)]I_{10} \cdot MeCN$ $I \cdots I$ interactions resulted in extended donor–acceptor arrays, contributing to the self-assembly of the compound. In the case of the Co complex, the authors showed that the positive charge on the cation $[Co([9]aneS_3)_2]^{3+}$ is balanced by three anions of I_3^-. These anions together with a neutral I_2 molecule formed an extended structure of I_{11}^{3-} that contain chains of alternating I_{11}^{3-} rings and complex cations. The structure contained $I \cdots I$ interactions which are less than 4.0 Å. In the complexes containing Pd, the extended structures contained relatively longer $I \cdots I$ contacts of 4.04, 4.11 and 4.17 Å, which resulted in the assembly of the polyiodide anions into 3-D network.

In another study, Westra *et al.* [7] investigated the reaction of different halogens including iodine (I_2) with metal complexes of N-alkyl- and N,N-dialkyl-N-benzoylthioureas. The authors showed that the oxidative addition reaction of I_2 molecules to Pt(II) complexes occurs under mild conditions, resulting in Pt(IV) complexes of these ligands. However, the authors observed that the addition of I_2 to Pt (II) complexes could result in the formation of another I_2 inclusion compound, which contain infinite $I-Pt(II)-I\cdots I-Pt(II)-I$ chains. Short intermolecular $I\cdots I$ distances of 3.45 Å between I_2 and coordinated iodide ions were observed. Similar results have been observed by other authors for Pt(IV) [8] and Pd(II) [9].

In 2013, Titi *et al*. [10] also observed the presence of intermolecular $I\cdots I$ interactions in Sn (IV) complexes of tetrakis(4-iodophenyl)porphyrin. The authors investigated the synthesis and crystallization of two complexes, namely bis(pyridine-3-carboxylato)-[tetrakis(4-iodophenyl)porphyrinato]Sn(IV) and bis(pyrimidine-5-carboxylato)[tetrakis(4 iodophenyl)porphyrinato]Sn(IV). They showed that the existence of $I\cdots I$ interactions in these complexes resulted in the supramolecular assembly of the porphyrin ligand into iodine-bonded layers. Each molecule interacts with other four molecules within the same layer via eight $I\cdots I$ interactions at 3.8 and 4.0 Å.

Allan *et al*. [11] also observed similar $I\cdots I$ interactions, occurring at relatively high pressures in diiodo complexes containing Pd and Pt. The authors studied the pressure-induced crystallization of various thioether macrocyclic dihalide complexes of Pd(II) and Pt(II). They showed that the formation of short $I\cdots I$ interactions in $[PdI_2([9]aneS3)]$ and $[PtI_2([9]aneS3)]$ ([9]aneS3 = 1,4,7-trithiacyclo-nonane) at 19 kbar had a significant effect on the energetics of these complexes, which resulted in a reduction in the interaction distance between iodine atoms. Similar $Br\cdots Br$ interactions were observed in $[PdBr_2([9]aneS3)]$ and $[PtBr_2([9]aneS3)]$, which occurred at higher pressures of 58 kbar.

Svensson and Kloo [12] investigated the synthesis of a binary metal-iodide···iodine compound utilizing a reaction between $HgI_2(C_6N_4H_{12})$ and HI in ethanol. Their results confirmed the presence of an intermolecular $I\cdots I$ interaction between I_2 molecules and the metal iodide ions. The authors showed that the resultant complex (i.e., $[C_6N_4H_{13}]_2(Hg_2I_6)_{1/2}(HgI_3).^1/_2I_2)$ has a structure that contains $C_6N_4H_{13}^+$ cations and distinct HgI_3^- ions as well as $Hg_2I_6^{2-}$ chains, which are linked by I_2 molecules $[\cdots Hg_2I_6^{2-}\cdots I_2\cdots Hg_2I_6^{2-}$

···]. The I_2 molecules coordinated with other bridging iodines in the $Hg_2I_6^{2-}$ dimers, which resulted in the formation of infinite chains in the crystallographic *b* direction. The intramolecular I–I distance was found to be at 2.74 Å, which is longer than the I–I distance observed for pure iodine in the solid state (2.72 Å) and in the gas phase (2.67 Å) [13,14]. This indicates that there was a significant I···I interaction between I_2 molecules and the $Hg_2I_6^{2-}$ ions, which played the role of I⁻ donor in pure polyiodides. The intermolecular I···I distances of iodine in the chain were found to be 3.44 Å, which is in the range observed in polyiodide compounds [15].

4.3 Determination of the nature and physical properties of I···I interactions

It is known that halogen bonding such as the I···I interaction occurs as a donor-acceptor interaction, which can be influenced by its surrounding environment [16]. In our study, the structure, type and physical properties of I···I interactions in dimers of different metal-iodide complexes were studied. This was done in order to determine the effect of varying the transition metal on the I···I interaction. All crystal structures containing the I···I interaction were investigated with the aid of Mercury V3.3 by visually inspecting each interaction and classifying the shape of the interaction. Results showed that there are two different types of I···I interactions found among the studied complexes, namely intermolecular and intramolecular interactions.

However, our focus was on the intermolecular interactions, where two I–M–I moieties interact via an I···I contact. These intermolecular interactions exist in various shapes (i.e., conformations), which include boat, linear, chair, zigzag chain, >···<–shaped, Z-shaped, \···<>–shaped, <>···<>–shaped, <>/<>–shaped, and bent. Schemes 4.1 and 4.2 show schematic representations of all the I···I interaction geometry that have been observed and identified in our study. These interactions exist in different types including single, double, bifurcated and even multiple interactions as shown in Scheme 4.3.
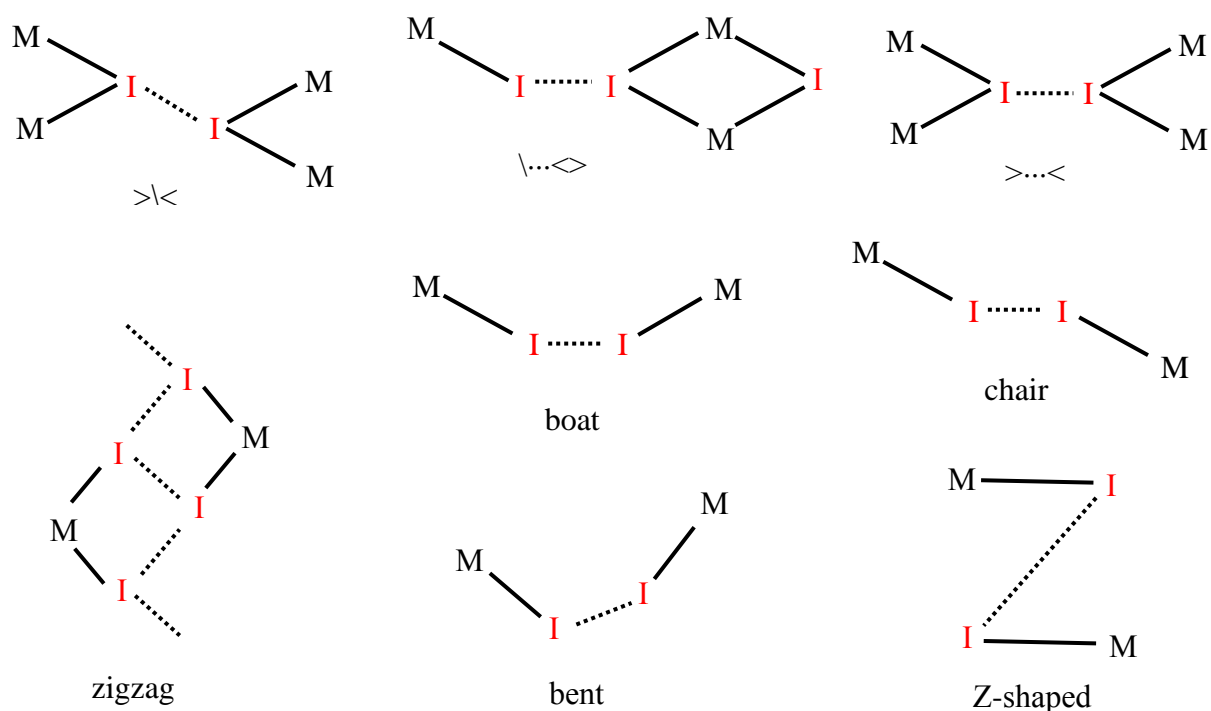
Scheme 4.1: Interaction shapes found most commonly in dimers of transition metal-iodide complexes, where M is the transition metal and I is an iodine atom (the interaction between I atoms is represented by a dotted line).
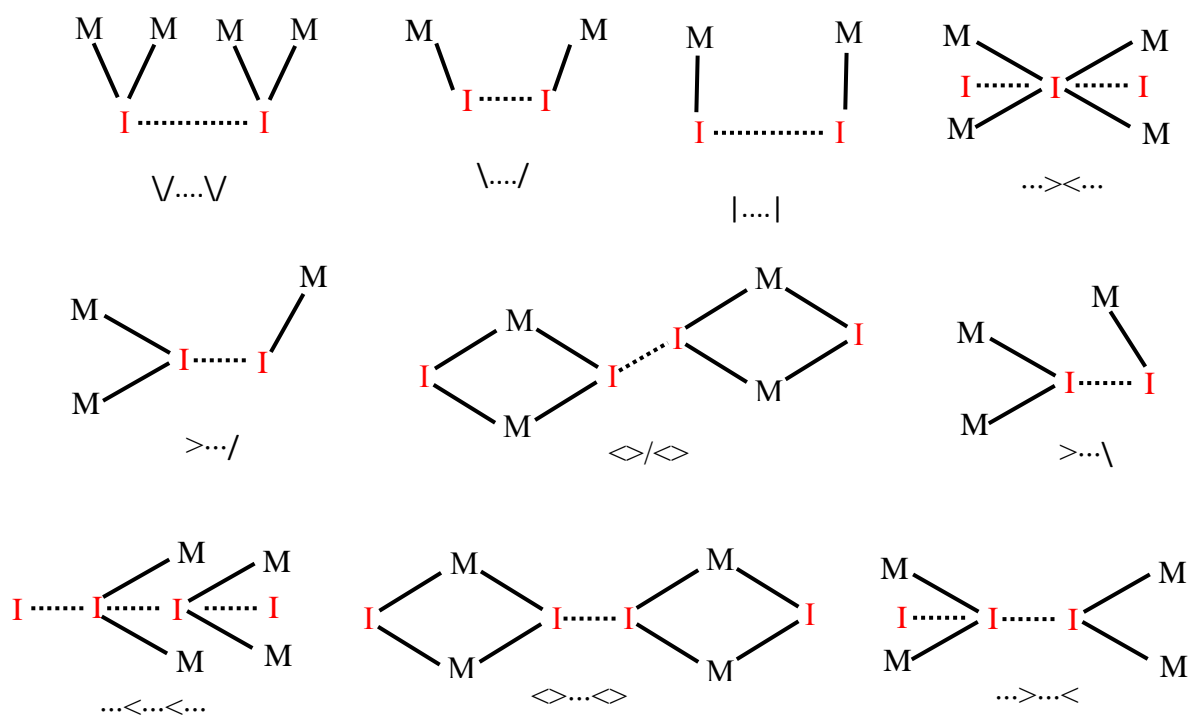
Scheme 4.2: Interaction shapes found less commonly in dimers of transition metal-iodide complexes, where M is the transition metal and I is an iodine atom (the interaction between I atoms is represented by a dotted line).

single

double

bifurcated

multiple
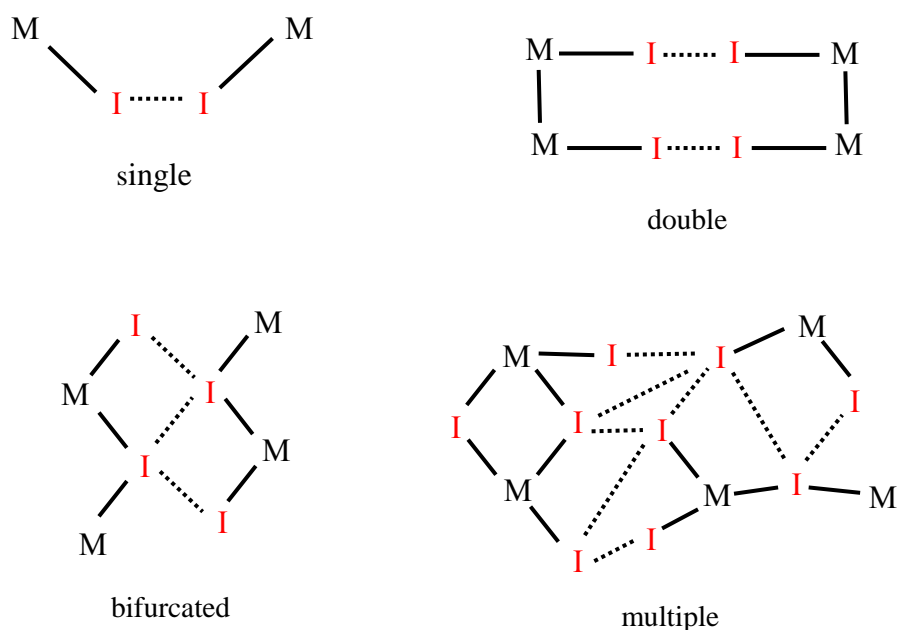
Scheme 4.3: Various interaction types found in dimers of transition metal-iodide complexes, where M is the transition metal and I is an iodine atom (the interaction between I atoms is represented by a dotted line).

Results indicated that these intermolecular interactions may exist in various types, where some interaction shapes or conformations are more commonly observed than other structures. In order to better explain the conformations shown in Schemes 4.1-4.3 examples of some selected structures containing different transition metals are displayed in Figures 4.1-4.5, which show various intermolecular interactions existing between the dimeric fragments. The refcodes of these complexes and their chemical formula as well as the resultant conformations are given in Table 4.4. Figure 4.1 shows an example of the chair shape observed in the dimer of DIGZAU (Ga complex). It can be seen that a single I···I interaction occurs at a distance of 3.9 Å, where the two fragments are in the *anti*-position (opposite sides).
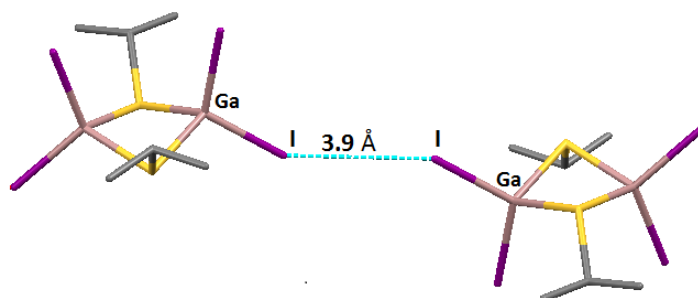
Figure 4.1: An example of a single I···I interaction in the Ga complex in DIGZAU ($C_6H_{14}Ga_2I_4S_2$) showing the chair shape.

Table 4.4: Refcodes, chemical formula and the resultant conformation of selected metal-iodide complexes that contain different transition metals.

Transition metal	Ref code	Formula	Conformation
Ga	DIGZAU	$C_6H_{14}Ga_2I_4S_2$	Chair
Bi	EVINUT	$2(C_6H_{10}N_2^{2+}). Bi_2I_{10}^{4-}. 4(H_2O)$	Boat
Bi	BAYHIT	$3(C_{10}H_{12}NS_3^{+}). Bi_2I_9^{3-}$	Bent
Cu	NILQOO	$2(C_{15}H_{33}KNO_6^{+}). Cu_4I_6^{2-}$	>···<
Sn	NEWKIJ	$C_{16}H_{18}I_4Sn_2$	zigzag
Cu	AFUDIO	$(C_{28}H_{32}Cu_4N_4S_2)$	◇···◇
Cd	BOGHEL	$Cd_2I_6^{2-}. C_{12}H_{30}CdN_6O_6^{2+}$	◇/◇
Cd	LAJLEN	$C_8H_{20}Cd_2I_4Sb_2$	Z-shaped
Pd	WEQXAR	$2(C_{19}H_{34}N^{+}). I_6Pd_2^{2-}$	\···◇
Hg	OBAQEP	$C_{19}H_{23}Cu Hg_2 I_5N_2O_3S_4.CH_2Cl_2$	Linear
Cu	DEHFIG	$C_{22}H_{20}Cu_4I_4N_4S_2$	Boat
Re	FUZVAX	$C_6I_8O_6Re_4$	Bent
Pt	GITVUA	$C_2I_4 O_2Pt_2$	Z-shaped
Cu	BOMLUK	$(C_6H_{14}N_3^{+})_n. 0.5n(Cu_2I_4^{2-})$	Bent
Pd	AGAHOF	$2(C_{12} H_{28} N^{+}). I_6 Pd_2^{2-}$	Chair

Another commonly observed single I···I interaction shape is shown in Figure 4.2, which displays a boat-shape structure observed for a Bi complex. As can be seen, the two fragments in the dimeric form of EVINUT are on the same side resembling the boat structure. Furthermore, the I···I interaction occurs at a slightly shorter distance of 3.7 Å than that observed for Ga in Figure 4.1. Figure 4.3 also shows another Bi complex that displays a different shape, namely bent (observed in the dimer of BAYHIT). This shape was also commonly observed. Similar to EVINUT, the two fragments in Figure 4.3 are on the same side but the structure is slightly bent with the I···I interaction occurring at a longer distance of 4.1 Å than that observed for EVINUT (Figure 4.2).

56
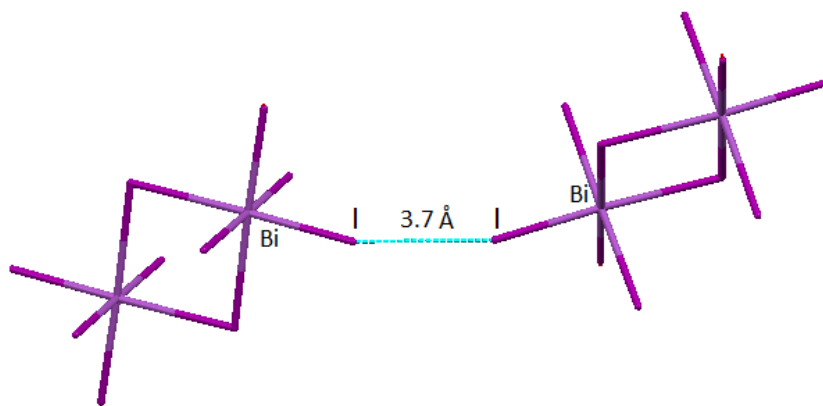
Figure 4.2: An example of a single I⋯I interaction in the Bi complex in EVINUT $(2(C_6H_{10}N_2^{2+}).Bi_2I_{10}^{4-}. 4(H_2O)$ showing the boat shape.
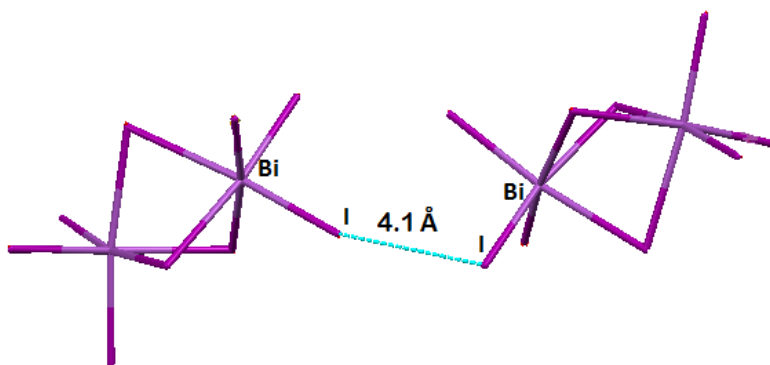
Figure 4.3: An example of a single I⋯I interaction in the Bi complex in BAYHIT $(3(C_{10}H_{12}NS_3^{+}).$ $Bi_2I_9^{3-})$ showing the bent shape structure.

Figure 4.4 shows an example of the most commonly observed shape found in Cu complexes, namely the $>\cdots<$-shaped structure. In this structure, each I atom is covalently linked to two Cu atoms in each fragment. The I $\cdots$ I interaction occurs at 4.2Å, a similar distance to that given in Figure 4.3.
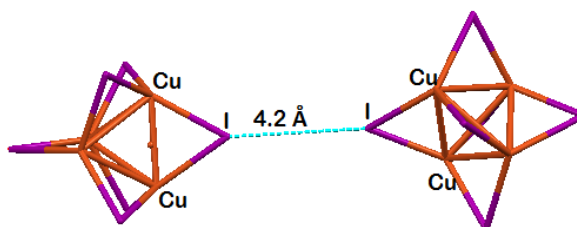
Figure 4.4: An example of a single I⋯I interaction in the Cu complex of NILQOO $(2(C_{15}H_{33}KNO_6^{+}).Cu_4I_6^{2-})$ showing the $>\cdots<$ structure.

It can be seen that all common structures shown in Figures 4.1-4.4 have a single $I \cdots I$ interaction between the two fragments. However, more than one interaction is possible, leading to the zigzag chain shape shown in Figure 4.5, which displays a dimer of the Sn complex in NEWKIJ. Here, the two fragments have an $I \cdots I$ interaction that occurs in a multiple, bifurcated manner with relatively longer interaction distances of 4.3 Å.
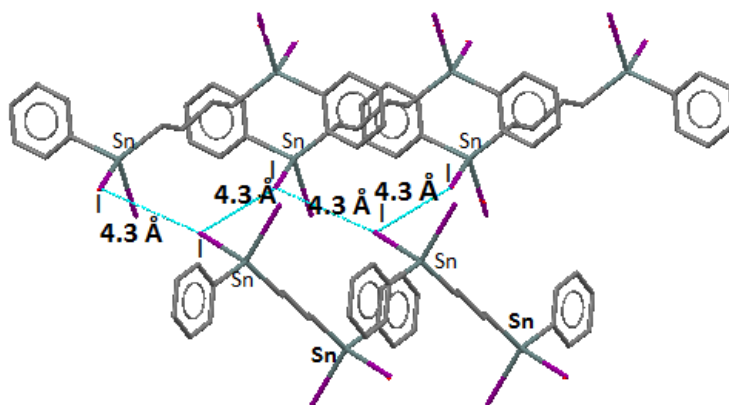
Figure 4.5: An example of a multiple bifurcated $I \cdots I$ interaction in the Sn complex in NEWKIJ ($C_{16}H_{18}I_4Sn_2$) showing a zigzag chain shape.

Other less common conformations that were observed in our study include $\diamond \cdots \diamond$–shaped, $\diamond/\diamond$-shaped, Z-shaped and $\backslash \cdots \diamond$–shaped. Examples of these structures are given in Figures 4.6-4.11, respectively. Figure 4.6 shows the dimeric form of the Cu complex in AFUDIO, which resembles the $\diamond \cdots \diamond$ shape. Each I atom bonds to two Cu atoms in each segment, where an $I \cdots I$ interaction occurs at a distance of 4.1 Å.

Figure 4.7 shows the dimeric form of BOGHEL, which resembles the $\diamond/\diamond$ structure. It can be seen that the structure is very similar to that given in Figure 4.6, where each I atom bonds to two Cd atoms in each segment with a similar $I \cdots I$ interaction distance of 4.1 Å. However, as can be seen in Figure 4.7 the M–I$\cdots$I–M form of BOGHEL is slightly bent compare to that of AFUDIO in Figure 4.6, which is linear.
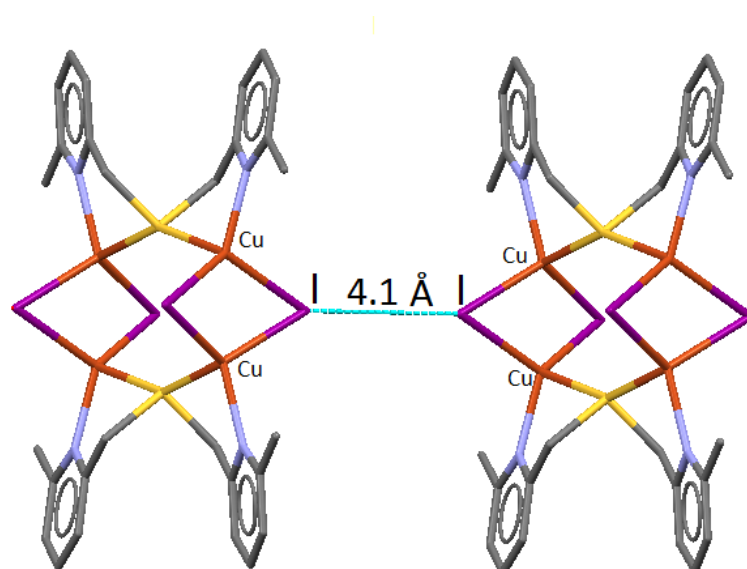
Figure 4.6: An example of a single I···I interaction in the Cu complex in AFUDIO ($C_{28}H_{32}Cu_4N_4S_2$) showing the <>···<> structure.
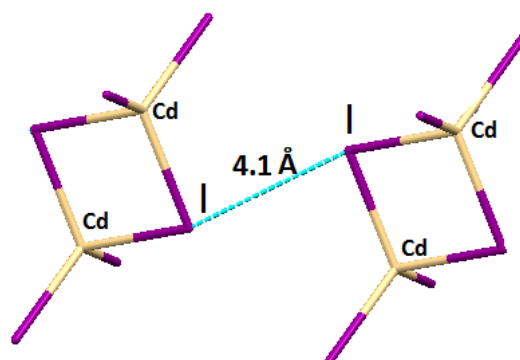
Figure 4.7: An example of a single I···I interaction in the Cd complex in BOGHEL ($Cd_2I_6^{2-}$.$C_{12}H_{30}CdN_6O_6^{2+}$) showing the <>/<> shape.

An example of a Z-shaped structure is clearly shown in Figure 4.8, which displays the crystal structure of the dimeric form of LAJLEN. It can be seen that this conformation is an extreme form of the chair conformation. Similarly, 4.9 shows an example of another structure of the less commonly observed shapes, namely the \···<> shape. The I···I interaction occurs at a similar distance of 4.2 Å to that given in Figure 4.8 for the Cd complex.

59
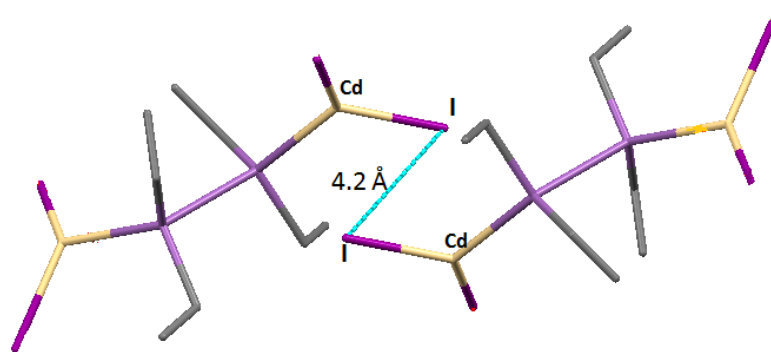
Figure 4.8: An example of a single I···I interaction in the Cd complex in LAJLEN ($C_8H_{20}Cd_2I_4Sb_2$) showing the Z-shape.
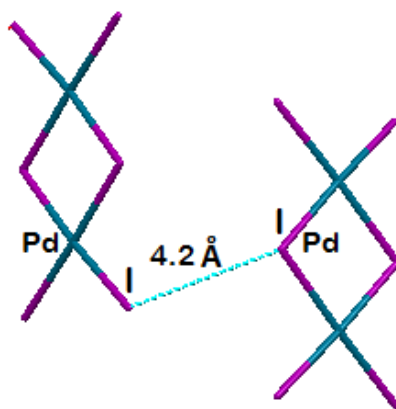
Figure 4.9: An example of a single I···I interaction in the Pd complex in WEQXAR ($2(C_{19}H_{34}N^+)$. $Pd_2I_6^{2-}$) showing \···<> shape.

All structures given in Figures 4.6-4.9 show examples of a single I···I interaction, however the results also indicate that other forms of interactions such as double, bifurcated and even multiple interactions may occur. Figure 4.10 shows an example of a double I···I interaction in the Hg complex in OBAQEP. There is a double I···I interaction occurring in a linear manner between the two fragments, resulting in a ring. Furthermore, both observed I···I interactions occur parallel to each other at the same distance of 3.97 Å (see Figure 4.10), due to a centrosymmetric arrangement of the complexes.

Figure 4.11 shows the crystal structure of DEHFIG ($C_{22}H_{20}Cu_4I_4N_4S_2$), which also contains the I···I double interaction, but this time each I···I interaction exhibits the >···<–shape. The I···I intermolecular interaction is represented by a black dotted line with a distance between I atoms of 4.09 Å. Figure 4.12 shows an example of a multiple, bifurcated interaction. This

60

was found in the Re complex of FUZVAX, where each I atom interacts with two I atoms in the other fragment. The I$\cdots$I interaction distances range between 3.9 to 4.2 Å (see Figure 4.12). Figure 4.13 gives the crystal structure of GITVUA ($C_2I_4O_2Pt_2$), which shows the I$\cdots$I interaction with a bifurcated structure in a Z-shaped form. The I$\cdots$I intermolecular interactions are represented by I$\cdots$I distances of 4.212 and 4.237 Å.
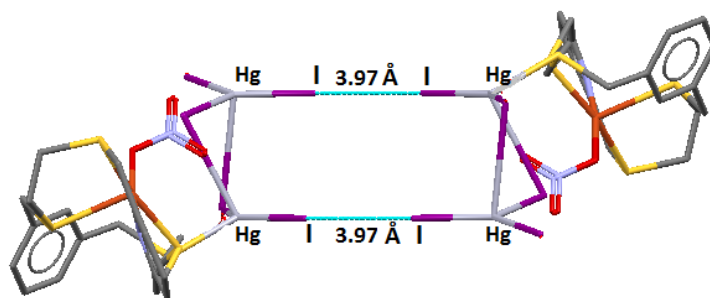
Figure 4.10: An example of a double I$\cdots$I interaction in the Hg complex in OBAQEP ($C_{19}H_{23}Cu\ Hg_2\ I_5N_2O_3S_4.CH_2Cl_2$) showing a double type of interaction.
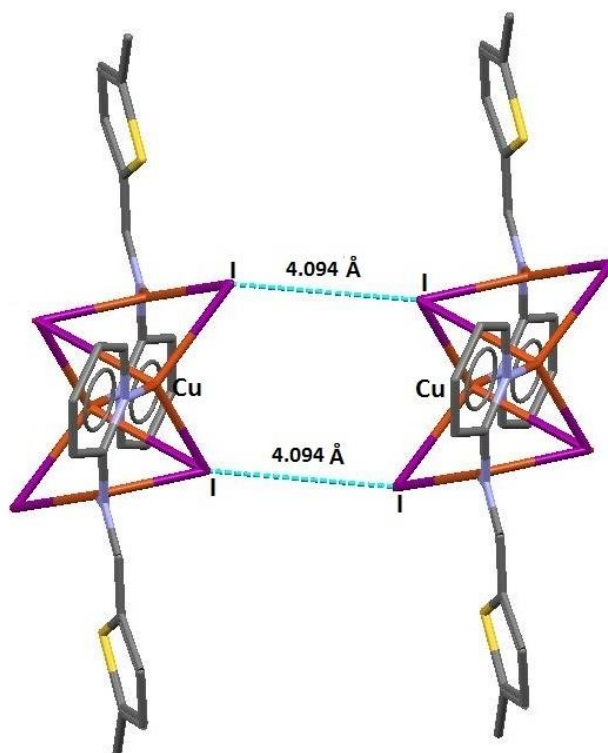
Figure 4.11: An example of a double interaction in the Cu complex in DEHFIG ($C_{22}H_{20}Cu_4I_4N_4S_2$), showing the boat shape.

61
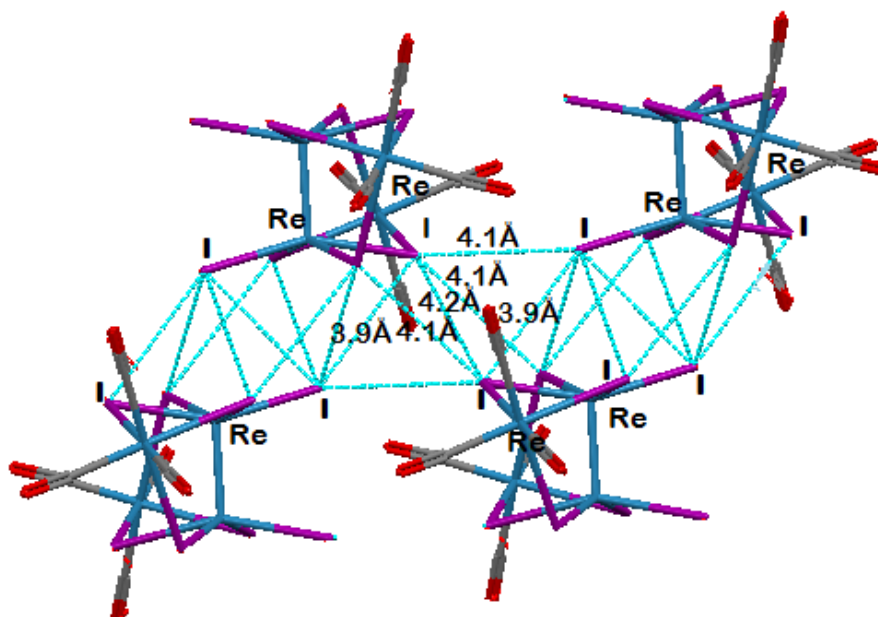
Figure 4.12: An example of a multiple I···I interaction in the Re complex in FUZVAX ($C_6I_8O_6Re_4$).
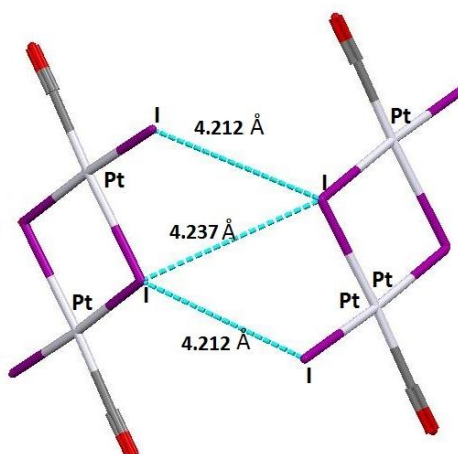
Figure 4.13: An example of a bifurcated I···I interaction in the Pt complex in GITVUA ($C_2I_4 O_2Pt_2$), showing the combination of \···< and >···< interactions.

Results also show that some metal-iodide complexes exhibit <u>intramolecular</u> I···I interactions such as those that contain Mn, Ga, Sn, As or Cu. An example of these <u>intramolecular</u> interactions found in Cu complex is represented in Figure 4.14, which displays the molecular structure of BOMLUK $(C_6H_{14}N^{3+})_n.0.5n(Cu_2I_4^{2-})$. The I···I <u>intramolecular</u> distance is found to be at 4.24 Å.
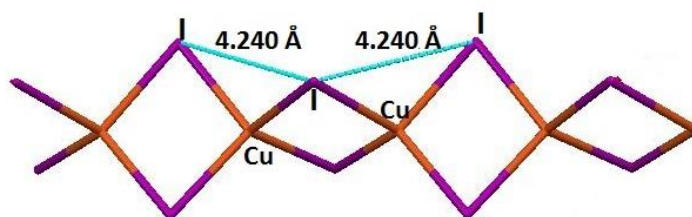
Figure 4.14: An example of <u>intramolecular </u>interactions in the Cu complex in BOMLUK $(C_6H_{14}N_3{}^+)_n.0.5n(Cu_2I_4{}^{2-})$, showing the I···I distance of 4.24 Å.

The transition metal found in the complex plays a significant role in the nature of the I···I interaction. For instance, some metals such as Pt can lead to a strong interaction (will be discussed in more details in Chapter 5), while others such as Hg can lead to weaker I···I interactions. Tables 4.5-4.7 summarize all the results of metal-iodide complexes containing intermolecular I···I interactions obtained through the analysis of the CSD. Table 4.5 shows the types of interaction, average distance of interaction and the most common shapes (conformations) observed in the dimeric form (I–M–I···I–M–I) of metal-iodide complexes for first row transition metals. Tables 4.6 and 4.7 show types of interaction, average distance of interaction and the most common shapes observed in the dimer form (I–M–I···I–M–I) of metal-iodide complexes for the second and the third row transition metals, respectively. Excel sheets showing the structural properties of interest for all analyzed metal complexes are given in the digital supplementary information (see page 126 for details).

Table 4.5: Most common types of interaction, average interaction distance and M–I⋯I–M conformations in 1st-row metal-iodide complexes reported in the CSD.

M	Ti	Fe	Co	Cu	Zn	Ga	Ge	As	Se
No. of complexes	4	1	6	34	7	53	6	33	1
Most common type of interaction*	multiple (100)	double (100)	bifurcated (36)	single (91)	double (43)	double (15)	bifurcated (67)	double (18)	multiple (100)
Most common shapes*	>⋯< (100)	bent (100)	chair (45)	>⋯< (48)	chair (57)	chair (48)	chair (67)	chair (61)	chair (100)
d_{avg} (I⋯I)**	4.2(1)	4.2	3.9(1)	4.1(2)	4.1(1)	4.1(1)	4.1(1)	4.0(2)	3.9

* Percentages (%) of metal-iodide complexes exhibiting this common type and shape out of the total number of complexes are indicated in parentheses.

**Standard deviation is given in parentheses.

Table 4.6: Most common types of interaction, average interaction distance and M–I···I–M conformations in 2nd-row metal-iodide complexes reported in the CSD.

M	Zr	Nb	Mo	Ru	Rh	Pd	Ag	Cd	In	Sn	Sb	Te
No. of complexes	3	3	18	2	4	10	9	29	21	22	57	25
Most common type of interaction*	double (50)	single (100)	single (28)	multiple (50)	multiple (100)	single (100)	single (78)	bifurcated (27)	single (48)	bifurcated (36)	bifurcated (21)	bifurcated (48)
Most common shapes*	chair (50)	>···< (100)	chair (44)	boat (50)	zigzag (100)	chair (30)	>···< (56)	chair (31)	chair (38)	bent (32)	chair (30)	chair (36)
d_{avg} (I···I)**	4.2(1)	3.9(2)	4.1(1)	4.0(1)	3.9(2)	4.0(2)	4.1(2)	4.1(1)	4.1(1)	4.1(2)	3.9(2)	3.9(2)

* Percentages (%) of metal-iodide complexes exhibiting this common type and shape out of the total number of complexes are indicated in parentheses.

** Standard deviation is given in parentheses.

From Table 4.5, one can see that transition metals in the first row undergo various types of interactions (with different conformations), including single, double and multiple interactions. However, some of these elements have a small number of iodide complexes such as Fe (1 complex), Se (1 complex), Co (6 complexes), Ge (6 complexes) and Ti (4 complexes). It can also be seen that the most common shapes for these complexes is chair-shaped structure, although bent and >···<–shaped are also formed depending on the metal involved. In addition, most metal complexes exhibit more than one type of conformation. For instance, 34 Cu complexes have a single I···I interaction with >···<–shaped as the most common conformation (48%), while (21%) of complexes form <>···<>–shaped interactions. Similarly, As and Ga have a high numbers of 33 and 53 complexes, respectively. However, these two elements undergo different types of interactions when compared to Cu, i.e., double interaction with the chair shape as the most common conformation (As, 61% and Ga, 48%). The average interaction distance ranged from 3.9 to 4.2 Å (see Table 4.5). The main group elements typically show chair conformations, while the transition metals form more varied conformations.

Results shown in Table 4.6 indicate that compared to the first row, the second row transition metals generally show an increased number of metal-iodide complexes (more than 10) that have the I···I interaction, while the average I···I distance was found to be very similar to the interactions of transition metals in the 1st-row, ranging from 3.9-4.1 Å. Furthermore, complexes of metals in the 2nd-row exhibit a wider range of shapes, including chair, boat, zigzag, >···<–shaped and bent. However, the chair shape was again found to be the most common in complexes of 2nd-row metals, particularly the main group metals. The most common shapes observed for 2nd-row metals are: Zr (50% chair), Ru (50% boat), Rh (100% zigzag), Ag (56% >···<–shaped), Mo (44% chair), and La (33% >···<–shaped). Furthermore, all these metals share the same type of interaction which are double and multiple, except in the case of Nb (100% >···<–shaped) and Pd (30% chair) which have the single type of interactions.

From Table 4.6, we can see that for instance that Pd has 10 complexes with dimeric form. Some of these complexes have the single type of interaction with a chair shape as the most common form (30%). The average I···I interaction distance is 4.0 Å. Mills *et al*. [17] observed a slightly shorter I···I distance when they investigated the preparation of a model

66

compound utilizing an oxidative addition reaction of dihalides (X_2) to d^8 transition metal complexes. The authors attempted to prepare 2,6-bis-(dimethylaminomethyl)phenyl-C,N,N′-iodo-palladium(II) bis(di-iodine) [Pd(NCN)I$_5$] by adding I_2 to a solution of [Pd(NCN)I] in CH_2Cl_2. They observed the formation of two-dimensional networks of [Pd(NCN)I$_5$], where relatively strong interactions of 3.6 Å (significantly shorter than the sum of the vdW radii interactions in the crystal structure of I_5^- (3.96 Å) between the I_5^- anions exist. The authors showed that these I_5^- anions are actually adducts of iodide ions and I_2 molecules (i.e., $I^-·2I_2$), which link the complexes together. They indicated that each two of the neutral I_2 molecules interact with the iodide ion in the [Pd(NCN)I] complex via $I \cdots I$ interactions with distances of 3.27 and 3.29 Å. The authors mentioned that this is also considerably shorter than the interaction distance of 3.5 Å observed in the crystal structure of I_2. Figure 4.15 displays the crystal structure of AGAHOF ($2(C_{12}H_{28}N^+)·Pd_2I_6^{2-}$), showing the $I \cdots I$ intermolecular interaction distance of 4.17 Å with a single chair shape.
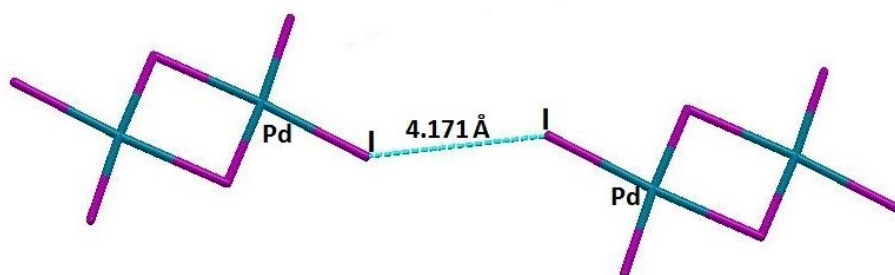
Figure 4.15: An example of a single I⋯I interaction in the Pd complex in AGAHOF ($2(C_{12}H_{28}N^+)·Pd_2I_6^{2-}$), showing the chair shape.

Metals such as Cd, In, Sn, Sb, and Te have the highest number of metal-iodide complexes with more than 20 complexes (see Table 4.6). The average $I \cdots I$ distance was similar to that observed in 1st-row transition metals ranging from 3.9-4.1 Å. These metals exhibit mainly two types of interaction (i.e., double and bifurcated) with the chair shape as the most common as follows: Cd (31%), Pd (30%) and Sb (30%), Te (36%), In (38%) and Sn (bent 32%).

Svensson *et al*. [18] studied the crystal structure of a binary metal-iodide⋯iodine compound containing Cd, namely [Me$_3$S][Cd$_2$I$_6$]$_{1/2}$·3I$_2$. The synthesis was achieved by the reaction of [Me$_3$S][I$_5$] with CdI$_2$ at 80 °C. Using X-ray diffraction and Raman spectroscopy, the authors showed that the resultant complex structure contains layers of Cd$_2$I$_6^{2-}$ dimers, which are bridged by neutral I_2 molecules. These dimers formed infinite chains which are interspaced

by I_{10} units with I_2 molecules co-ordinating in a zigzag manner via strong $I \cdots I$ interactions. The I_2 molecules in the $[Me_3S][Cd_2I_6]_{1/2}.3I_2$ complex interacted between the terminal iodides in the dimeric $Cd_2I_6{}^{2-}$ units at a distance of 3.37 and 3.51 Å, which are in the range observed in polyiodides. The authors also observed the presence of other I_2 molecules which were intercalated between the cadmium-containing layers. These intercalated I_2 molecules interacted with the terminal iodides in $Cd_2I_6{}^{2-}$ unites with slightly longer distance ranging between 3.41-3.56 Å.

Table 4.7 shows that 3rd-row metals such as Pt (36 complexes), Pb (23 complexes), Hg (99 complexes), and Bi (79 complexes) form a very high number of complexes that contain the $I \cdots I$ interaction. On the other hand, metals such as La (1 complex), W (6 complexes), Re (5 complexes) and Ir (5 complexes), Os (4 complexes), and Tl (2 complexes) have a relatively small number of complexes with $I \cdots I$ interaction. In general, the average $I \cdots I$ interaction distance in this row is found to be in the range of 3.9-4.3 Å. These complexes also exhibit a variety of different shapes with the bent-shape more common than the chair shape. Furthermore, the type of interaction also varies from single, bifurcated to multiple.

For instance, 15 Au complexes exhibit an $I \cdots I$ interaction, with an average distance of 3.9 Å (see Table 4.7). These metal iodide complexes generally form single interactions with the bent and chair shapes being equally common (40% bent, 40% chair). Söhnel *et al*. [19] studied the stability of gold iodides in the gas phase and the solid state at the *ab initio* and density functional level using relativistic and nonrelativistic energy-adjusted pseudopotentials for gold and iodine. The authors found that I_2 molecules could form strong $I \cdots I$ interactions with Au_2I_2, which are 23.2 and 12.6 kJ/mol at the relativistic and nonrelativistic B3LYP level, respectively (87.1 and 69.7 kJ/mol at the relativistic and nonrelativistic MP2 level, respectively). They also showed that the I–I distance of the terminal I_2 was very close to the calculated bond length for pure I_2 (i.e., 2.71 Å at the relativistic B3LYP level and 2.69 Å at the nonrelativistic level). Furthermore, the authors determined that the structural parameters such as the Au-I distance varied considerably, which is very dependent on the method applied. From Tables 4.5, 4.6 and 4.7, we can also see that the average $I \cdots I$ distance observed in 1st-row, the 2nd-row and 3rd-row metals is between 3.9-4.2 Å. However, strong interactions were observed a shorter distance of 3.4-3.8 Å (see CSD results in the digital supplementary information).

Table 4.7: Most common types of interaction, average interaction distance and M–I···I–M conformations in 3rd-row metal-iodide complexes reported in the CSD.

M	La	W	Re	Os	Ir	Pt	Au	Hg	Tl	Pb	Bi
No. of complexes	1	6	5	4	5	36	15	99	2	23	79
Most common type of interaction*	single (100)	bifurcated (50)	multiple (60)	single (75)	trifurcated (40)	bifurcated (19)	single (73)	bifurcated (35)	bifurcated (100)	single (91)	bifurcated (77)
Most common shapes*	chair (100)	bent (48)	>···< (45)	bent (50)	bent (40)	chair (31)	bent (40) chair (40)	bent (35)	bent (100)	boat (27)	bent (33)
d_{avg} (I···I)**	4.3	4.1(1)	4.1(1)	4.0(2)	4.0(1)	4.0(2)	3.9(2)	4.1(1)	3.9(2)	4.1(1)	4.0(2)

* Percentages (%) of metal-iodide complexes exhibiting this common type and shape out of the total number of complexes are indicated in parentheses.

** Standard deviation is given in parentheses.

4.4 Conclusion

The CSD was used to study all previously published experimental crystal structures containing metal iodides. The CSD search was used to establish which complexes containing the I–M–I moieties are able to form dimers containing I$\cdots$I interactions in the solid state (M is a transition metal and I is an iodine atom). The analysis showed that some metal-iodide complexes which contain the I–M–I moiety did not exhibit I$\cdots$I interactions (e.g., Cr, V, Sc, Ni, Mn, Y, Tc, Po, and Ta). However, the results showed that some other metal-iodide complexes have a high number of compounds that form dimers as a result of the presence of I$\cdots$I intermolecular interactions. These include complexes that contain Au (21%), Hg (21%), In (26%), Ti (25%), Nb (37%), Bi (40%), Ga (42%) or Sb (65%) which have the highest number of compounds with the I$\cdots$I intermolecular interaction. The most common conformations of all metal iodide complexes containing I$\cdots$I interactions (i.e., having the dimeric I–M–I$\cdots$I–M–I form) in the solid state were identified. These include chair, boat, bent, >$\cdots$<–shaped and zigzag forms.

Results also showed that these intermolecular interactions can be single, double, multiple and bifurcated interactions. In general, the average distance that led to a strong interaction in such complexes is between 3.9 – 4.2 Å. The most common shapes in which these metals are likely to have a shorter distance between iodine atoms (i.e., stronger I$\cdots$I interaction) were also investigated. A strong interaction (i.e., a shorter distance between I atoms) is most likely to occur where the relative orientation of the two I–M–I moieties is in the chair form. To the best of our knowledge, this is the first comprehensive study to investigate the type, nature and strength of such interactions in metal-iodide complexes.

4.5 References

1. Allen, F., *The Cambridge Structural Database: a quarter of a million crystal structures and rising.* Acta Crystallographica Section B **2002**, 58, 380-388.

2. Lydia C. Gilday, Sean W. Robinson, Timothy A. Barendt, Matthew J. Langton, Benjamin R. Mullaney, and Paul D. Beer., *Halogen Bonding in Supramolecular Chemistry.* Chemical Reviews **2015**, *115* (15), 7118–7195.

3. Bruno, I.J., Cole, J.C., Edgington, P.R., Kessler, M., Macrae, C.F., McCabe, P., Pearson, J., and Taylor, R., *New software for searching the Cambridge Structural Database and visualizing crystal structures.* Acta Crystallographica Section B **2002**, 58(3 Part 1), 389-397.

4. Macrae, C.F., Edgington, P.R., McCabe, P., Pidcock, E., Shields, G.P., Taylor, R., Towler, M., and van de Streek, J., *Mercury: visualization and analysis of crystal structures.* Journal of Applied Crystallography **2006**, 39(3), 453-457.

5. Blake, A.J., Li, W.-S., Lippolis, V., Parsons, S., and Schröder, M., *Extended structures of polyiodide salts of transition metal macrocyclic complexes.* Acta Crystallographica Section B **2007**, 63(1), 81-92.

6. Hitchcock, P.B., Hughes, D.L., Leigh, G.J., Sanders, J.R., De Souza, J., McGarry, C.J., and Larkworthy, L.F., *Preparation of new vanadium(II) iodides and crystal structure of hexakis(acetonitrile)vanadium(II)(tetraiodide).* Journal of the Chemical Society, Dalton Transactions **1994**(24), 3683-3687.

7. Westra, A.N., Bourne, S.A., Esterhuysen, C., and Koch, K.R., *Reactions of halogens with Pt(II) complexes of N-alkyl- and N,N-dialkyl-N-benzoylthioureas: oxidative addition and formation of an I_2 inclusion compound.* Dalton Transactions **2005**(12), 2162-2172.

8. Buse, K.D., Keller, H.J., and Pritzkow, H., *Reaction of molecular iodine with cis-dihalo(2,2'-bipyridyl)platinum(II) and cis-dihalo(1,10-phenanthroline)platinum(II). Oxidative addition and inclusion compounds.* Inorganic Chemistry **1977**, 16(5), 1072-1076.

9. Gray, L.R., Gulliver, D.J., Levason, W., and Webster, M., *Coordination chemistry of higher oxidation states. 5. Reaction of palladium(II) iodo complexes with molecular iodine and crystal and molecular structure of diiodo(cis-1,2-*

71

bis(diphenylphosphino)ethene)palladium(II)-diiodine (1/1). Inorganic Chemistry **1983**, 22(17), 2362-2366.

10.   Titi, H.M., Patra, R., and Goldberg, I., *Intermolecular iodine–iodine interactions in bis(pyridine-3-carboxylato)[tetrakis(4-iodophenyl)porphyrinato]tin(IV) and bis(pyrimidine-5-carboxylato)[tetrakis(4-iodophenyl)porphyrinato]tin(IV).* Acta Crystallographica Section C **2013**, 69(9), 1013-1016.

11.   Allan, D.R., Bailey, D., Bird, N., Blake, A.J., Champness, N.R., Huang, D., Keane, C.P., McMaster, J., Prior, T.J., Tidey, J.P., and Schröder, M., *High-pressure studies of palladium and platinum thioether macrocyclic dihalide complexes.* Acta Crystallographica Section B **2014**, 70(3), 469-486.

12.   Svensson, P.H. and Kloo, L., *Metal Iodides in Polyiodide Networks: Synthesis and Structure of Binary Metal Iodide−Iodine Compounds Stable under Ambient Conditions.* Inorganic Chemistry **1999**, 38(14), 3390-3393.

13.   Karle, I.L., *Anomalous Electron Scattering from Iodine Vapor.* The Journal of Chemical Physics **1955**, 23(9), 1739-1739.

14.   van Bolhuis, F., Koster, P.B., and Migchelsen, T., *Refinement of the crystal structure of iodine at 110 degrees K.* Acta Crystallographica **1967**, 23(1), 90-91.

15.   J. Blake, A., Li, W.-S., Lippolis, V., Schroder, M., A. Devillanova, F., O. Gould, R., Parsons, S., and Radek, C., *Template self-assembly of polyiodide networks.* Chemical Society Reviews **1998**, 27(3), 195-206.

16.   Brammer, L., Minguez Espallargas, G., and Libri, S., *Combining metals with halogen bonds.* CrystEngComm **2008**, 10(12), 1712-1727.

17.   Mills, A.M., Beek, J.A.M.v., Koten, G.v., and Spek, A.L., *{2,6-Bis[(dimethylamino)methyl]phenyl}iodopalladium(II) bis(diiodine).* Acta Crystallographica Section C **2002**, 58(5), m304-m306.

18.   H. Svensson, P., Bengtsson-Kloo, L., and Persson, P., *Metal iodides in polyiodide networks. The structural chemistry of CdI$_2$ with an excess of iodine.* Journal of the Chemical Society, Dalton Transactions **1998**(9), 1425-1429.

19.   Söhnel, T., Brown, R., Kloo, L., and Schwerdtfeger, P., *The Stability of Gold Iodides in the Gas Phase and the Solid State.* Chemistry – A European Journal **2001**, 7(14), 3167-3173.

Chapter 5

I–M–I···I–M–I structure optimization in the gas phase and in "solvents"

5.1 Introduction

In this chapter we describe an investigation into the nature and strength of the I···I interactions in metal iodide dimers by calculating the interaction energy of the conformations. The intermolecular distances of these interactions in some selected metal-iodide complexes were determined employing various levels of DFT theory. The calculations were carried out in the gas phase as well as in various solvents, in order to determine the effect of the electrostatic environment (i.e., solvent) on the I···I interaction distance and strength. Ligands in the studied metal-iodide complexes were simplified when necessary.

5.2 I–M–I···I–M–I structure optimization

Based on the CSD survey described in Chapter 4, it was shown that some metal-iodide complexes are more likely to have $I \cdots I$ interactions in the dimer form (i.e, I–M–I···I–M–I). These include iodide complexes of metals such as copper (Cu), mercury (Hg), gallium (Ga), silver (Ag), platinum (Pt), palladium (Pd) or bismuth (Bi), where large numbers of complexes display the $I \cdots I$ interaction (see Table 4.3 in Chapter 4). For instance, Hg has 99 complexes while Bi has 79 complexes that have $I \cdots I$ interactions.

Analyzing all these metal-iodide complexes will be computationally too expensive and very time consuming. Therefore, structure optimizations were carried out on some selected metal-iodide complexes containing Cu, Hg, Ga, Ag, Pt, Pd or Bi. For each metal one complex was chosen as a model compound, except for Pd where two complexes were used, to perform the $I \cdots I$ interaction studies. In some cases it was necessary to use simplified model complexes. Table 5.1 summarizes all metal-iodide complexes that were chosen for this study from the CSD, their chemical formulas and the codes given to the model complexes.

Table 5.1: Chemical formulas of metal-iodide complexes used for the optimization study.

Metal	CSD Refcode	Chemical formula of complex	Model code	Chemical formula of model
Cu	DEHKACO2	$(2(C_{24}H_{20}P^{+}). Cu_2I_4{}^{2-})$	D-Cu	$[Cu_2 I_4]^{2-}$
Pt	NUKCAY	$(2(0.5(C_{10}H_2I_2N_2Pt).0.5(C_{10}H_{22}I_2N_2Pt))$	N-Pt	$(PtI_2N_2H_3)$
Ga	OJAVIE	$(C_8H_{22}Ga_2I_4N_2)$	O-Ga	$(Ga_2I_4N_2H_6)$
Bi	ZUCKIR	$(C_{40}H_{37}BiI_2N_3O_2P_2{}^{+}. C_{10}H_{10}BiI_4N_2{}^{-}. C_5H_5N)$	Z-Bi	$(CH_{15}BiI_2N_3O_2P_2)^{+}$
Ag	PAWXOB	$(Ag_2I_5{}^{3-})_n. 2n(C_{11}H_{20}N_2{}^{2+}). n(I^{-}). 2n(H_2O)$	P-Ag	$[Ag_2I_6]^{4-}$
Hg	JAHCOK01	$(C_{36}H_{30}Hg_2I_4P_2)$	J-Hg	$(Hg_2P_2H_6I_4)$
Pd	HOVMAH	$(C_{20}H_{22}I_4N_2Pd_2S_2. C_2H_4Cl_2)$	H-Pd	$[Pd_2I_6]^{2-}$
Pd	AGAHOF	$2(C_{12}H_{28}N^{+}). Pd_2I_6{}^{2-}$	A-Pd	$[Pd_2I_6]^{2-}$

For each model compound, a single unit of the complex (i.e., I–M–I form) was optimized to obtain the minimum energy of the conformation. This optimized structure was then used to build the dimeric form (i.e., I–M–I···I–M–I), which was also optimized before calculating the

I···I interaction distance and energy. The optimized geometries were compared to those observed in the solid state, obtained from CSD as discussed in Chapter 4. The structures of these metal-iodide complexes using simplified ligands were investigated with the aid of the software package Gaussian 09 using different protocols as indicated in Table 3.1 (e.g. DFT functional, basis set and PCM solvent model) [1]. The basis set superposition error (BSSE) correction was applied in Gaussian by implementing the counterpoise=2 keyword [2, 3]. Calculation of the I···I interaction energy was carried out in the gas phase as well as in an implicit solvent environment (water, ethanol or chloroform). It should be mentioned that frequency calculations were performed on all optimized structures in this section to confirm that they were at minimum energy conformations.

5.2.1 Simplifying the ligands

Before any further calculations could be performed, it was important to simplify the model obtained from the crystal structure of the studied metal-iodide complexes, in order to reduce the amount of computational power and time required to do the calculations. Figure 5.1 shows the molecular structure of DEHKACO2 ($C_{24}H_{20}P^{+} \cdot Cu_2I_4^{2-}$), which was used as a model compound to study the I···I interactions in Cu complexes. The counterion, bis(tetraphenylphosphonium), is very bulky and so was removed entirely to afford the final model complex (i.e., $[Cu_2 I_4]^{2-}$). This is shown in Figure 5.2.
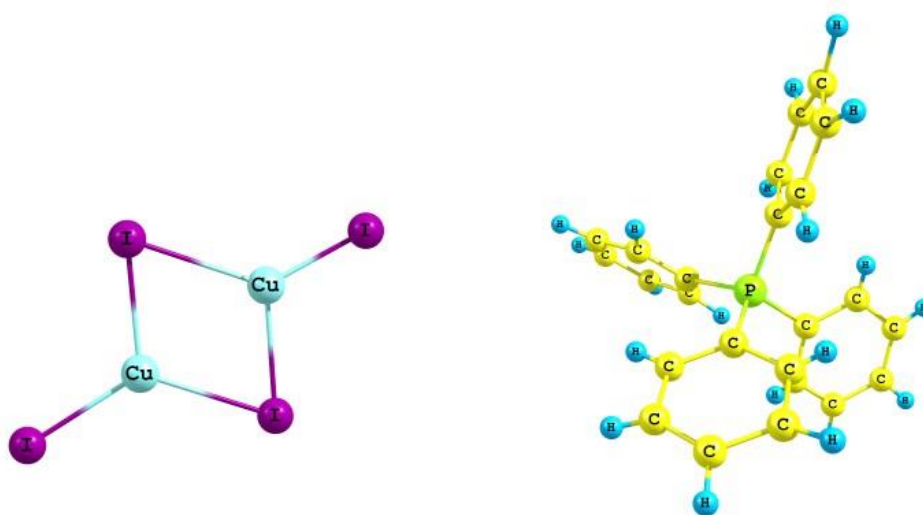
Figure 5.1: Molecular structure of DEHKACO2 showing the initial bulky structure before simplifying the ligand.

75
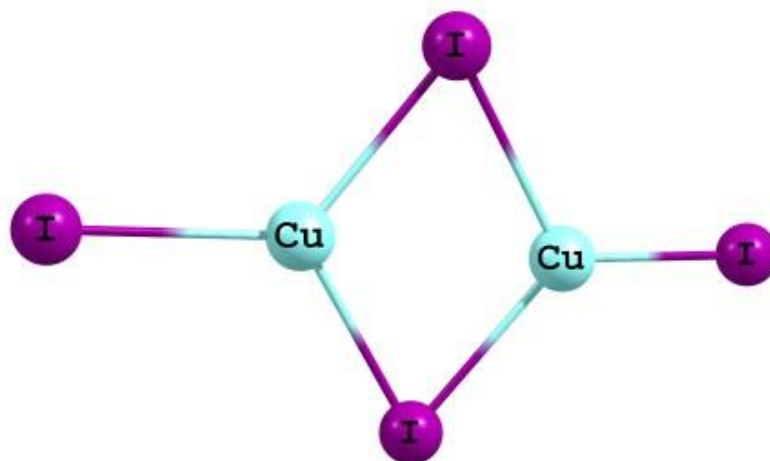
Figure 5.2: Model structure of D-Cu obtained from DEHKACO2 after removing the counterion.

Figures 5.3 (a) and (b) show the molecular structures obtained from the crystal structure of NUKCAY ($2(0.5(C_{10}H_{22}I_2N_2Pt)$. $0.5(C_{10}H_{22}I_2N_2Pt))$ in two different configurations. In this case it is the cyclopentanamine ligand in NUKCAY that is very bulky. The structure of the *trans*-conformation was chosen as model and simplified by replacing each cyclopentane ring with a hydrogen atom (H). This resulted in the formation of a new structure with two NH_3 groups attached to the central metal Pt atom ($PtI_2N_2H_3$) (see Figure 5.4).

a)

b)
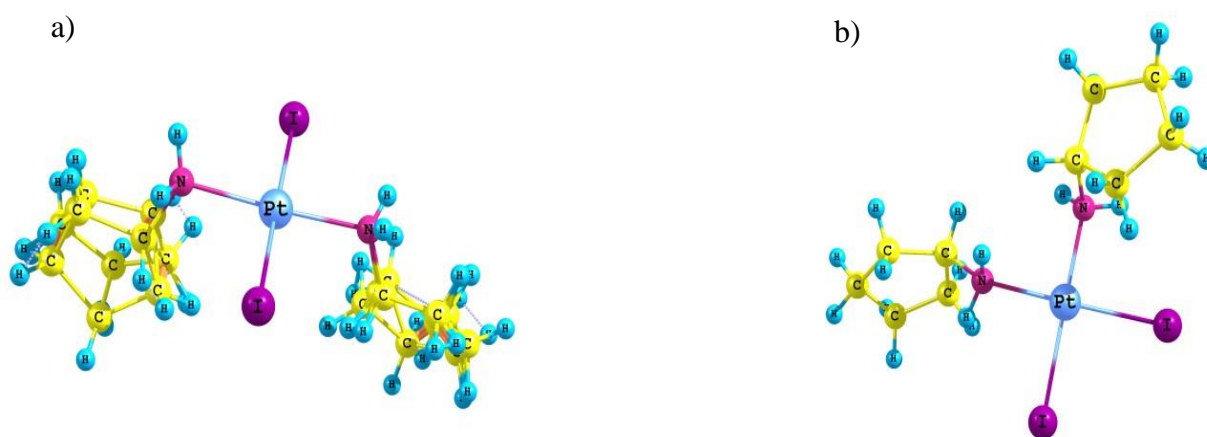
Figure 5.3: Molecular structure of NUKCAY showing the: (a*) trans* and (b) *cis* configurations of the two molecules in the asymmetric unit before simplification of the ligands.

76
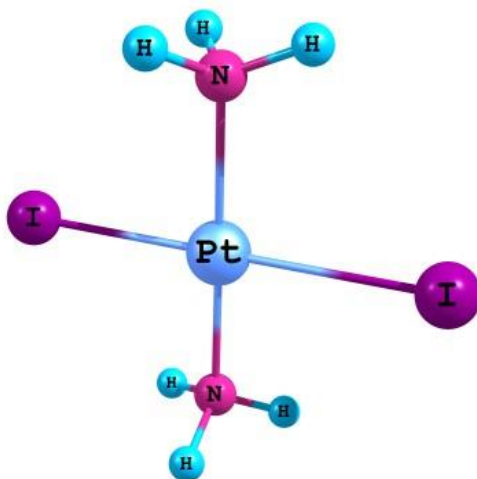
Figure 5.4: Model structure of N-Pt obtained from NUKCAY after simplifying the ligand.

Similar to NUKCAY, the bulky ligand in OJAVIE (model compound used to study the I···I interactions in Ga complexes) was simplified by replacing the *t*-butylamine group by a hydrogen atom. The initial structure of OJAVIE is shown in Figure 5.5, while the simplified structure after replacing the *t*-butylamine group by a hydrogen atom is shown in Figure 5.6 (i.e., $Ga_2I_4N_2H_6$). Similar to NUKCAY, the resultant simplified structure of OJAVIE contains two NH_3 groups covalently attached to the Ga atoms.
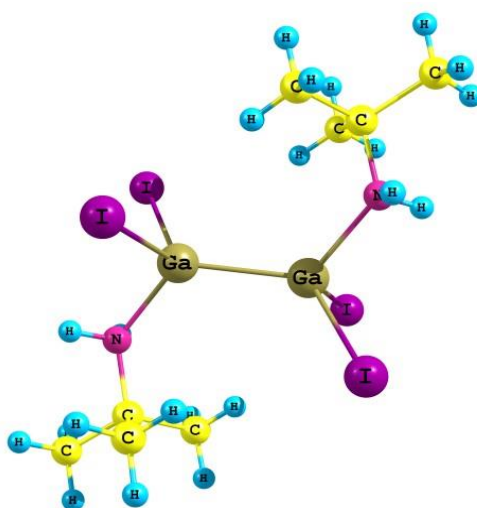
Figure 5.5: Molecular structure of OJAVIE before simplifying the ligand (i.e., $C_8H_{22}Ga_2I_4N_2$).
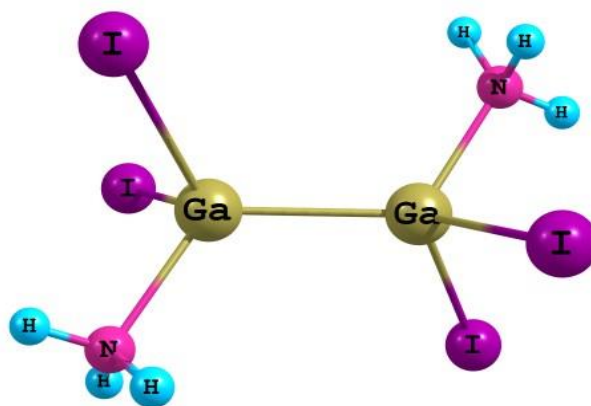
Figure 5.6: Model compound of O-Ga obtained from OJAVIE after simplifying the ligand $(Ga_2I_4N_2H_6)$.

Figure 5.7 shows the structure of the asymmetric unit of ZUCKIR before simplification (i.e., $C_{40}H_{37}Bi\ I_2N_3O_2P_2^+$. $C_{10}H_{10}BiI_4N_2^-$. C_5H_5N). It can be seen that there are two different bulky ligands, which are covalently attached to the central Bi atom. To simplify the structure, each benzene group attached to the phosphorus atom was replaced by a hydrogen atom. Furthermore, all pyridine groups attached to the central Bi atom were replaced by NH_3 groups. This resulted in the final simplified structure, which is a cation (i.e., $(CH_{15}BiI_2N_3O_2P_2)^+$), as shown in Figure 5.8.
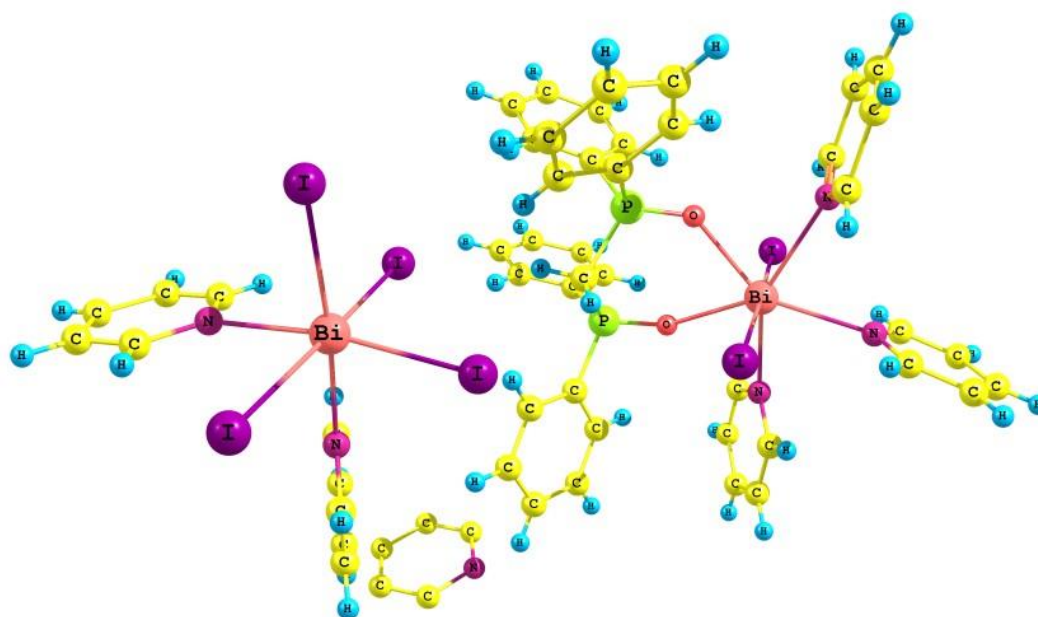
Figure 5.7: Model structure of the asymmetric unit of ZUCKIR before simplification (i.e., $C_{40}H_{37}BiI_2N_3O_2P_2^+.C_{10}H_{10}BiI_4N_2^-.C_5H_5N$).
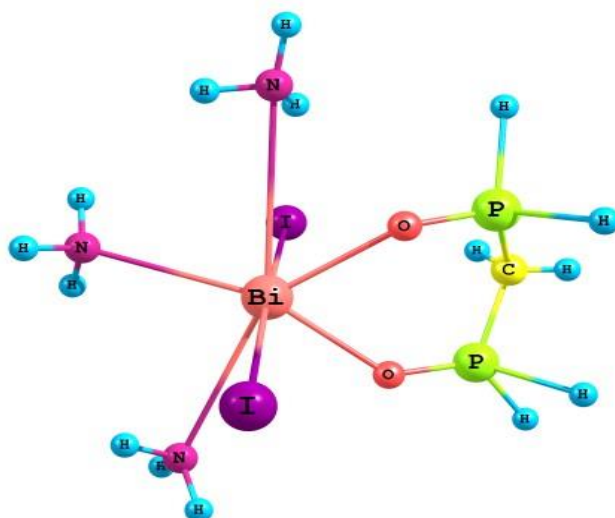
Figure 5.8: Model compound of Z-Bi obtained from ZUCKIR after simplifying the ligand.

The CSD survey showed that PAWXOB consists of ionic species $((Ag_2I_5^{3-})_n. 2n(C_{11}H_{20}N_2^{2+}).$ $n(I^-). 2n(H_2O))$ as shown in Figure 5.9. The structure was simplified by removing the amine and iodide counterions, while the polymeric silver iodide network was cut resulting in a new final simplified complex structure $[Ag_2I_6]^{4-}$, shown in Figure 5.10.
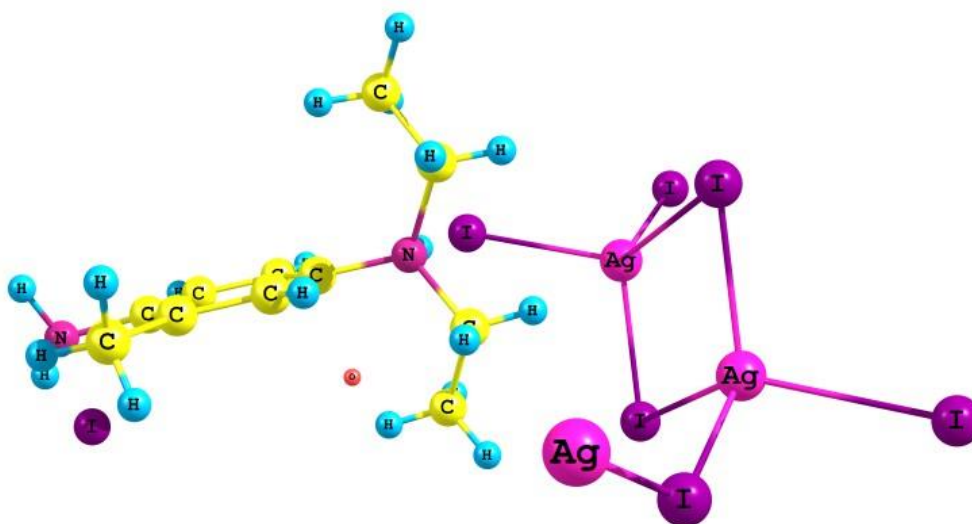
Figure 5.9: Structure of the asymmetric unit of PAWXOB before simplifying the polymeric complex $(Ag_2I_5^{3-})_n. 2n(C_{11}H_{20}N_2^{2+}). n(I^-). 2n(H_2O)$.

79
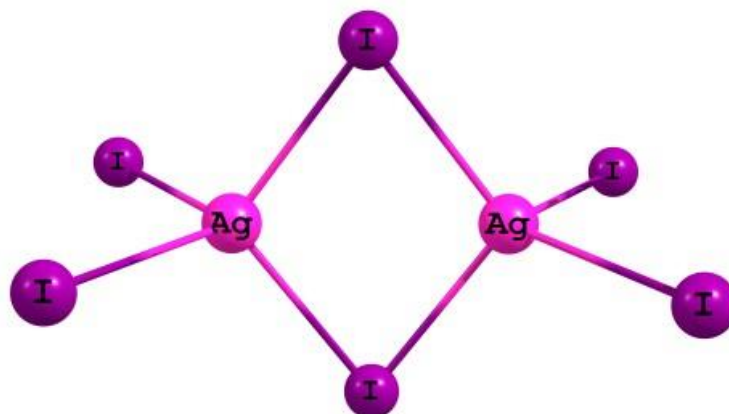
Figure 5.10: Model compound of P-Ag obtained from PAWXOB after simplification.

Figure 5.11 shows the molecular structure of JAHCOK01, which was used as a model compound to study the I⋯I interactions in Hg complexes. The large ligands are covalently attached to the Hg atoms through phosphorus atoms. The ligands were simplified by replacing each benzene group attached to the phosphorus atom with a hydrogen atom. This resulted in the formation of a simplified complex structure with a phosphine group (PH_3) attached to each of the Hg atoms (see Figure 5.12).
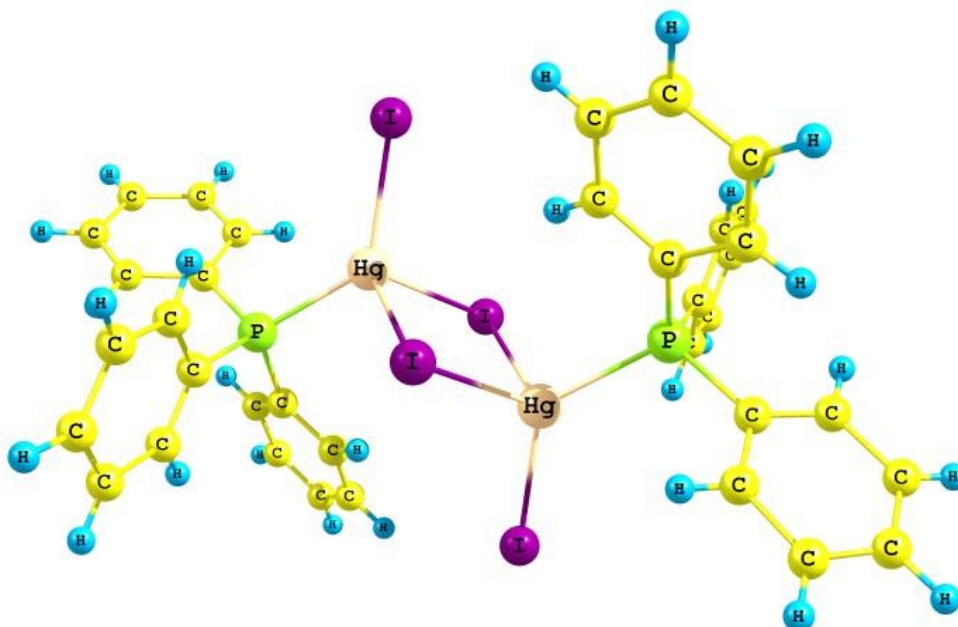
Figure 5.11: Molecular structure of JAHCOK01 before simplifying the ligands ($C_{36}H_{30}Hg_2I_4P_2$).

80
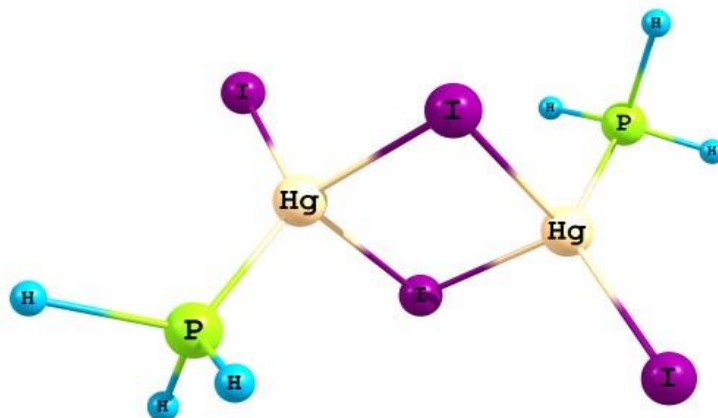
Figure 5.12: Model compound of J-Hg obtained from JAHCOK01 after simplifying the ligands ($Hg_2P_2H_6I_4$).

To study the $I \cdots I$ interactions in Pd complexes, two compounds which form two different M–I$\cdots$I–M orientations were used. This was done to study the effect of the final structure shape in the dimer form on the $I \cdots I$ interaction. Figure 5.13 shows the structure of HOVMAH ($C_{20}H_{22}I_4N_2Pd_2S_2$. $C_2H_4Cl_2$), where the M–I$\cdots$I–M interactions form a linear shape in the dimer form. The molecular structure of the other compound (AGAHOF), which has a chair shape in its dimer form, is shown in Figure 5.14. The initial molecular structure of HOVMAH has a bulky ligand and a disordered $C_2H_4Cl_2$ counterion, while the molecular structure of AGAHOF has a bulky counterion.
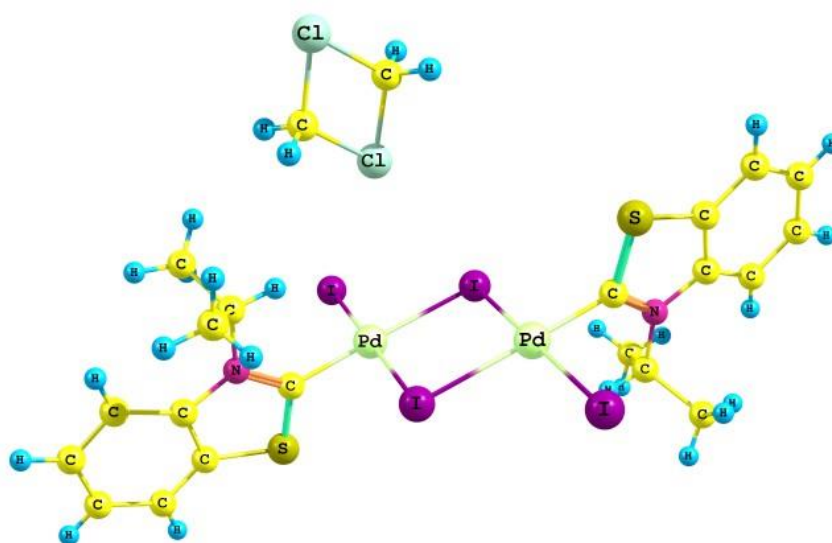
Figure 5.13: Molecular structure of HOVMAH before simplification ($C_{20}H_{22}I_4N_2Pd_2S_2$. $C_2H_4Cl_2$).
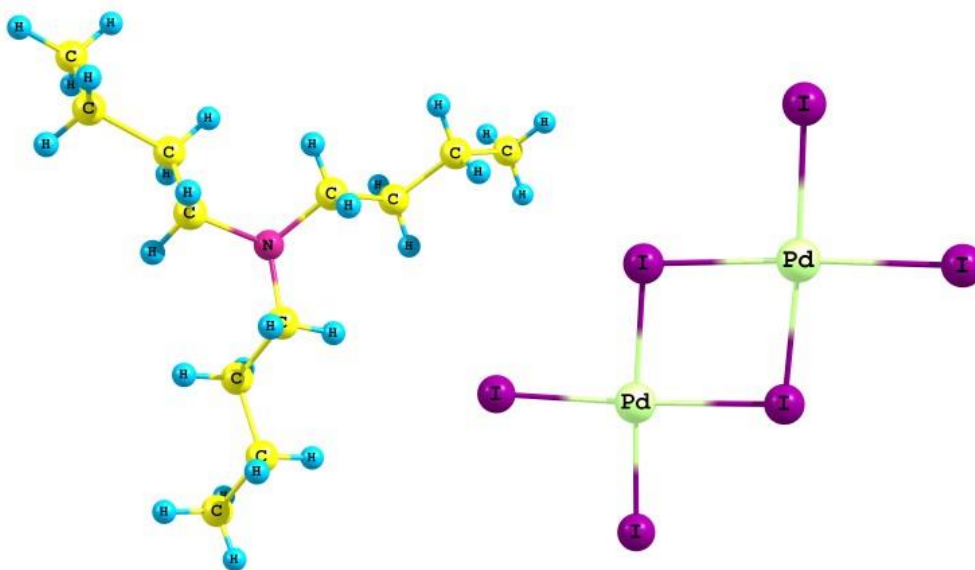
Figure 5.14: Molecular structure of AGAHOF before simplification ($2(C_{12}H_{28}N^+)$, $Pd_2I_6^{2-}$).

The final simplified structure was obtained from HOVMAH by replacing the bulky thiazolidine ligand with a hydrogen atom and removing the $C_2H_4Cl_2$ counterion entirely. This resulted in the formation in a new simplified structure containing two Pd and six iodide atoms as shown in Figure 5.15. The molecular structure of AGAHOF was also simplified by removing the bulky ligand completely. This is shown in Figure 5.16, which indicates that removing the tributylamine cation resulted in the formation of a similar structure to that obtained from HOVMAH.
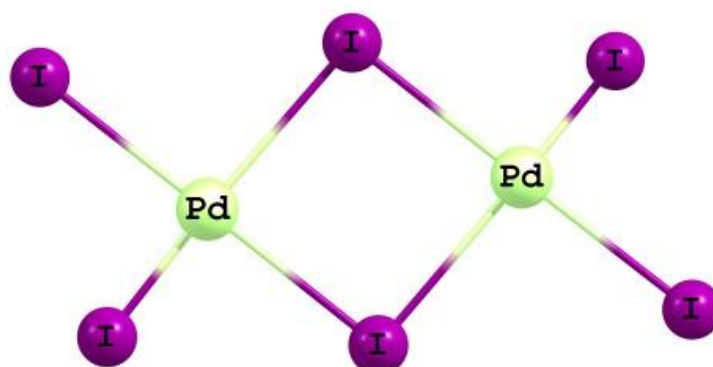
Figure 5.15: Model complex of H-Pd obtained from HOVMAH after simplification $[Pd_2I_6]^{2-}$.

82
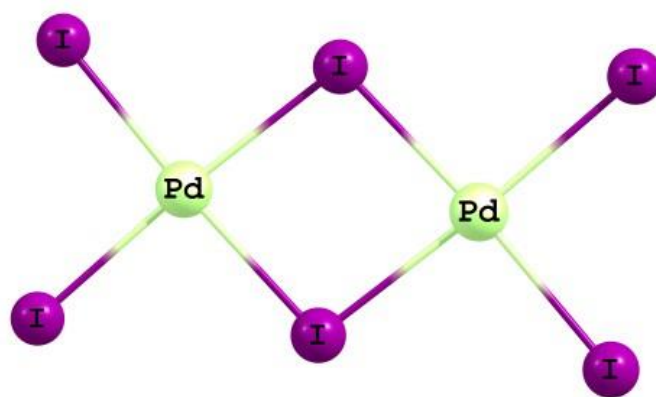
Figure 5.16: Model complex of A-Pd obtained from AGAHOF after simplification $[Pd_2I_6]^{2-}$.

### 5.2.2 Modelling of I···I interactions in the gas phase

Modelling in the gas phase was performed on metal-iodide complexes containing the following transition metals: Cu, Hg, Ag, Pt, Pd, Ga or Bi. One structure for each identified transition metal was investigated. The chemical formulas of these metal-iodide complexes (models) are shown in Table 5.1. For each model, the structure of the individual complex was optimized first and then used to build the dimeric form based on the orientations found as part of the CSD survey described in Chapter 4. All calculations were carried out by using Gaussian 09 utilizing different level of DFT theory (namely PBEPBE [4] and B3LYP [5, 6]) in combination with the aug-cc-pVTZ–pp [7, 8] and 6-31G(d) basis sets.

5.2.2.1 Intermolecular distance d (I···I)

To study the strength of the I···I interaction in metal-iodide complexes, it was important to calculate the distance between the iodine atoms in dimers in the gas phase. These calculations allowed us to investigate the intra- and intermolecular interactions (e.g. I···I interaction, van der Waals repulsion, etc.) without any influence from the surroundings, such as solvent effects. The latter will be discussed in details in Section 5.2.3. Figure 5.17 shows the initial and optimized monomeric structures of D-Cu in the gas phase. The latter was obtained at the minimum energy conformation (E of −1577.8785 a.u.). The optimized structure (Figure 5.17 (b)) exhibited significant changes in the I–Cu distances as well as I–Cu–I angles as compared to the initial monomeric structure shown in Figure 5.17 (a). The optimized structure was then used to build the dimeric structure of D-Cu (Figure 5.18) to perform the gas phase

calculations to determine the bond length and strength of the I···I interaction. The calculations were carried out at the PBEPBE level of theory in combination with aug-cc-pVTZ–pp and 6-31G(d) basis sets. The two D-Cu ions were found to repel each other in the gas phase and the optimization was stopped at the point shown in Figure 5.19 (at an energy of E = − 3155.67145555 a.u.). This can be attributed to a repulsive electrostatic interaction between the two D-Cu fragments of the dimer in the gas phase as a result of the charge on each fragment. This is similar to what has been found previously for triiodide ions, which repelled each other in the gas phase [1]. It should be noted here that the I–Cu–I and Cu–Cu–I angles in the two fragments also changed significantly during the optimization (see Figure 5.19).
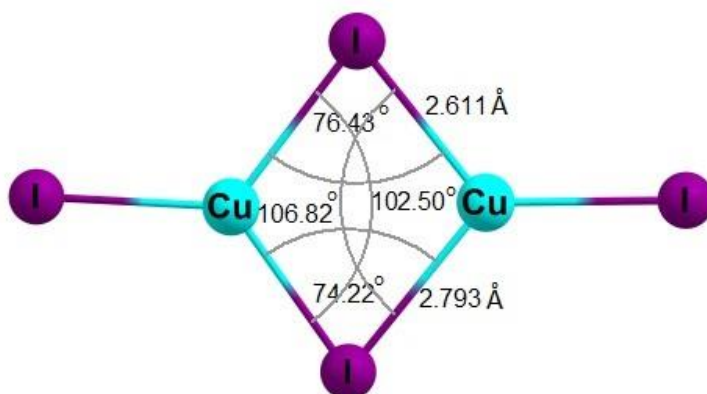
a)
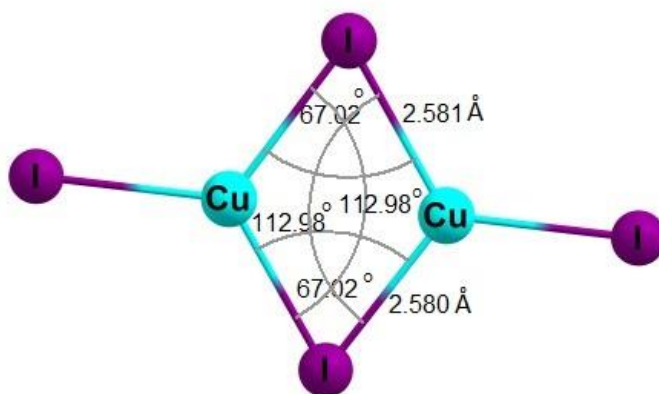
b)

Figure 5.17: (a) Initial monomeric structure of D-Cu and (b) optimized monomeric structure of D-Cu in the gas phase (E = − 1577.8785 a.u.).

84

The optimized structure of the complex model obtained from N-Pt in the minimum energy conformation (E = − 824.0755 a.u.) is shown in Figure 5.20. This structure was used to build a dimer based on the geometric parameters for the I⋯I interaction in N-Pt which is represented in Figure 5.21.
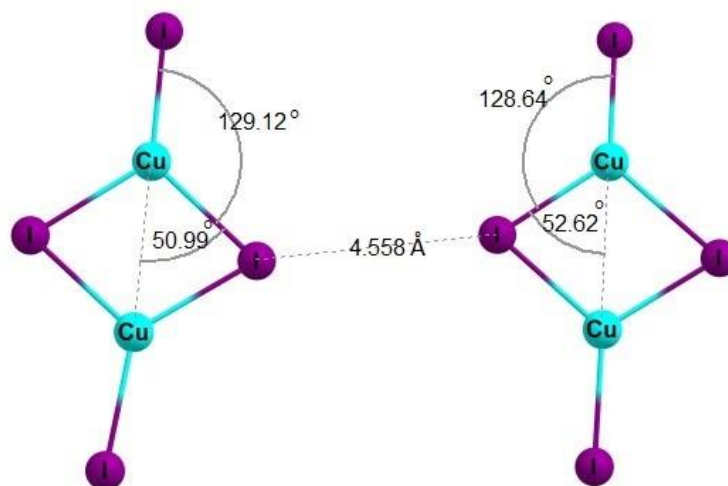

Figure 5.18: The initial dimeric structure of D-Cu in the gas phase, showing I⋯I distance of 4.558 Å (E = − 3155.757057 a.u.).
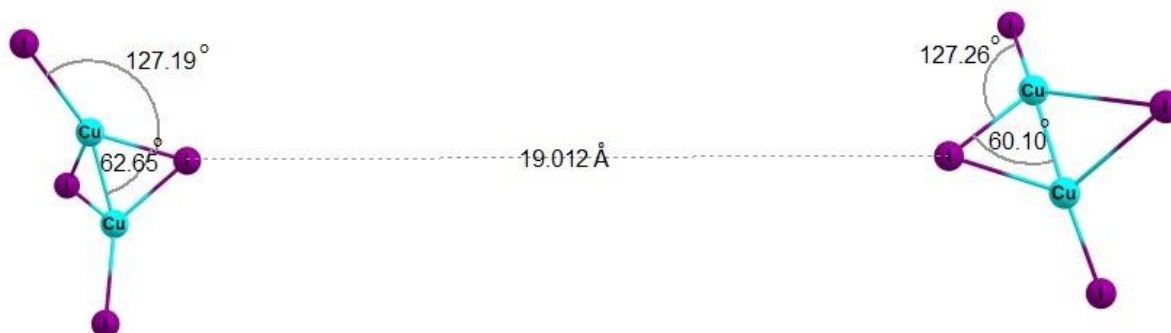

Figure 5.19: The incompletely optimized dimeric structure of D-Cu in the gas phase, showing a long I⋯I distince of 19.012 Å (E = − 3155.6714 a.u.) indicating the presence of repulsion.
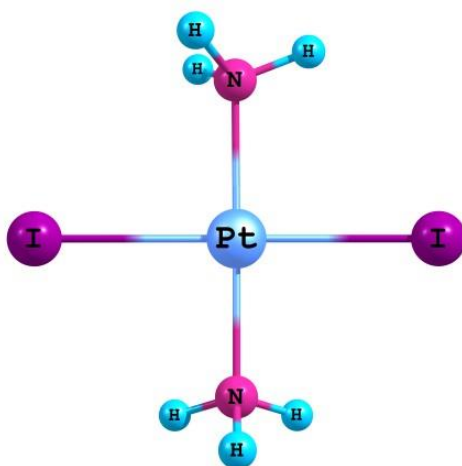
85

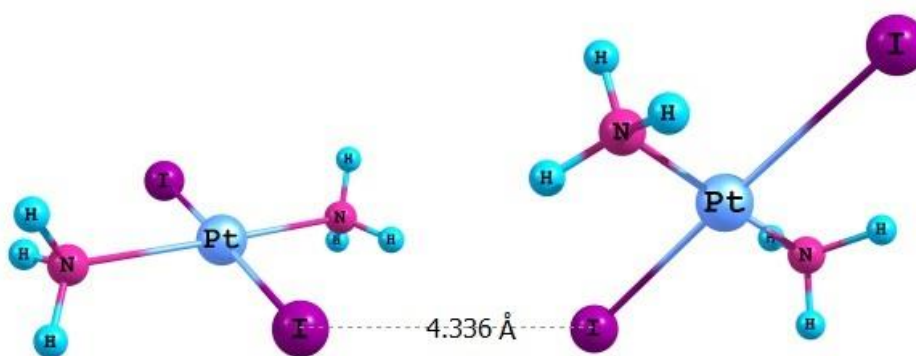**Figure 5.20:** Optimized structure of monomeric form of N-Pt in the gas phase.

Figure 5.21: Initial dimeric structure of N-Pt in the gas phase (I···I distance = 4.336Å).

Figure 5.22 shows the optimized structure of the N-Pt dimer obtained at the minimum energy conformation (E = − 1648.207 a.u.). As we can see in Figure 5.21 (based on results from the CSD), the I···I distance in N-Pt is 4.336 Å. After optimization, the two fragments have twisted such that they are positioned face on, with the two Pt atoms close to each other and the ligands staggered. This results in a significant increase in the I···I distance from 4.336 to 5.255 Å as shown in Figure 5.22.

This can be explained by the presence of a strong hydrogen bond with iodine (NH···I) in the Pt complex occurring at a short distance of 2.621 Å (see Figure 5.22). Since there are four such interactions that form, this conformation will be much more stable than a single, weak I···I interaction. These hydrogen bonds play a very significant role in keeping the two fragments close to each other.

86

In the case of the silver-iodide complex all attempts to optimize the monomeric form of P-Ag at the PBEPBE/aug-cc-pVTZ–pp level of theory failed. Optimization at a completely different level of theory (B3LYP/LANL2DZ) was also not successful. As seen in Figure 5.23, the structure unexpectedly started to break apart during the optimization process. Therefore, no further calculations to investigate the $I \cdots I$ interaction in P-Ag were carried out.
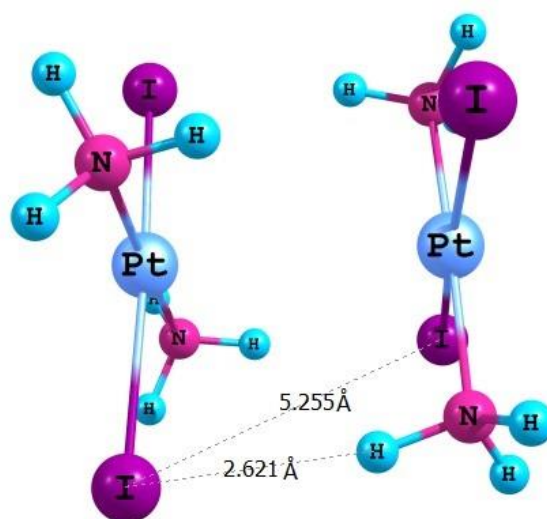

Figure 5.22: Optimized dimer structure of N-Pt in the gas phase indicating the presence of hydrogen bonding (NH···I) (distance = 2.621 Å) as well as the I···I distance.

Figure 5.23: Incompletely optimized of P-Ag, showing the structure breaking apart during optimization.

The initial structure of Z-Bi shows the presence of two Bi-I bonds with bond lengths of 3.009 and 3.083 Å (see Figure 5.24). The $I \cdots I$ interaction could also not be studied since several attempts at optimization failed, with the formation of new I–H and/or I–O bonds. Figure 5.25

87

(a) displays a non-optimized structure of Z-Bi, showing the formation of a new I-H bond with a bond length of 1.467Å. Figure 5.25 (b) displays another non-optimized structure of Z-Bi, showing the formation of I-H and I-O bonds with bond lengths of 1.526 and 2.097 Å respectively.
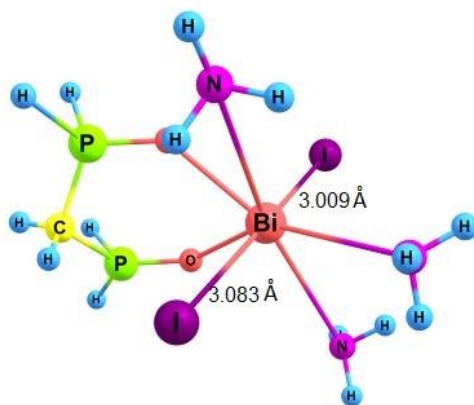

Figure 5.24: Initial molecular structure of Z-Bi used for optimization (Bi-I bond length = 3.083 Å and 3.009 Å).
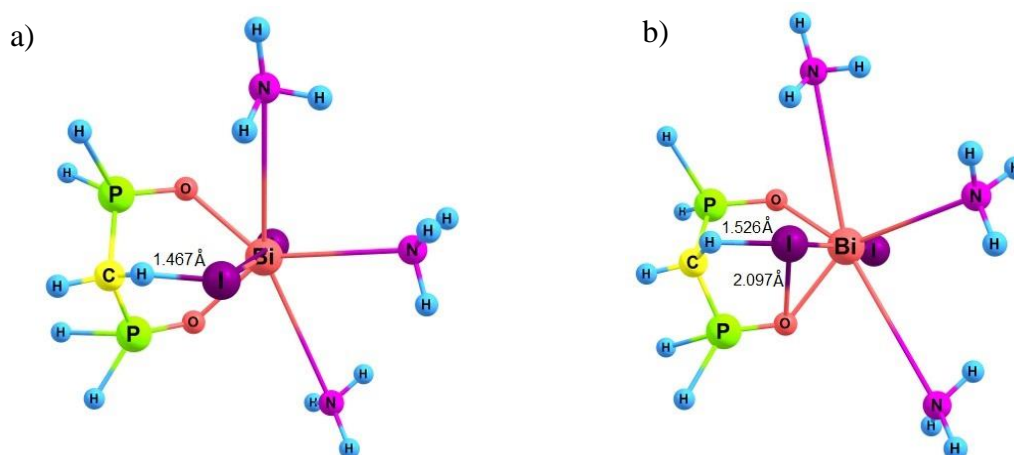

Figure 5.25: Non-optimized structures of Z-Bi showing: (a) the formation of an H-I bond at a distance of 1.467 Å and (b) the formation of H-I and O-I bonds at distances of 1.526 and 2.097 Å, respectively.

Since the optimization of the individual molecule was not successful, a dimeric form of the crystal structure was used as a basis for the optimization. A different level of theory, namely B3LYP/LANL2DZ, was used to obtain the final optimized structures of the monomeric and dimeric forms. Figure 5.27 shows the initial dimeric structure of Z-Bi before optimization.

88

Based on the CSD data, Z-Bi has a chair shape with an I···I distance of 4.184 Å in the dimer form.
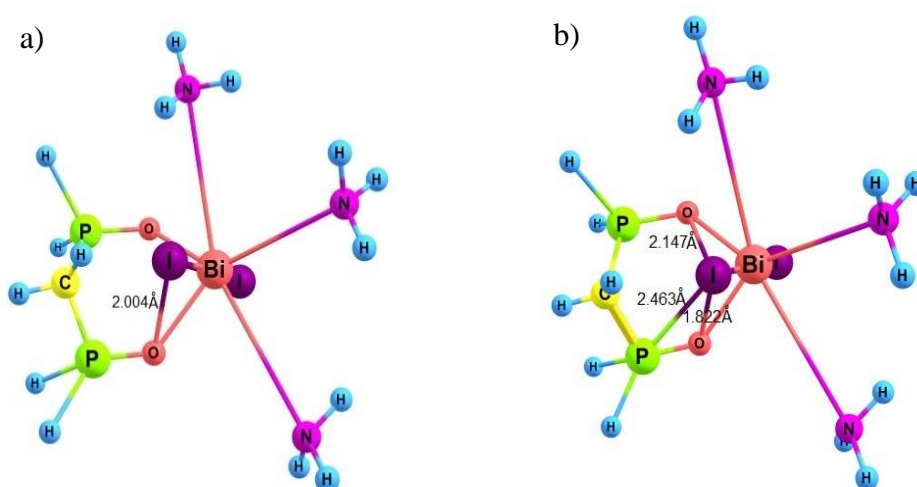
Figure 5.26: Non-optimized structures of Z-Bi showing the disappearance of H-I bonds and the formation of other new bonds: (a) O-I at a distance of 2.004 Å and (b) O-I at a distance of 1.822 and 2.147 Å.

Figure 5.27: Initial dimeric structure of Z-Bi in the gas phase (I···I distance = 4.187 Å).

During optimization attempts, an increase in the I···I distance from 4.184 Å to 6.439 Å was observed, however no minimum energy conformation was obtained. The distance between the iodine and the central Bi atom was frozen using the Modredundant option, but still

89

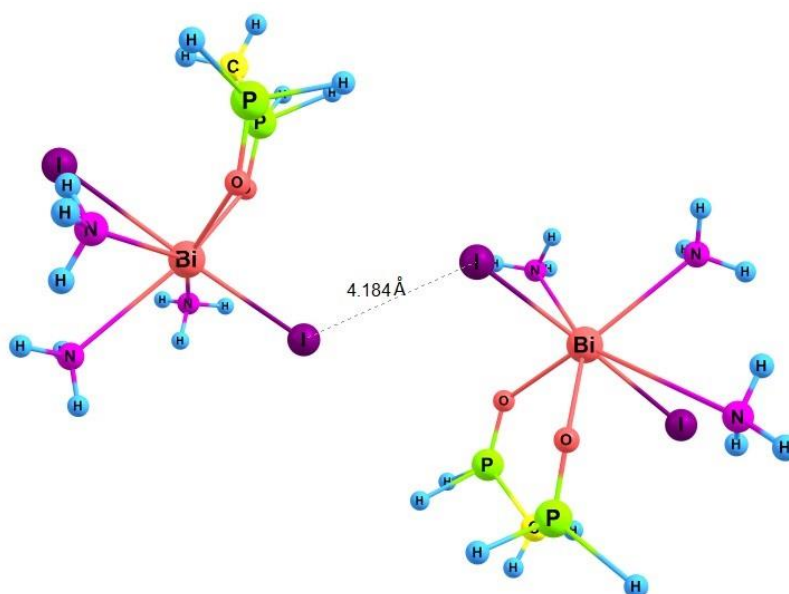showed an increase in the I···I distance from 4.184 Å to 6.266 Å with no convergence to minimum energy conformation. Additional constraints on the angle between the I and the Bi resulted in no significant change in the I···I distance (i.e., I···I distance changed only from 4.184 to 4.187 Å). Relaxation of the frozen coordinates eventually resulted in the minimum energy conformation of Z-Bi being obtained. This is shown in Figure 5.28, where a significant change in the I···I distance from 4.184 to 6.027 Å was observed.
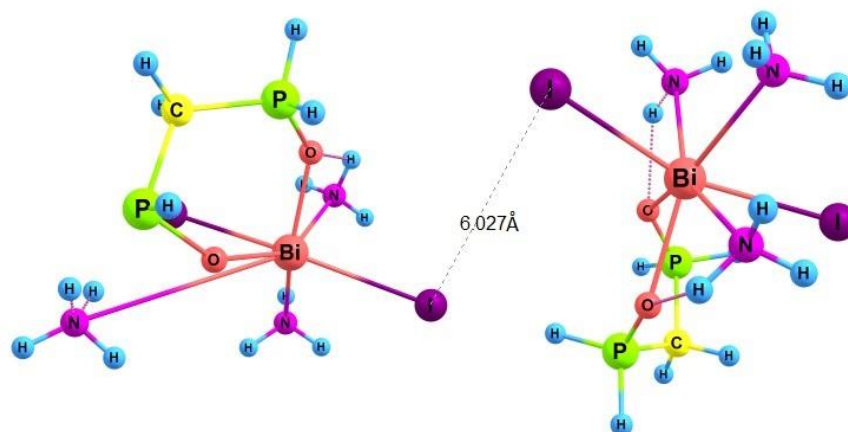

Figure 5.28: Final optimized dimeric structure of Z-Bi in the gas phase (I··I distance = 6.027 Å) at the B3LYP/LANL2DZ level of theory.

Similar to the Bi complex, first attempts to optimize the Hg complex using the PBEPBE/aug-cc-pVTZ–pp level of theory again failed, hence B3LYP/LANL2DZ was used to optimize the structure of J-Hg (E = − 147.8260 a.u.). Based on the structure obtained from the CSD, the J-Hg dimer has a bent shape with an I···I distance of 4.184 Å as indicated in Figure 5.29. Figure 5.29 also shows the presence of an interaction between two fragments via hydrogen bonding (PH···I) with a distance of 3.011 Å. We assume that the presence of hydrogen bonds contributes significantly to the stabilization of the final optimized structure of J-Hg (see Figure 5.30), which showed a minimum energy conformation of E = − 295.6871 a.u.

As can be seen in Figures 5.29 and 5.30, the I···I distance has slightly increased (by 0.307 Å) from 4.184 Å in the initial structure to 4.491 Å in the final optimized structure. One can also see that the Hg–I bond has been broken and the interaction distance between the two fragments via hydrogen interaction (PH···I) decreased considerably from 3.011 and 6.013 Å to 3.003 and 3.096 Å respectively. It thus appears that the iodine-hydrogen interaction plays

a significant role in keeping the two of fragments together, rather than the intermolecular I···I interaction, which is probably much weaker.
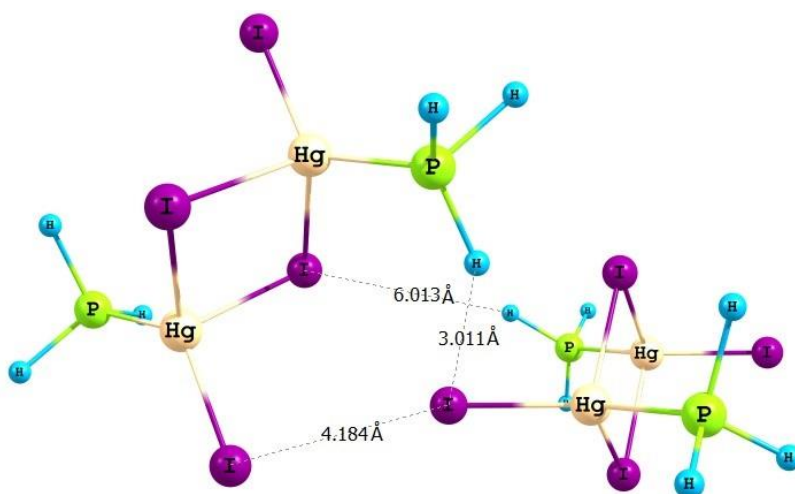
Figure 5.29: Initial dimeric structure of J-Hg in the gas phase (I···I distance = 4.184 Å).
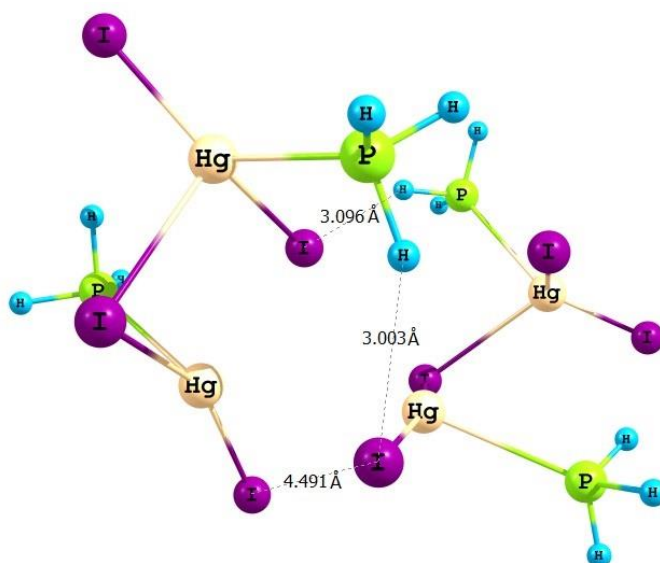
Figure 5.30: Optimized dimeric structure of J-Hg in the gas phase (I···I distance = 4.491 Å).

It was shown in Section 5.2.1 that for the Pd complex ($Pd_2I_6^{2-}$), two different models, namely those obtained from HOVMAH and AGAHOF were used. These two models have different I ··· I interaction shapes (a linear and chair shape) in the dimer form. When the ligands were simplified the same final structure was obtained as was shown in Figures 5.15 and 5.16. Figure 5.31 shows the initial dimeric structure of AGAHOF in the gas phase, which displays

an I⋯I distance of 4.171 Å. For the optimization of HOVMAH, two levels of theory (namely PBEPBE/aug-cc-pVTZ–pp and B3LYP/LANL2DZ) were tested. However, no minimum energy conformation was obtained when either levels of theory were used. No further optimization studies were tested for this model. Similarly, no optimized structure was obtained for the AGAHOF, when the PBEPBE/aug-cc-pVTZ–pp was used, while when the B3LYP/LANL2DZ level of theory was used, repulsion resulted in the ions moving away from each other. Optimization was stopped at the point shown in the Figure 32. The I⋯I distance increased significantly from 4.171 to 25.489 Å (E = − 644.4234512 a.u.).
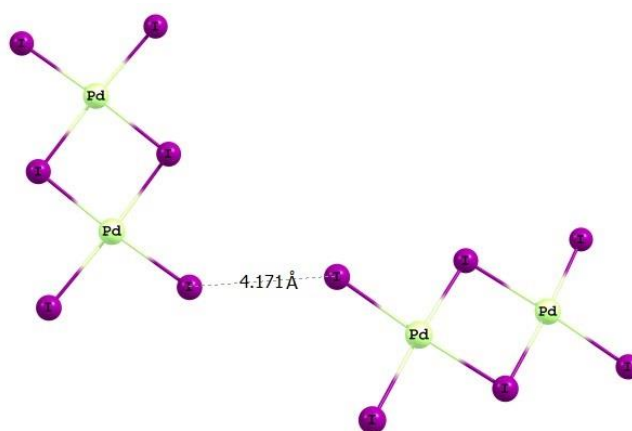
Figure 5.31: Initial dimeric structure of A-Pd in the gas phase, showing I⋯I distance of 4.171 Å.
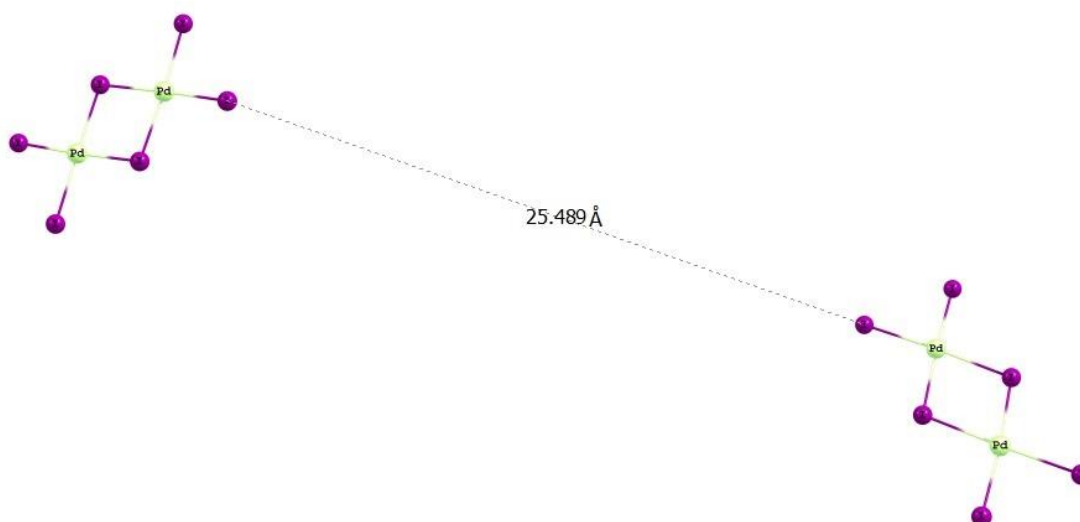
Figure 5.32: Incompletely optimized dimeric structure of A-Pd in the gas phase showing I⋯I distance of 25.489 Å.

92

The PBEPBE/aug-cc-pVTZ–pp level of theory was used successfully for the optimization of the molecular structure of O-Ga. Figure 5.33 shows the final optimized monomeric structure of O-Ga (E = − 1815.12104331 a.u.).
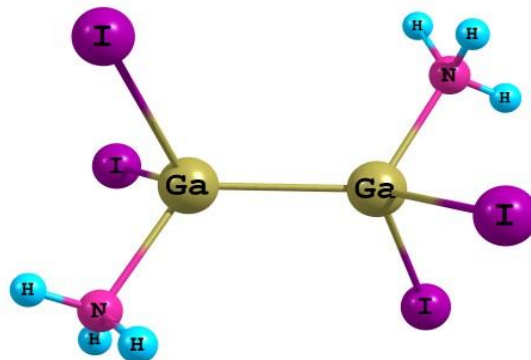
Figure 5.33: Optimized monomeric structure of O-Ga in the gas phase (E = − 1815.12104331 a.u.).

Figure 5.34 shows that initial dimer structure of O-Ga model, with an I⋯I distance of 4.021 Å. Optimization of this dimeric form of the O-Ga, at the PBEPBE/aug-cc-pVTZ–pp level of theory failed. Similarly, no convergence to a minimum energy was obtained with a different level of theory (B3LYP/aug-cc-pVTZ–pp) as the two Ga atoms moved away from each other. In an attempt to find a minimum energy geometry, which succeeded, therefore, the Ga–Ga distance in each fragment was initially frozen and then released. It can be seen that there was a slight increase in I⋯I distance from 4.021 to 4.255 Å (see Figure 5.35).
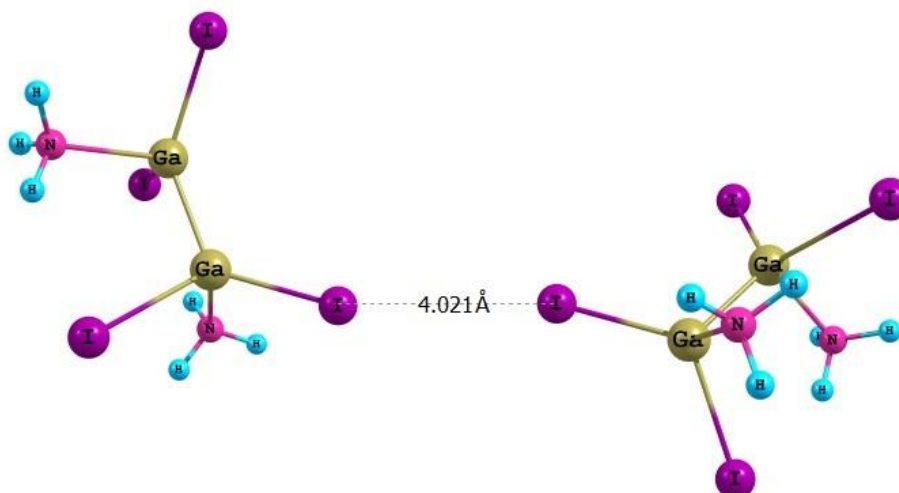
Figure 5.34: Initial dimeric structure of O-Ga in the gas phase (I⋯I distance = 4.021 Å).
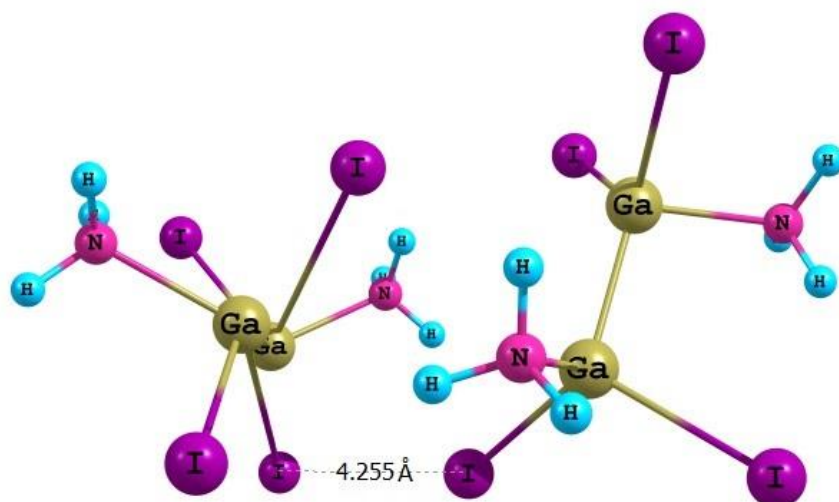
Figure 5.35: Optimized dimeric structure of O-Ga in the gas phase (I···I distance = 4.255 Å) (E = − 3631.5858116 a.u.).

It should be mentioned here that during optimization, a hydrogen bonding interaction formed, which played a significant role to keep the fragments very close to each other. This is displayed in Figure 5.36, which shows the presence of hydrogen-iodine interactions (NH···I) with distances of 2.835 and 2.971 Å in the optimized structure. Table 5.2 summarizes the intermolecular distances that were obtained for selected metal-iodide complexes containing Pd, Ga, Cu, Bi, Hg or Pt. The I···I distances obtained from the CSD are also included for comparison.
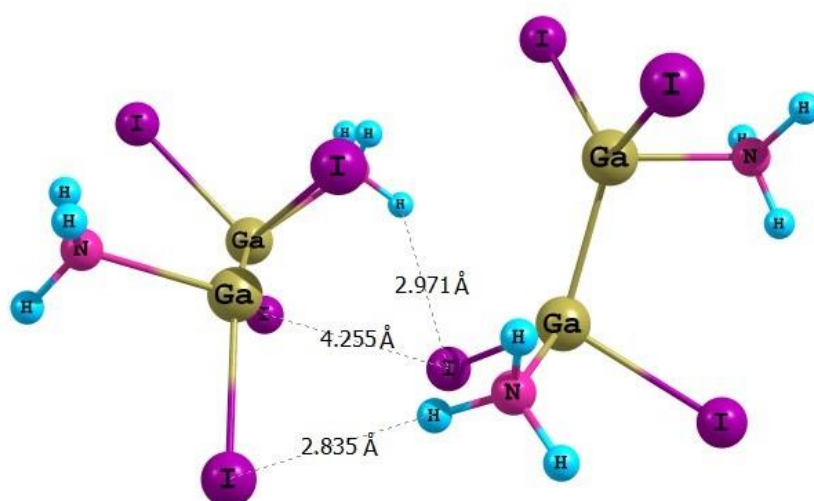
Figure 5.36: A different view of the optimized dimeric structure of O-Ga in the gas phase, showing the presence of NH···I interactions with distances of 2.835 and 2.971 Å.

Table 5.2: Summarized results of intermolecular I⋯I distances observed in the gas phase compared to data obtained from the CSD.

Metal	Model	d (I⋯I) (Å)	
		CSD	Gas phase
Cu	DEHKACO2	4.097	*
Pt	NUKCAY	4.251	5.255
Bi	ZUCKIR	4.184	6.027
Hg	JAHCOK01	4.184	4.491
Ga	OJAVIE	4.021	4.255
Pd[a]	AGAHOF	4.171	*
Pd[b]	HOVMAH	3.825	**
Ag	PAWXOB	4.238	**

* Optimization was stopped–the lowest energy conformation will be an infinite distance apart.

** No minimum energy conformation could be identified.

From Table 5.2, one can see that based on results from the CSD, the order of increasing intermolecular distance is as follows:

$$Pd^b < Ga < Cu < Pd^a < Bi, Hg < Pt$$

However, our results show that there are significant differences between the I⋯I intermolecular distance calculated for the gas phase compared to data obtained from the CSD. Our observations indicate that the order of increasing intermolecular distance in the gas phase is as follows:

$$Ga < Hg < Pt < Bi < Cu = Pd^a$$

The differences between the I⋯I distances in the gas phase and crystal structure can be attributed to the effect of the chemical surroundings in the crystal structure, which can reduce the electronic repulsion. On the other hand, in the case of N-Pt, J-Hg and O-Ga hydrogen bonding occurred in the gas phase, which played a large role in keeping the two fragments close to each other. This resulted in a slight difference in the I⋯I intermolecular distance in the metal complexes of Pt, Hg, and Ga (see Table 5.2).

5.2.2.2 I⋯I interaction energy (E$_{INT}$)

The interaction energies (E$_{INT}$) between metal-iodide complexes exhibiting the I⋯I interaction can be calculated by:

$$E_{INT} = E_{dimer} - 2\,(E_{monomer}) \qquad\qquad 5.1$$

However, since for many cases either optimization of the monomer or dimer failed it was only possible to determine E$_{INT}$ for the Pt complex. This is displayed in Table 5.3. However, this interaction energy is not exclusively due to the I⋯I interaction, but primarily due to the NH⋯I hydrogen bonds.

Table 5.3: Interaction energy (E$_{INT}$) observed in the gas phase.

	E$_{INT}$ (kcal/mol)	
Metal	Model	Gas phase
Pt	N-Pt	− 35.4

This result is not unexpected, since I_3^-⋯I_3^- interactions were found to be repulsive in the gas phase [1]. However, calculations in a solvent showed that the electrostatic environment stabilized the system to the extent the I_3^-⋯I_3^- interaction become attractive in solvents with high dielectric constants. Hence the next step in this study was to apply the same method to the metal-iodide complexes.

5.2.3 Modelling of the I⋯I interactions in an implicit solvent environment

Modelling of I⋯I interactions within dimers of selected metal-iodide complexes was performed in an implicit solvation model, i.e., the polarizable continuum model [9, 10]. All calculations were performed using of the Gaussian 09 rev. B.01 package [11], utilizing different levels of DFT theory (namely PBEPBE and B3LYP) in combination with the aug-cc-pVTZ–pp (for the metal atoms) and 6-31G(d) (for all other atoms) basis sets. The influence of the surrounding environment on the I⋯I intermolecular interactions in metal-iodide complexes was thus investigated. Different environments were achieved by changing the solvent to have different dielectric constants, such as water (ε = 78.3553), ethanol

(ε = 24.852), and chloroform (ε = 4.7113). The effect of these solvents on the intermolecular distance d ($I \cdots I$) and the ($I \cdots I$) interaction energy was investigated. Groenewald *et al*. [1] also performed an extensive theoretical investigation, where they studied the influence of the electrostatic environment on the $I_3^- \cdots I_3^-$ interaction. Optimizations in the gas phase and in an implicit polarizable continuum solvent model with a variety of solvents showed that there is a significant dependence of the $I_3^- \cdots I_3^-$ interaction energy on the dielectric constant. The authors concluded that $I_3^- \cdots I_3^-$ interactions can be favored in the appropriate environment, where the strength of the $I_3^- \cdots I_3^-$ interaction energy converges as the dielectric constant increases.

5.2.3.1 Intermolecular distance *d* (I $\cdots$ I)

In general, the approach of undertaking the calculations in solvent was successful – only the Pd complex did not yield a stable dimeric complex in solvents, as compared to the gas phase where no complexes other than Pt formed stable dimeric structures. In order to determine if there is any substantial dependence of the $I \cdots I$ interaction energy on the dielectric constant of the solvent as was found for the I_3^- species [1], the $I \cdots I$ intermolecular distances of the optimized structures were compared to the values obtained from the CSD. Table 5.4 shows a summary of the $I \cdots I$ distances obtained in different solvents. In addition, the $I \cdots I$ distance for the gas phase has been included for comparison.

Table 5.4: A summary of the I$\cdots$I distances in different solvents and the gas phase, along with the CSD value as a benchmark.

			d(I$\cdots$I) (Å)			
Metal	Model	CSD	Gas phase	Chloroform (ε = 4.7113)	Ethanol (ε=24.852)	Water (ε=78.3553)
Cu	DEHKACO2	4.097	19.012*	38.378*	4.414	4.321
Pt	NUKCAY	4.251	5.255	4.043	4.069	4.069
Bi	ZUCKIR	4.184	6.027	5.932	5.171	5.144
Hg	JAHCOK01	4.184	4.491	4.380	4.742	4.805
Ga	OJAVIE	4.021	4.255	**	**	4.117
Pd	AGAHOF	4.171	25.489*	37.928*	41.152*	40.542*

* Optimization was stopped, the lowest energy conformation will be an infinite distance apart.

** No minimum energy conformation could be identified.

Table 5.4 shows that most metal-iodide complexes such as those containing Pt, Ga, Bi or Hg showed only minor changes in the $I \cdots I$ distances observed in the gas phase and in solvent environment compared to that obtained from the CSD. However, the Cu complexes showed a dramatic variation in $I \cdots I$ distances compared to the distance obtained from the CSD, when different solvents were used as electrostatic environments. Although there were slight increases in the $I \cdots I$ distance of 0.224 and 0.317 Å observed in water and ethanol respectively, the Cu complex did not form a stable adduct when chloroform was used as the solvent.

In the gas phase, electrostatic repulsion due to the close proximity of the two anions dominates over the dispersion component of the interaction since there is no significant influence by the surrounding. When the dimer is placed in different electrostatic environments it is possible to obtain stable adducts for Cu with reasonably short $I \cdots I$ distances if the dielectric constant of the surroundings is high (4.321 and 4.414 Å when the dimer is placed in water and ethanol, respectively). This indicates that there is a stabilizing effect due to the presence of water and ethanol. Furthermore, there is a slight increase of about 0.1 Å in the intermolecular distance in ethanol as compared to water. The reason for the stabilization is that the dielectric field surrounding the anions damps the electrostatic repulsion, thus the attractive dispersion plays a more important role, stabilizing the overall interaction. In agreement with our findings, Groenewald et al. [1] observed a slight decrease in the $I_3^- \cdots I_3^-$ intermolecular distance (i.e., 0.1 Å) when a dimer of $I_3^- \cdots I_3^-$ was placed in water compared to ethanol. They attributed this to the fact that water has a more polar structure compared to ethanol, which provides more stabilization to the dimer.

For Pd the dispersion component of the interaction is so weak that even placing the dimer in an electrostatic environment does not stabilize it sufficiently to form a stable adduct. This disagrees with results published in 2011 by Grimme and Djukic [12], who reported a theoretical study on the interactions between ions with the same sign of charge. The authors studied cation-cation interactions in a dimer of rhodium complex ($[(PhNC)_4Rh]_2^{2+}$) in the gas phase and acetonitrile. Although there was a repulsion (40 kcal/mol) present at equilibrium, a stable structure was obtained. They indicated that the driving force behind the formation of a stable doubly charged complex can be attributed to the presence of dispersion interactions. The authors mentioned that a "proper tuning of their energetic contribution may stabilize

molecular aggregates, which would be otherwise highly unstable by virtue of other overwhelming repulsive terms" [12]. They also concluded that dispersion corrections are essential when utilising DFT functionals to study these complexes, hence our use of Grimme's D3 dispersion correction in this study.

For the Pt complex which formed a weak interaction in the gas phase, as indicated by a longer I⋯I distance compared to data obtained from the CSD, when the dimer is placed in an electrostatic environment (i.e., solvent) the I⋯I distance decreases considerably. All solvents used showed a similar effect, where the I⋯I distance decreased by ~1.2 Å compared to the value observed in the gas phase, and about 0.2 Å compared to the experimental structure. This was attributed to the presence of hydrogen bonding in the gas phase (NH⋯I), which plays a significant role in stabilizing the dimer, thus breaking the I⋯I. In solvents the hydrogen bonding is weaker, allowing the dispersion-driven I⋯I interaction to dominate.

Figures 5.37, 5.38, and 5.39 show the optimized structures of N-Pt in water, ethanol and chloroform respectively. In general, there was a significant decrease by 1.2 Å in the I⋯I distance compared to that observed in the gas phase, while the NH⋯I distance increased compared to the gas phase structure. As seen in Figures 5.37 and 5.38 the dimer exhibited the same I⋯I distance of 4.069 Å when the dimer was placed in water and ethanol as compared to that observed in the gas phase (5.255 Å). However, when chloroform was used as the solvent lower I⋯I distance of 4.043 Å was obtained as compared to both water and ethanol. This can be attributed to the substantial dependence of hydrogen bond length on the electrostatic environment, i.e., solvent used.
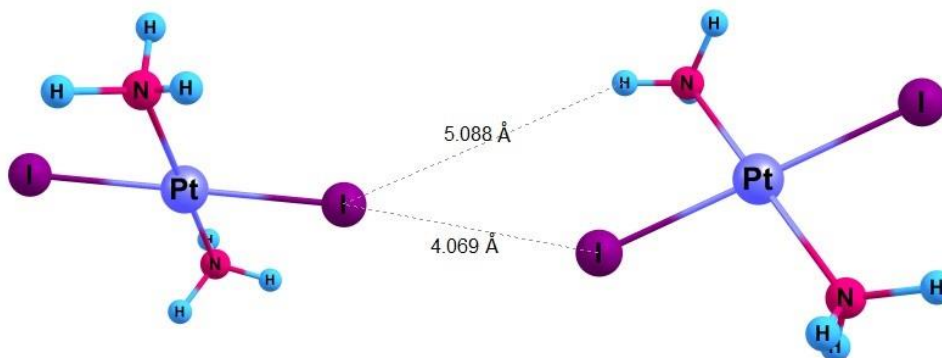
Figure 5.37: Optimized structure of N-Pt in water, showing the I⋯I distance of 4.069 Å and NH⋯I distance of 5.088 Å.

99
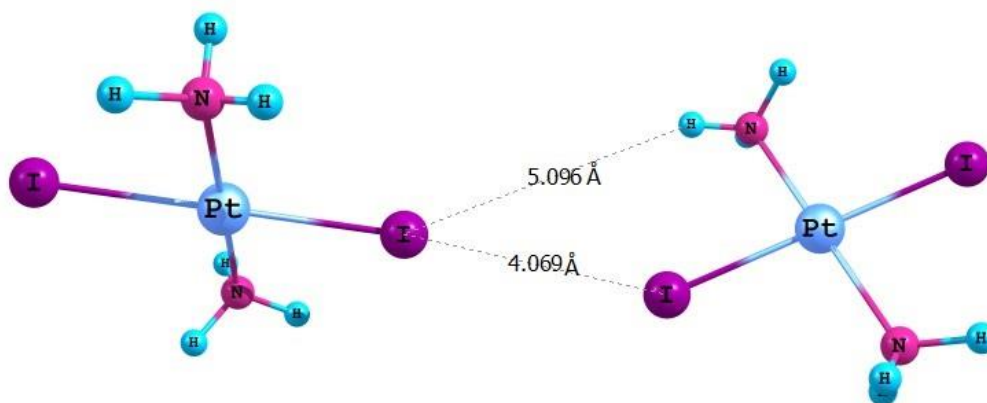
Figure 5.38: Optimized structure of N-Pt in ethanol, showing the I···I distance of 4.069 Å and NH···I distance of 5.096 Å.
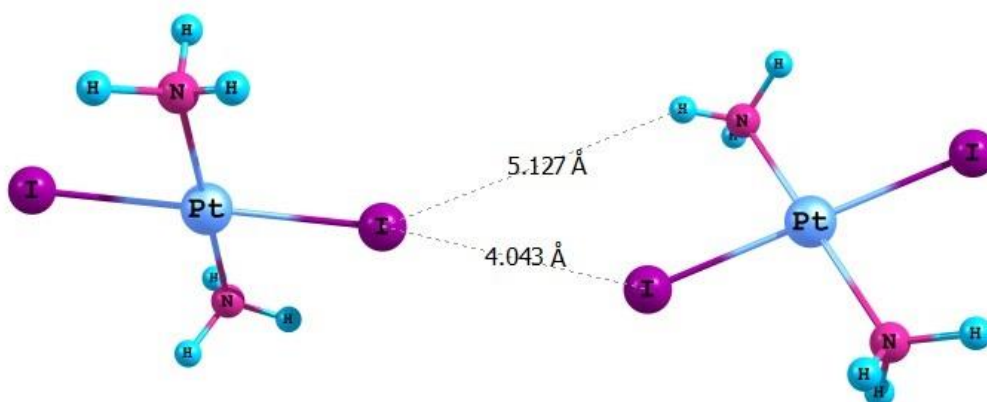
Figure 5.39: Optimized structure of N-Pt in chloroform, showing the I···I distance of 4.043 Å and NH···I of 5.127 Å.

From Figures 5.37, 5.38, and 5.39, one can clearly see that there is a significant increase in hydrogen bond length as the solvent changed from water or ethanol to chloroform. In other words, the increase in the dielectric constant of the solvent resulted in a significant increase in the hydrogen bond strength, which led to a significant decrease in the I···I distance. This is in a good agreement with the findings of Aquino *et al.* [13] who investigated the effect of different solvents on the hydrogen bonding observed in dimers of acetic acid and in complexes of acetic acid with several polar molecules utilizing DFT. Three solvents of different polar strength (heptane, water and dimethyl sulfoxide) and their effect on the formation of stable structures were analyzed. The authors indicated that highly polar solvents will stabilize the strong hydrogen bonding interactions formed in the neutral complexes. As

100

the polarity of the solvent used decreases, there is a lengthening of the hydrogen bonds, which also results in a significant decrease in the stabilization of these bonds. On the other hand, polar solvents may lead to breaking the weak hydrogen bonding completely. In general, weaker hydrogen bonding occurred at longer distances due to the effect of a strong polar solvent in cyclic and neutral dimers. Thus, the distance between the hydrogen bonding decreased with increasing the polarity of the solvent. Although it was shown that several factors could affect the stabilization of the investigated complexes in different polar environments, the authors concluded that as the dielectric constant of the solvent increases, the intermolecular interaction decreases considerably.

A similar theoretical study was performed by Lu *et al.* [14] on halogen bonding (X-B) in solution, where they found similar solvent-dependent behavior to that found for hydrogen bonding. The authors studied the influence of the surrounding medium on weak halogen bonds, where a series of dimeric complexes of halobenzene (PhX) with three electron donors (H_2O, HCHO, and NH_3) were investigated by means of DFT calculations. The PCM implicit solvation model was used to study the effect of three different solvents, which have a wide range of dielectric constants (i.e., cyclohexane, chloroform, and water). The authors indicated that the solvent has a slightly destabilizing effect on weak halogen bonds, where the length of the halogen bonds are found to decrease in solution, which result in the formation of C-X bonds that are elongated. It has been shown that the influence of the solvent on the intermolecular interactions can be attributed to the decrease in the contribution of the electrostatic interactions to the total interaction energy which occurs as the dielectric constant increases [4, 6, 7].

Our results are opposite to these studies since in the gas phase the electrostatic interactions are repulsive. In solvents the electrostatic interaction (repulsion rather than attraction in the literature studies) is reduced, leading to stabilization of the system.

For Bi the I⋯I distance decreased considerably in the presence of a solvent as compared to the gas phase. Compared to the CSD, the I⋯I distance increased in water (0.96 Å), in ethanol (0.99 Å) and in chloroform (1.75 Å), although the interactions are still considerably longer than in the crystal structures. It should be noted that the I⋯I distances in water and ethanol are shorter than in chloroform, as might be expected due to the decrease in electrostatic repulsion.

101

Hg showed a different behavior, where the I⋯I distance increased from the gas phase value by 0.314 Å in water and 0.251 Å in ethanol, however a decrease of 0.111 Å was observed in chloroform as compared to the gas phase. This can be attributed to the change that occurs in each fragment in the optimized structure in an electrostatic environment. The presence of the dimer in the solvent resulted in the breakage of the Hg–I bond as was shown in Figure 5.30. In a study performed by Sone *et al.* [15], the authors investigated the effect of different solvents on the bonding of Hg (II) with halides (X). The authors showed that the strength of the Hg–X bond (i.e., Hg–I) in solvents decreases significantly relative to the gas phase. They attributed this to the fact that the solvent molecules tend to assemble around the central Hg atom in the linear HgI_2 molecule and coordinate to it. This will lead to the accumulation of the negative ends of the solvent molecules around the Hg atom, which substantially weakens the Hg–I bond.

The Ga complex showed a similar behavior to the complex containing Bi when the dimer was placed in water, however no stable structure could be obtained when ethanol and chloroform were used. As seen in Table 5.4, the I⋯I distance decreased by about 0.14 Å in water as compared to the gas phase, which was attributed to the added stabilization provided by water. It should be mentioned that when we tried to optimize the structure in both ethanol and chloroform at the B3LYP/aug-cc-pVTZ–pp level of theory no convergence to a minimum energy structure was obtained despite all efforts. Assuming that a length-strength relationship holds it appears that in water the I–M–I⋯I–M–I interaction decreases as follows based on the I⋯I distances: Pt > Ga > Cu > Hg > Bi > Pd. However, it is necessary to calculate E_{INT} values to confirm this.

5.2.3.2 I⋯I interaction energy (E_{INT})

The interaction energies (E_{INT}) between complexes containing Cu, Pt or Pd have been investigated (see Table 5.5). It can be seen that E_{INT} in the copper complex changed considerably in the solvent model compared to the gas phase. The strength of I⋯I interaction in these different solvents was as follows: water > ethanol > chloroform. This can be attributed to the different polarity of these solvents. Here, we should note that the I⋯I interaction energy in water (+0.53 kcal/mol) is less repulsive than that calculated in ethanol (+4.35 kcal/mol) and chloroform (+6.19 kcal/mol), due to the polarity of water.

102

It has been shown that the E_{INT} depends greatly on the level of theory and the basis sets used. In an extensive study, Volkov *et al.* [16] explored the dependence of the intermolecular electrostatic interaction energy in molecular systems on the DFT method used. They investigated different dimers of α-glycine at various level of theory using different basis sets. DFT with the pure PBEPBE functional as well as with the hybrid B3LYP functional were used in combination with the aug-cc-pVTZ–pp and 6-31G** basis sets. The authors showed that electrostatic interaction energies obtained from the B3LYP functional are in very good agreement with those obtained by advanced correlated methods such as MP2, when augmented triple-zeta or quadruple-zeta basis sets are used.

Table 5.5 also shows that E_{INT} for Pt complex in the gas phase is much stronger than that observed in water, ethanol or chloroform. Similar to Cu, the strength of the I⋯I interaction in these different solvents is as follows: water > ethanol > chloroform. Weak interaction energies (–2.22 to –2.60 kcal/mol) were obtained with all solvents, as compared to the gas phase, as the strong NH⋯I hydrogen bonds stabilizing the gas phase structure were not formed in the solvents. Similarly, the Pd complex showed strongly a repulsive interaction energy between two anions in chloroform (+5.5 kcal/mol), where the interaction energy in water (–0.22 kcal/mol) and in ethanol (+0.78 kcal/mol) are weakly repulsive due to the polarity of water and ethanol. As the optimization continued the two fragments started to move away from each other (similar to Figure 5.32), which resulted in a significant decrease in the I⋯I interaction energy. Thus, the I⋯I interaction energy was calculated at the point where optimization was stopped.

Table 5.5: The interaction energy (E_{INT}) between I⋯I in different transition metal-iodine complexes.

Metal	Model	Gas phase	E_{INT} (kcal/mol)		
			Chloroform (ε = 4.7113)	Ethanol (ε=24.852)	Water (ε=78.3553)
Cu	D-Cu	*	+ 6.19*	+ 4.35	+ 0.53
Pt	N-Pt	− 35.4	− 2.22	− 2.50	− 2.60
Pd	A-Pd	*	+ 5.5*	+0.78*	− 0.22*

* At the point where optimization was stopped.

103

It should be mentioned here that it was not possible to obtain the interaction energies for Ga, Hg and Bi. Attempts to optimize the Ga complex structure in a solvent model failed as discussed in Section 5.2.2.1. Similarly, optimization of Bi and Hg complexes resulted in the breakage of the bond between the I atom and the metal atom even in solvents (similar to Figures 5.28 and 5.30). Figure 5.40 shows the E_{INT} of Cu and Pt as a function of the dielectric constant. It can be seen that the studied metal complexes exhibit slightly different behavior.
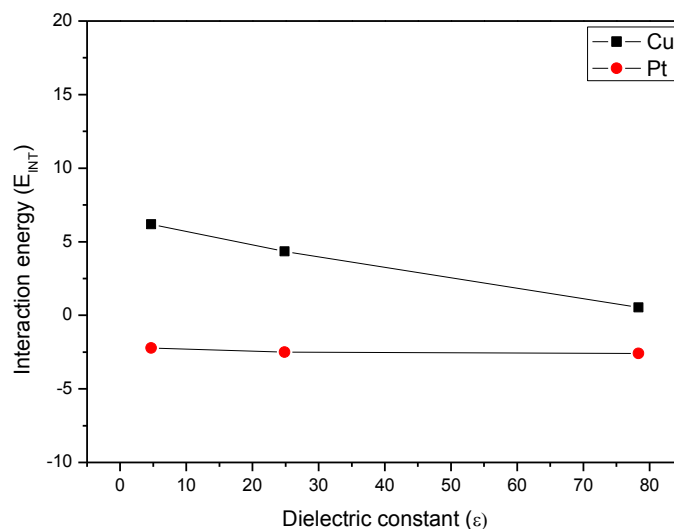
Figure 5.40: E_{INT} for selected dimers containing Cu or Pt in various solvents: water, ethanol and chloroform.

However, in general we can conclude that the strength of the interaction energy observed in different solvents decreases in the following order (E_{INT} increases as the dielectric constant increases):

$$E_{INT} \text{ (water)} > E_{INT} \text{ (ethanol)} > E_{INT} \text{ (chloroform)}$$

As discussed above, the $I \cdots I$ interaction energies in water, ethanol and chloroform summarized in Table 5.5 show a substantial dependence on the surrounding environment. It is clear that the interaction energy depends on the dielectric constant of the solvent used. The same trend can be observed for all studied metal complexes, where the two fragments are more attracted to each other in water compared to ethanol and chloroform. In other words, as the dielectric constant increases, the $I \cdots I$ intermolecular distance decreases while the

interaction energy (E_{INT}) increases. It should be noticed here that the interaction energy (E_{INT}) of Pt is greater than for Cu.

5.3 Conclusion

The strengths of the I$\cdots$I interactions in the dimer form (i.e, I–M–I$\cdots$I–M–I) were calculated using DFT methods for the selected metal iodides. These include complexes containing the following metals: copper (Cu), mercury (Hg), gallium (Ga), silver (Ag), platinum (Pt), palladium (Pd) or bismuth (Bi). For some metal iodides, optimization for pairs of complexes was successfully achieved at the PBEPBE/aug-cc-pVTZ–pp, B3LYP/aug-cc-pVTZ–pp, or B3LYP/LANL2DZ levels of theory, where values of the minimum interaction energies involving I$\cdots$I interactions in these metal-iodide complexes were obtained. The optimized geometries were then used to calculate the interaction energies. The effect of the electrostatic environment (i.e., solvent) on the I$\cdots$I interaction strength was also studied utilizing an implicit solvent model. Solvents of different polarity including water, ethanol and chloroform, which describe the effect of the electrostatic environment, were used. Results indicated that there are considerable differences between the I$\cdots$I distances calculated in different solvents compared to values obtained from the CSD. Generally speaking, the I$\cdots$I intermolecular distance decreases as the dielectric constant increases, hence most metal-iodide complexes formed stable I$\cdots$I linked dimers in water, as opposed to the gas phase when only Pt iodide formed a stable dimer. The order of increasing I$\cdots$I intermolecular distances based on the CSD is as follows: Ga < Cu < Pd < Bi = Hg < Pt. However, our results showed that the order of increasing the I$\cdots$I intermolecular distances observed in water is in the following order: Pt < Ga <Cu < Hg < Bi. This might be attributed to the presence of hydrogen bonds in Pt and Ga complexes, while for Hg and Bi no such bonds were observed.

In addition, the I$\cdots$I distances in Cu showed a dramatic change when various solvents with different polarity were used as the electrostatic environment showing that higher dielectric constants were required to make the I$\cdots$I interaction attractive than for Pt. Confirming the trends in the I$\cdots$I distances, the interaction study also showed that there is a substantial change in the I$\cdots$I interaction energy (E_{INT}) depending on the electrostatic environment in which the complex is found. Results indicated that as the dielectric constant increases the stabilizing E_{INT} increases. It was shown that the strength of the I$\cdots$I interaction energy in our

selected solvents decreases as follows: E_{INT} (water) > E_{INT} (ethanol) > E_{INT} (chloroform). This was attributed to a substantial dependency of I$\cdots$I interaction energy on the dielectric constant of the solvent, due to damping of the repulsive electrostatic interactions. Furthermore, results showed that the I$\cdots$I interaction energy in metal-iodide complexes are only attractive for the Pt complex.

5.4 References

1. Groenewald, F., Esterhuysen, C. and Dillen, J., *Extensive theoretical investigation: influence of the electrostatic environment on the $I_3^-\cdots I_3^-$ anion–anion interaction.* Theoretical Chemistry Accounts **2012**, 131(10), 1-12.

2. Boys, S.F. and Bernardi, F., *The calculation of small molecular interactions by the differences of separate total energies. Some procedures with reduced errors.* Molecular Physics **1970**, 19(4), 553-566.

3. Simon, S., Duran, M., and Dannenberg, J., *How does basis set superposition error change the potential surfaces for hydrogen‑bonded dimers?* The Journal of Chemical Physics **1996**, 105(24), 11024-11031.

4. Perdew, J.P., Burke, K., and Ernzerhof, M., *Generalized Gradient Approximation Made Simple.* Physical Review Letters **1996**, 77(18), 3865-3868.

5. Xu, X. and Goddard, W.A., *The X3LYP extended density functional for accurate descriptions of nonbond interactions, spin states, and thermochemical properties.* Proceedings of the National Academy of Sciences of the United States of America **2004**, 101(9), 2673-2677.

6. Becke, A.D., *Density-functional thermochemistry. V. Systematic optimization of exchange-correlation functionals.* The Journal of Chemical Physics **1997**, 107(20), 8554-8560.

7. Dunning, T.H., *Gaussian basis sets for use in correlated molecular calculations. I. The atoms boron through neon and hydrogen.* The Journal of Chemical Physics **1989**, 90(2), 1007-1023.

8. Woon, D.E. and Dunning, T.H., *Calculation of the electron affinities of the second row atoms: Al–Cl.* The Journal of Chemical Physics **1993**, 99(5), 3730-3737.

9. Tomasi, J., Mennucci, B., and Cammi, R., *Quantum Mechanical Continuum Solvation Models.* Chemical Reviews **2005**, 105(8), 2999-3094.

10. Miertuš, S., Scrocco, E., and Tomasi, J., *Electrostatic interaction of a solute with a continuum. A direct utilizaion of AB initio molecular potentials for the prevision of solvent effects.* Chemical Physics **1981**, 55(1), 117-129.

11. Frisch, M.J., Trucks, G.W., Schlegel, H.B., Scuseria, G.E., Robb, M.A., Cheeseman, J.R., Scalmani, G., Barone, V., Mennucci, B., Petersson, G.A., Nakatsuji, H., Caricato, M., Li, X., Hratchian, H.P., Izmaylov, A.F., Bloino, J., Zheng, G., Sonnenberg, J.L., Hada, M., Ehara, M., Toyota, K., Fukuda, R., Hasegawa, J., Ishida,

M., Nakajima, T., Honda, Y., Kitao, O., Nakai, H., Vreven, T., Montgomery Jr., J.A., Peralta, J.E., Ogliaro, F., Bearpark, M.J., Heyd, J., Brothers, E.N., Kudin, K.N., Staroverov, V.N., Kobayashi, R., Normand, J., Raghavachari, K., Rendell, A.P., Burant, J.C., Iyengar, S.S., Tomasi, J., Cossi, M., Rega, N., Millam, N.J., Klene, M., Knox, J.E., Cross, J.B., Bakken, V., Adamo, C., Jaramillo, J., Gomperts, R., Stratmann, R.E., Yazyev, O., Austin, A.J., Cammi, R., Pomelli, C., Ochterski, J.W., Martin, R.L., Morokuma, K., Zakrzewski, V.G., Voth, G.A., Salvador, P., Dannenberg, J.J., Dapprich, S., Daniels, A.D., Farkas, Ö., Foresman, J.B., Ortiz, J.V., Cioslowski, J., and Fox, D.J., *Gaussian 09, Revision B.01*, Gaussian, Inc., **2009**: Wallingford, CT, USA.

12. Grimme, S. and Djukic, J.-P., *Cation−Cation "Attraction": When London Dispersion Attraction Wins over Coulomb Repulsion.* Inorganic Chemistry **2011**, 50(6), 2619-2628.

13. Aquino, A.J., Tunega, D., Haberhauer, G., Gerzabek, M.H., and Lischka, H., *Solvent Effects on Hydrogen Bonds A Theoretical Study.* The Journal of Physical Chemistry A **2002**, 106(9), 1862-1871.

14. Lu, Y., Li, H., Zhu, X., Liu, H., and Zhu, W., *Effects of solvent on weak halogen bonds: Density functional theory calculations.* International Journal of Quantum Chemistry **2012**, 112(5), 1421-1430.

15. Sone, K., Aritaki, M., Hiraoka, K., and Fukuda, Y., *Solvent Effect on the Raman Spectra of Mercury(II) Halides.* Bulletin of the Chemical Society of Japan **1976**, 49(7), 2015-2016.

16. Volkov, A., King, H.F., and Coppens, P., *Dependence of the Intermolecular Electrostatic Interaction Energy on the Level of Theory and the Basis Set.* Journal of Chemical Theory and Computation **2006**, 2(1), 81-89.

Chapter 6

Study of the I–M–I⋯I–M–I interactions by Natural Bond Orbital and Atoms in Molecules analyses in the gas phase and in "solvents"

6.1 Introduction

In this chapter we describe the investigation of the nature and properties of the $I \cdots I$ intermolecular interactions in dimers of two different transition metal-iodide complexes, containing Cu and Pt. These were chosen as they were the only two complexes that could be optimized resulting in the successful calculation of the $I \cdots I$ interaction energy. Various parameters with regards to the $I \cdots I$ interaction were investigated based on Natural Bond Orbital (NBO) and Atoms in Molecules (AIM) analyses. The calculations were performed in the gas phase as well as in an implicit solvent model using various solvents with a wide range of dielectric constants (i.e., water, ethanol and chloroform). Utilizing NBO calculations, the $I \cdots I$ interactions were analyzed using the distribution of electron density in two different types of orbitals, which are most important for characterising the donor-acceptor nature of these types of interaction. These are the lone pair (LP) orbitals, which represent the donor orbitals and the Rydberg orbitals (RY*) that act as acceptor orbitals. The stabilization energy (ΔE_S) of these donor-acceptor $I \cdots I$ intermolecular interactions was also estimated. Moreover, three AIM parameters, the electron density $\rho_b(r)$, Laplacian of the electron density $L(\rho_b(r))$ and the total energy density $H_b(r)$, were determined at the $I \cdots I$ intermolecular bond critical points (BCPs). The NBO and AIM parameters thus were obtained employed to aid in the understanding and classification of the $I \cdots I$ interactions (i.e., as van der Waals or hydrogen-bonding type) existing in metal-iodide complexes in the gas phase and in solution. The calculated values for AIM parameters of $I \cdots I$ [i.e., $\rho_b(r)$, $L(\rho_b(r))$ and $H_b(r)$] were also be compared to those obtained for $I_3^- \cdots I_3^-$ in the literature [6].

6.2 Natural Bond Orbital analysis

Natural Bond Orbital (NBO) [1] calculations were used to study the donor-acceptor component of the $I \cdots I$ intermolecular interactions in dimers of two metal iodide complexes, namely Cu and Pt. These are D-Cu, which is the simplified anionic part of DEHKACO2 ($[Cu_2I_4]^{2-}$), and N-Pt ($PtI_2N_2H_6$) that was obtained from NUKCAY. The focus was on studying the NBO parameters of the two orbitals involved in the donor-acceptor interaction, namely the valence lone pair (LP) which is an occupied orbital (with a normal occupancy of 2 electrons) and a Rydberg orbital (RY^*). The latter typically contains 0 electrons, although it may contain more if there is electron donation from an LP orbital, but usually much less than that in the lone pair orbital [2]. By examining the occupancies in these orbitals we will be able to determine if there is any electron transfer between iodine atoms, thus pointing to the formation of an $I \cdots I$ interaction in the dimer indicated by deviations from 2 for the LP and 0 for the RY^* orbital. The stabilization energy between these orbitals is also estimated in the NBO calculation. Higher stabilization energies are indicative of stronger interactions. The calculations were carried out in the gas phase and in a solvent model using various solvents with different dielectric constants (i.e., water, ethanol and chloroform), which will allow us to understand the nature of the $I \cdots I$ interactions and the effect of the surrounding environments (gas phase and solvent) on these interactions.

6.2.1 Analysis of the I···I interaction in the D-Cu dimer

Figure 6.1 shows the dimeric structure of D-Cu (the anionic part of DEHKACO2, $[Cu_2I_4]^{2-}$) with the $I \cdots I$ interaction distance of 4.558 Å as obtained from the CSD. The analysis was focussed on the interaction between atoms I3 and I7 where the interaction is indicated by a dotted line as shown in Figure 6.1. The results are given in Table 6.1, which shows the electron occupancies of the lone pair orbital with the lowest occupancy (LP) and the empty orbital (RY^*) containing the highest occupancy for atoms I3 and I7 in the D-Cu dimer in the gas phase, water, ethanol and chloroform. The stabilization energy between these orbitals is also shown in Table 6.1.
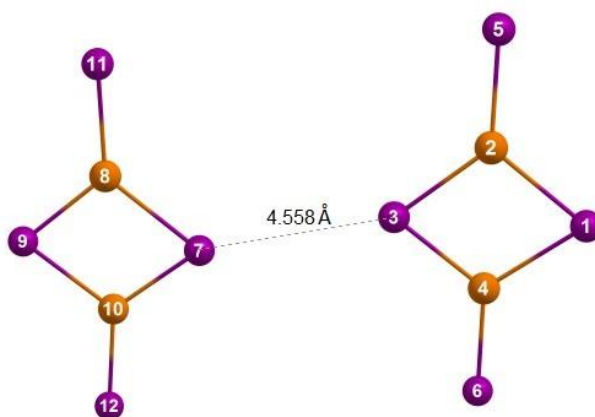
Figure 6.1: Dimeric structure of D-Cu ($[Cu_2I_4]^{2-}$), showing the I3···I7 distance of   4.558 Å as obtained from the CSD. Iodine atoms are indicated as purple spheres and Cu atoms are indicated as brown spheres.

Table 6.1: LP, RY* and ΔE_S values for atoms I3 and I7 in the D-Cu dimer in the gas phase, chloroform, ethanol and water.

Atom No./ Environment	$I3_{(LP)} \rightarrow I7_{(RY*)}$		ΔE_S (kcal/mol)	$I7_{(LP)} \rightarrow I3_{(RY*)}$		ΔE_S (kcal/mol)
Gas phase	1.969	0.001	0.42	1.972	0.001	0.38
Chloroform	1.932	0.000	0.07	1.969	0.001	0.30
Ethanol	1.970	0.001	0.19	1.970	0.001	0.19
Water	1.970	0.001	0.17	1.970	0.001	0.22

One can clearly see that in all cases (i.e., $I3_{(LP)} \rightarrow I7_{(RY*)}$ and $I7_{(LP)} \rightarrow I3_{(RY*)}$) the LP orbitals occupancies are close to 2.0 and the RY* orbitals occupancies are close to 0.0, which indicates that there is no significant electron transfer. Furthermore, the number of electrons in the LP and RY* orbitals observed for I3 and I7 in the gas phase and solution are similar (see Table 6.1). One can clearly see that interactions between these orbitals (i.e., LP and RY*) generally exhibited weak stabilization energies, where the calculated values of ΔE_S are in the range of 0.07-0.42 kcal/mol in both the gas phase and solvent model. This explains the very weak interaction between iodine atoms in the I···I moiety in both the gas phase, water, ethanol and chloroform, since there is no significant covalent component.

111

6.2.2 Analysis of the I···I interaction in the N-Pt dimer

Figure 6.2 gives the structure of the dimer of N-Pt (obtained from NUKCAY, $PtI_2N_2H_6$), showing the I···I interaction distance of 4.336 Å (based on the CSD). The interaction between atoms I1 and I12, indicated by a dotted line as shown in Figure 6.2, was analyzed. The results are tabulated in Table 6.2, which gives the occupancies of the LP and RY^* orbitals as well as the stabilization energy (ΔE_S) between these orbitals for atoms I1 and I12 in the N-Pt dimer in the gas phase, water, ethanol and chloroform.
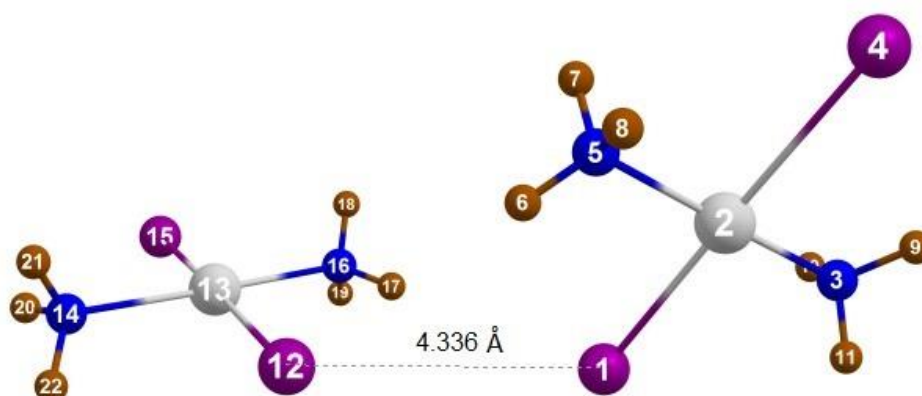

Figure 6.2: Dimeric structure of N-Pt ($PtI_2N_2H_6$), showing the I1···I12 distance of 4.336 Å as obtained from the CSD. Iodine atoms are indicated as purple spheres, Pt as grey spheres, H atoms as brown spheres and N atoms as blue spheres.

Table 6.2: LP, RY^* and ΔE_S values for atoms I1 and I12 in the N-Pt dimer in the gas phase, chloroform, ethanol and water.

Atom No./ Environment	$I1_{(LP)} \to I12_{(RY*)}$		ΔE_S (kcal/mol)	$I12_{(LP)} \to I1_{(RY*)}$		ΔE_S (kcal/mol)
Gas phase	1.927	0.000	1.04	1.927	0.000	1.04
Chloroform	1.958	0.001	0.48	1.961	0.001	0.12
Ethanol	1.959	0.001	0.49	1.963	0.001	0.13
Water	1.959	0.001	0.49	1.963	0.001	0.14

It can be seen in Table 6.2 that the values of LPs observed for I1 and I12 in the gas phase and in solution are very similar. This indicates that the surrounding environment had no effect on the number of electrons in the LP and RY* orbitals of interest on atoms I1 and I12, which

112

remained the same. The results in Table 6.2 also show that there is no electron transfer to the RY* orbitals, thus no confirmation of the presence of the I⋯I interaction in the dimer. We can also observe that the stabilization energies in the N-Pt dimer are very weak in both the gas phase and in all solvents used. The values of ΔE_S for these two orbitals are in the range of 0.48-1.04 kcal/mol.

6.3 Atoms In Molecules (AIM) analysis

The nature of the I⋯I interactions in D-Cu and N-Pt dimers was further investigated using AIM analysis [3, 4]. Three AIM parameters, namely the electron density $\rho_b(r)$, Laplacian of the electron density $L(\rho_b(r))$ and the total energy density $H_b(r)$ were determined at the bond critical points (BCPs) of the I⋯I interaction. The calculations were carried out in the gas phase and in an implicit solvent model using various solvents with different dielectric constants (water, ethanol and chloroform).

Nakanishi *et al.* [5] used AIM to perform a dual-parameter analysis of weak to strong interactions between various molecules and adducts. Interactions examined in their work are those in van der Waals (vdW) adducts, hydrogen-bonded (H-bond) complexes, molecular complexes and hypervalent adducts through charge transfer (CT) interactions, as well as some classical covalent bonds. The authors mentioned that there is a typical range for each one of these parameters ($\rho_b(r)$, $L(\rho_b(r))$ and $H_b(r)$), which corresponds to the type of interaction in the complex dimer. Table 6.3 gives the typical ranges for (ρ_b), $L(\rho_b)$, and H_b for H-bond, vdW interactions and the charge transfer in trigonal bipyramidal (CT-TBP) adducts as obtained by Nakanishi *et al*.

Table 6.3: Typical ranges for (ρ_b), $L(\rho_b)$, and H_b (au) for H-B, vdW interactions and the CT-TBP. [a]

Interaction	(ρ_b)	$L(\rho_b)$	H_b
Hydrogen Bonds	$0.01 < (\rho_b) < 0.04$	$0.04 < [L(\rho_b)] < 0.12$	$-0.004 < H_b < 0.002$
van der Waals	$0.00 < (\rho_b) < 0.01$	$0.00 < [L(\rho_b)] < 0.04$	$0.000 < H_b < 0.002$
CT-TBPa	$0.03 < (\rho_b) < 0.1$	$-0.01 < [L(\rho_b)] < 0.1$	$-0.06 < H_b < -0.003$

[a] Values obtained from reference [5].

113

Groenewald *et al*. [6] investigated the same three AIM parameters for $I_3^- \cdots I_3^-$ interactions using DFT functionals and the MP2/a-TZ level of theory. The authors observed that there is a substantial increase in the absolute value for each parameter in the gas phase compared to solution, which they attributed to the decrease in the $I_3^- \cdots I_3^-$ intermolecular distance. Table 6.4 summarizes the results obtained by Groenewald *et al*., which shows the $I_3^- \cdots I_3^-$ intermolecular distance (Å) and the three AIM parameters obtained at the $I \cdots I$ BCP of the dimer in the gas phase, water, ethanol, and chloroform.

Table 6.4: $I_3^- \cdots I_3^-$ intermolecular distance (Å), electron density ($\rho_b(r)$), the Laplacian of the electron density ($L(\rho(r))$) and the total electronic energy density (H_b) various BCPs in atomic units (a. u.) of the dimer in the gas phase, chloroform, ethanol and water.[a]

Environment	$d(I_3^- \cdots I_3^-)$(Å)	$\rho_b(r)$	$L(\rho(r))$	H_b
Gas	3.901	0.0072	0.0186	0.0007
Chloroform	3.574	0.0132	0.0319	-0.0006
Ethanol	3.561	0.0137	0.0328	-0.0003
Water	3.562	0.0137	0.0328	0.0005

[a] Values obtained from reference [6].

Parthasarathi *et al*. [7] also studied the strength of hydrogen bonding in a number of intermolecular complexes. The authors observed a significant increase in electron density and Laplacian of electron density in a linear relationship that led to a change in the nature of the interaction from a vdW interaction (weak H-bond) to a medium (classical H-bond) to strong H-bond. The calculated values of $\rho_b(r)$, $L(\rho_b(r))$, and $H_b(r)$ of $I \cdots I$ interaction of D-Cu and N-Pt were compared to values obtained by Nakanishi *et al*. [5], Groenewald *et al*. [6] and Parthasarathi *et al*. [7]. This allowed us to understand the nature and properties of $I \cdots I$ interactions in metal-iodide complexes and the effect of the surrounding environments (gas phase and solvent) on these $I \cdots I$ interactions.

6.3.1 AIM analysis of the I ··· I interaction in the D-Cu dimer

The interaction energy between iodine atoms in the D-Cu dimer was calculated in Chapter 5 (see section 5.2.3.2), which showed that there is a significant influence of the surrounding environment on the interaction energy obtained. In order to confirm the existence of the I ··· I interaction in the dimer, the structure was analyzed utilizing the AIMAll (v.14.06.12) [8] software package. The influence of various surrounding environments, i.e. the gas phase and solvents, on the three selected AIM parameters was also investigated. Figure 6.3 shows the two-dimensional contour plot of the electron density for a dimer of D-Cu in the gas phase. Figures 6.4 and 6.5 show the two-dimensional contour plots of the D-Cu dimer in water and ethanol, respectively. Table 6.5 summarizes all the AIM parameters related to the BCP_S shown in Figures 6.4 and 6.5. These include the calculated values for the ρ_b, $L(\rho_b)$ and H_b at BCP # 1 in water and BCP # 2 in ethanol.
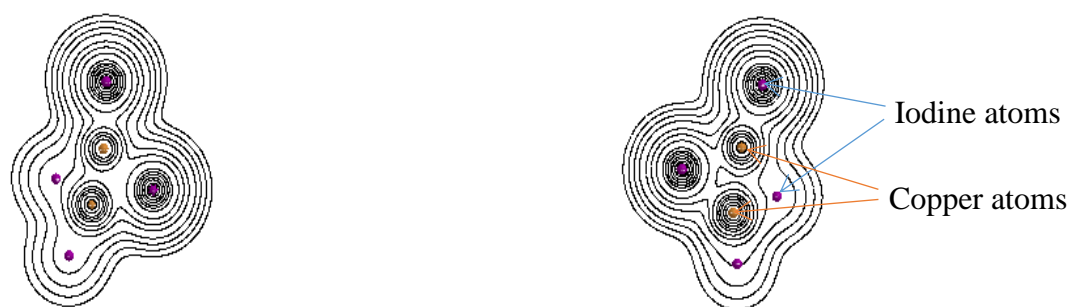

Figure 6. 3: Two-dimensional contour plot of electron density (ρ_b) of the D-Cu dimer in the gas phase; iodine atoms are indicated as purple spheres, Cu atoms as brown spheres.
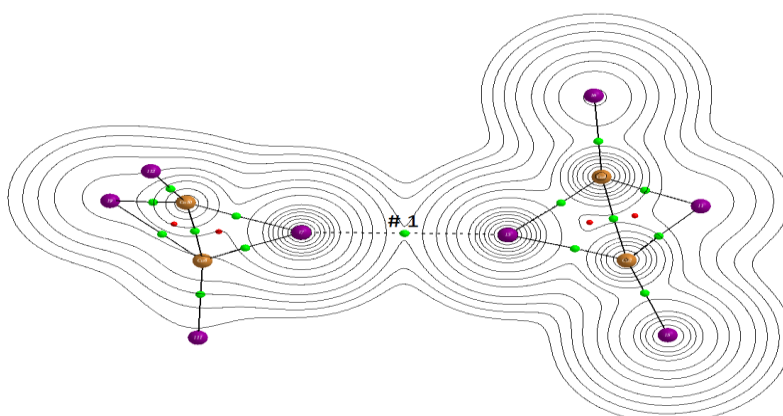

Figure 6.4: Two-dimensional contour plot of electron density (ρ_b) of the D-Cu dimer in water; iodine atoms are indicated as purple spheres, Cu atoms as brown spheres, BCPs as a green spheres, the bondpath is indicated by a (solid) blue line and the atomic interaction line is indicated by a dotted black line.

The I$\cdots$I intermolecular distances and AIM parameters at the BCPs between the two fragments in the dimer are included in Table 6.5. It should be mentioned here that there is no BCP between the iodine atoms when the dimer was placed in the gas phase and chloroform. This indicates that there is no I$\cdots$I interaction in these cases, which is attributed to the increase in the repulsive electrostatic force between the two fragments in the dimer of the D-Cu complex. It was shown in Chapter 5 (see Section 5.2.2.1) that the ions in the D-Cu dimer repelled each other in the gas phase and chloroform.
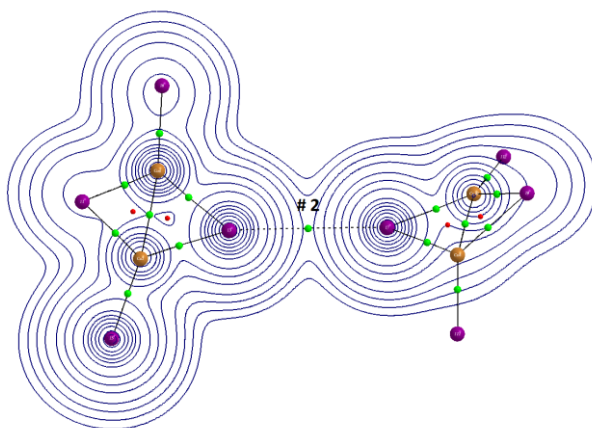

Figure 6. 5: Two-dimensional contour plot of electron density (ρ_b) of the D-Cu dimer in ethanol; iodine atoms are indicated as purple spheres, Cu atoms as brown spheres, BCPs as a green spheres, the bondpath is indicated by a (solid) blue line and the atomic interaction line is indicated by a dotted black line.

Table 6.5: The I$\cdots$I intermolecular distance (Å), electron density (ρ_b) at the BCP, the Laplacian of the electron density L($\rho(r)$) and the total electronic energy density (H$_b$) in atomic units (a.u.) at the BCP of the D-Cu complex dimer in water and ethanol.

Gas/Solvent	d(I$\cdots$I)(Å)	BCP #	Atoms	$\rho_b(r)$	L($\rho_b(r)$)	H$_b$
Gas	_	_	_	_	_	_
Chloroform	_	_	_	_	_	_
Ethanol	4.42	2	I3-I7	0.0035	0.0084	-0.0005
Water	4.33	1	I3-I7	0.0041	0.0097	-0.0005

From Table 6.5, we can see that reasonable values for all the parameters at BCP #1 and #2 for the I$\cdots$I moiety in water and ethanol were obtained. The electron density and Laplacian of the electron density in water increased by 14% compared to those observed in ethanol. Similarly, there was an increase of about 8.2% in the value of H$_b$ in water, as compared to ethanol.

116

If we compare our calculated values for these three AIM parameters listed in Table 6.5 to those obtained by Groenewald *et al*. listed in Table 6.4 we observe that the ρ_b and $L(\rho_b)$ values for the D-Cu dimer are lower than those for the I_3^- dimer in water and ethanol. This indicates that the transition metal (i.e., Cu) plays a significant role in increasing the repulsive force between the iodine atoms and thus a weaker $I \cdots I$ interaction occurs. We suspect that the reason for the weakening of the $I \cdots I$ interaction is that the I–Cu distance in the D-Cu dimer is shorter than I–I (by 29%), which suggests that it is a concomitantly stronger bond.

Surprisingly, we observed negative values for H_b for $I \cdots I$ in the D-Cu dimer in water compared to a positive H_b value for $I_3^- \cdots I_3^-$ as observed by Groenewald *et al*. This means that the electron density between iodine atoms in our studied dimers (M–I⋯I–M) is less than that between $I_3^- \cdots I_3^-$ dimers (the interaction between the $I_3^- \cdots I_3^-$ dimers is stronger). This strange result can be attributed to the presence of a transition metal atom in our studied dimer, which is known to give spurious results for the H_b values. Thus, negative H_b values observed in the gas phase may be due to the use of effective core potentials in the calculations, which are known to give incorrect H_b values [9]. These results nevertheless indicate that the presence of a Cu atom results in a relatively weaker interaction between iodine atoms than in the related triiodide species.

The AIM analysis also indicated that when the dimer is placed in water or ethanol, the calculated values for these three AIM parameters fall within the range of vdW interactions as classified by Nakanishi *et al.* (see Table 6.3). Our results are also in a good agreement with the values obtained by Parthasarathi *et al*., where we can see that the calculated values of these three AIM parameters (ρ_b, $L(\rho_b)$ and H_b) for D-Cu dimer again falls within the range for vdW interactions.

6.3.2 Analysis of the I⋯I interaction in the dimer of N-Pt

Figure 6.6 shows the two-dimensional contour plot of electron density (ρ_b) along with the BCPs for the N-Pt dimer in the gas phase. Figures 6.7, 6.8 and 6.9 show the two-dimensional plots of the electron density for the N-Pt dimer in water, ethanol and chloroform, respectively. The calculated values for the ρ_b, $L(\rho_b)$ and H_b at BCPs of N-Pt dimer in water, ethanol and chloroform are listed in Table 6.6. In the gas phase, no BCP is found along the

I···I line, since the NH···I hydrogen bonding interactions dominate. Therefore, no AIM parameters between atoms I1 and I12 were obtained. Instead, values for the AIM parameters at the BCPs for hydrogen bonding (H6-I12, H17-I1, H21-I4 and H10-I15) in the gas phase were observed. In fact, these values are in good agreement with our findings in Chapter 5, where we observed the existence of hydrogen bonding in the N-Pt dimer. They also correspond well to the values for hydrogen bonds according to Nakanishi's classification that is given in Table 6.3. From Table 6.6, we can see that the calculated values of ρ_b, $L(\rho_b)$ and H_b at BCP # 4, BCP # 5, BCP # 6 and BCP # 7 between H6-I12, H17-I1, H21-I4 and H10-I15 in the gas phase are the same due to symmetry.
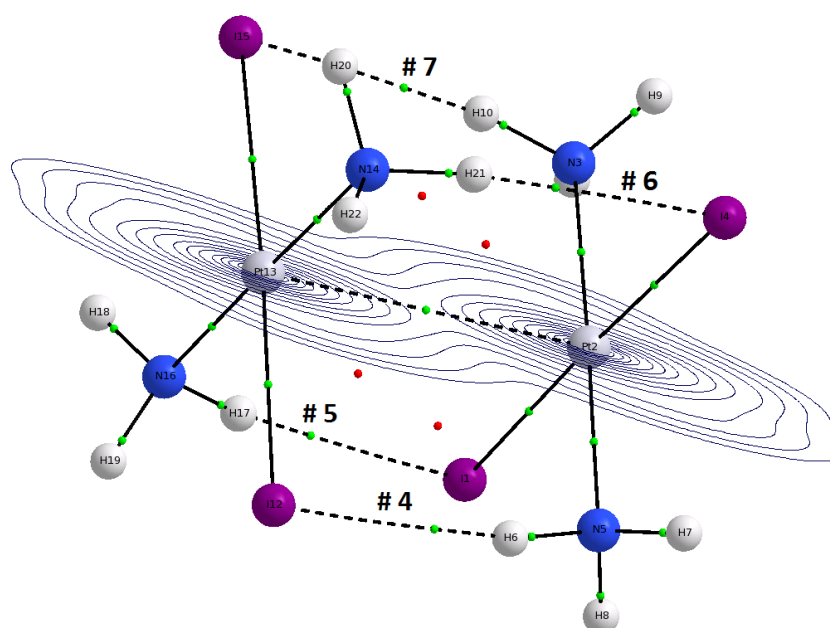

Figure 6.6: Two-dimensional contour plot of electron density (ρ_b) of the N-Pt dimer in the gas phase, showing the BCPs between H6-I12, H17-I1, H21-I4 and H10-I15.
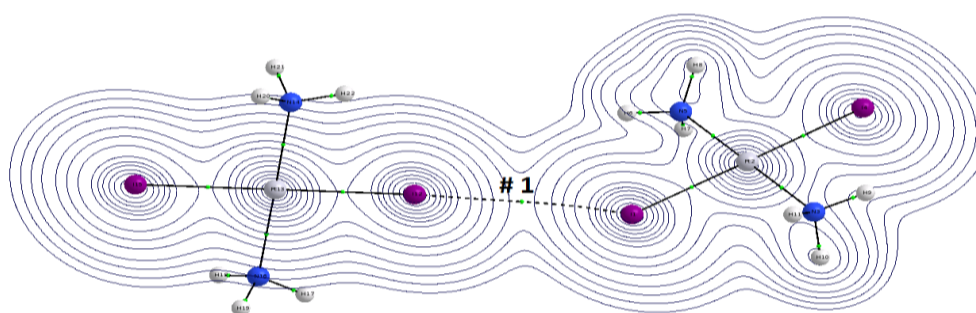

Figure 6.7: Two-dimensional contour plot of electron density (ρ_b) of the N-Pt dimer in water; I atoms as purple spheres, Pt atoms as grey spheres, H atoms as grey spheres, N atoms as blue spheres, the BCP as a green spheres, the bondpath is indicated by a (solid) blue line and the atomic interaction line is indicated by a dotted black line.

118

Figure 6.8: Two-dimensional contour plot of electron density (ρ_b) of the N-Pt dimer in ethanol; iodine atoms are indicated as purple spheres, Pt atoms as grey spheres, H atoms as grey spheres, N atoms as blue spheres, the BCP as a green spheres, the bondpath is indicated by a (solid) blue line and the atomic interaction line is indicated by a dotted black line.
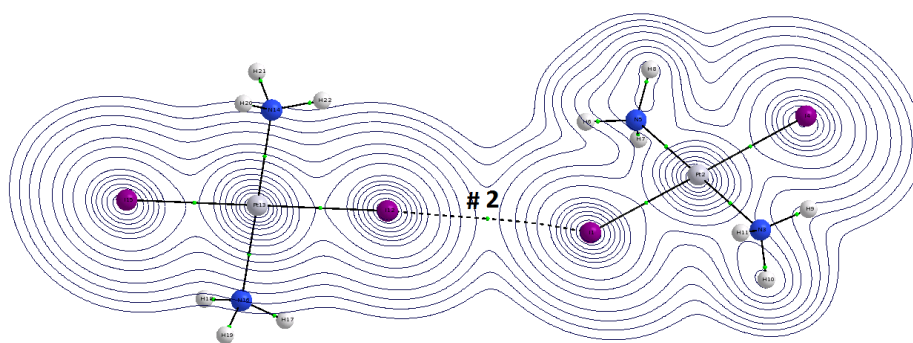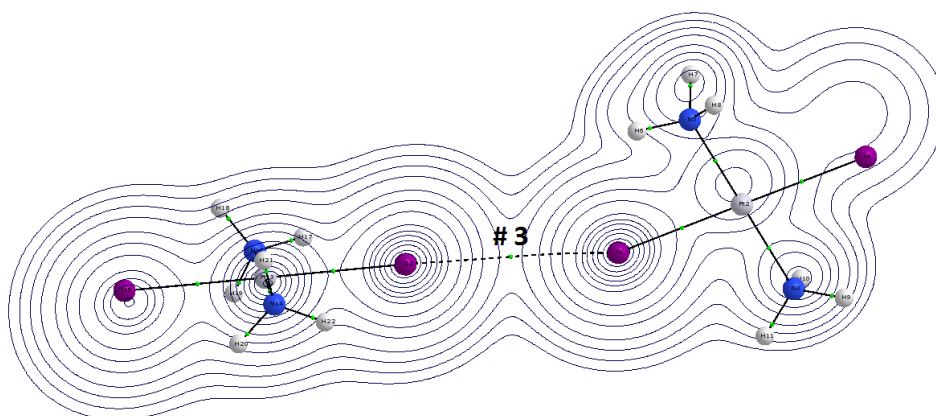

Figure 6.9: Two-dimensional contour plots of electron density (ρ_b) of the N-Pt dimer in chloroform; iodine atoms are indicated as purple spheres, Pt atoms as grey spheres, H atoms as grey spheres, N atoms as blue spheres.

Parthasarathi *et al*. [7] constructed plots utilizing the stabilization energy against the electron density (ρ_b) and Laplacian of electron density ($L(\rho_b)$), where they observed that the values of ρ_b and $L(\rho_b)$ could describe the strength of the H-bond. From this they were able to classify different types of H-bond as weak to medium (classical) or strong H-bonds. Our results indicate that the calculated values for ρ_b and $L(\rho_b)$ in the gas phase fall in the range of moderate H-bond (see Table 6.6).

Furthermore, when we consider the AIM parameters listed in Table 6.6 at the $I \cdots I$ BCPs we observe that there is no significant change in the calculated values when the dimer is placed in water, ethanol or chloroform. This indicates that changing the solvent from water to

119

ethanol does not play a large role in determining the calculated values of these three AIM parameters, i.e., (ρ_b, L(ρ_b), and H$_b$). Compared to the values defined by Nakanishi *et al.* we see that ρ_b and L(ρ_b) values for the N-Pt dimer are within the range for vdW interactions. Moreover, when we compare our findings to those obtained by Groenewald *et al.* for $I_3^- \cdots I_3^-$ dimers, it is clear that the presence of Pt atom resulted in a significant decrease in all three AIM parameters (ρ_b, L(ρ_b), and H$_b$) in solution. In other words, the Pt atom plays significant role in decreasing the interaction between iodine atoms.

Table 6.6: The I···I intermolecular distance (Å), the electron density (ρ_b), the Laplacian of the electron density and the total electronic energy density (H$_b$) in atomic units (a.u.) at the BCPs of the N-Pt dimer in the gas phase, chloroform, ethanol and water.

Gas/Solvent	d(I···I)(Å)	BCP #	Atoms	ρ_b	L($\rho_b(r)$)	H$_b$
Gas	_	_	I1-I12	_	_	_
Gas	2.65[a]	4	H6-I12[a]	0.0182[b]	0.0384[b]	-0.0005[b]
chloroform	4.05	3	I1-I12	0.0063	0.0147	+0.0006
ethanol	4.079	2	I1-I12	0.0059	0.0141	+0.0006
water	4.079	1	I1-I12	0.0060	0.0141	+0.0006

[a] hydrogen bond.

[b] Values are the same for H17-I1, H21-I4 and H10-I15.

6.4 Conclusion

NBO and AIM analyses were used to study the I···I intermolecular interactions in dimers of metal-iodide complexes containing two different transition metals, namely Cu and Pt. The analyses were performed in the gas phase as well as in various solvents with different dielectric constants, i.e., water, ethanol and chloroform. NBO results showed that there is no electron transfer between iodine atoms involved in the I···I interaction in both dimers (i.e., D-Cu and N-Pt) in the gas phase and solvent models. The ΔE_S values for the two dimers were also estimated and found to be very weak. This indicates that the two fragments in the dimers interact via dispersion or electrostatic interactions only.

Calculations showed that there was no BCP between the I atoms in both dimers in the gas phase, indicating that there is no I···I interaction. This was attributed to the presence of a repulsive force acting between the two fragments in the dimers. In the case of the N-Pt dimer,

the presence of hydrogen bonding decreased the repulsive force between the two fragments in the gas phase, however there was no I $\cdots$ I BCP. Therefore, no AIM parameters for this dimer could be obtained. On the other hand, when the dimers were placed in a solvent, AIM parameters were obtained which may depend on the environment (i.e., dielectric constant of the solvent). For instance, an increase in the dielectric constant, resulted in a very slight increase in the AIM parameters calculated for the D-Cu dimer, but had no effect on these calculated for the N-Pt dimer.

AIM analysis also indicated that the N-Pt dimer exhibited a slightly higher electron density between the iodine atoms in the I $\cdots$ I interaction compared to that in the D-Cu dimer in water and ethanol. This may be attributed to the transition metal in the metal-iodide complex. Thus, Pt provides a relatively better environment to increase the strength of the interaction between the iodine atoms in the I $\cdots$ I moiety, relative to that of Cu. However, the AIM analysis shows that neither metal is efficient in strengthening the I $\cdots$ I interaction compared to that found for dimers of I_3^-.

6.5 References

1. *NBO version 3.1,* E. D. Glendening, A. E. Reed, J. E. Carpenter, F. Weinhold. **1998**.

2. Weinhold, F. and Landis, C.R., *Natural Bond Orbitals and Extensions of Localized Bonding Concepts.* Chemistry Education Research and Practice **2001**, 2(2), 91-104.

3. Bader, R.F.W., *Atoms in molecules.* Accounts of Chemical Research **1985**, 18(1), 9-15.

4. Bader, R.F.W., *Atoms in Molecules: A Quantum Theory*: Oxford University Press, Oxford, U.K **1990**.

5. Nakanishi, W., Hayashi, S., and Narahara, K., *Atoms-in-Molecules Dual Parameter Analysis of Weak to Strong Interactions: Behaviors of Electronic Energy Densities versus Laplacian of Electron Densities at Bond Critical Points.* The Journal of Physical Chemistry A **2008**, 112(51), 13593-13599.

6. Groenewald, F.G., *Computational study of anion-anion intermolecular interactions between I_3^- ions in the gas phase, solution and solid state*, MSc thesis, Stellenbosch University: Stellenbosch, South Africa, 2012.

7. Parthasarathi, R., Subramanian, V., and Sathyamurthy, N., *Hydrogen Bonding without Borders: An Atoms-in-Molecules Perspective.* The Journal of Physical Chemistry A **2006**, 110(10), 3349-3351.

8. AIMAll (Version 15.09.12), Todd A. Keith, TK Gristmill Software, Overland Park KS, USA, 2015 (aim.tkgristmill.com).

9. Keith, T.A. and Frisch, M.J., *Subshell Fitting of Relativistic Atomic Core Electron Densities for Use in QTAIM Analyses of ECP-Based Wave Functions.* The Journal of Physical Chemistry A **2011**, 115(45), 12879-12894.

Chapter 7

Conclusion and future work

7.1 Conclusion

A comprehensive search analysis of previously published experimental crystal structures of transition metal-iodide complexes was carried out utilizing the Cambridge Structural Database (CSD). The analysis was performed in order to identify all complexes that contain an I–M–I moiety and exhibit $I \cdots I$ interactions. The $I \cdots I$ interaction distance was chosen as the sum of the van der Waals radii of the iodines (4.3 Å) plus 0.3 Å, to ensure that even weak interactions are identified. The CSD revealed that metal-iodide complexes containing copper (Cu), mercury (Hg), gallium (Ga), silver (Ag), platinum (Pt), palladium (Pd) or bismuth (Bi) are most likely to have $I \cdots I$ interactions.

The structures of dimers containing $I \cdots I$ interactions were visualized and analyzed utilizing the program Mercury V3.3 to determine the most common orientations (i.e., conformations) of the two I–M–I moieties relative to each other. The studied complexes exhibited different types of $I \cdots I$ intermolecular interactions including single, double, multiple and bifurcated interactions. The average $I \cdots I$ distance was between 3.9 – 4.2 Å, and the most common conformations of these interactions in the solid state are chair, boat, bent, $>\cdots<$–shaped and zigzag shapes. However, it was found that a strong interaction (i.e., a shorter $I \cdots I$ distance) is most likely to occur where the relative orientation of the two I–M–I moieties is in the chair form. To the best of our knowledge, this is the first comprehensive study of this type of interaction in metal-iodide complexes.

DFT was used to analyze the nature and strength of the $I \cdots I$ intermolecular interactions in dimers of complexes containing Cu, Hg, Ga, Pt, Pd or Bi. Optimization of pairs of these complexes (i.e., I–M–I$\cdots$I–M–I) was undertaken at the PBEPBE/aug-cc-pVTZ–pp, B3LYP/ aug-cc-pVTZ–pp, or B3LYP/LANL2DZ levels of theory, where values of the $I \cdots I$ interaction energies in these metal-iodide complexes was calculated. Optimizations of complexes containing Cu or Pt resulted in stable dimers both in the gas phase and in an implicit polarizable continuum solvent model using various solvents with a wide range of

dielectric constants (water, ethanol or chloroform). However, attempts to optimize dimers of complexes containing Bi or Pd in the gas phase failed, producing unstable structures. Similarly, complex dimers containing Hg, Pd, Bi or Ga (the Ga complex was only stable in water) were unstable in all solvents used (i.e., water, ethanol or chloroform). In general, optimizations in the gas phase and solvent model showed that there is a significant dependence of the $I \cdots I$ interaction energy and distance on the dielectric constant of the solvent used. As the dielectric constant of the solvent increases so does the E_{INT} (due to electrostatic stabilization), while the $I \cdots I$ intermolecular distance decreases significantly.

NBO and AIM analyses were used to study the nature and properties of the NBO $I \cdots I$ interactions. The analyses were carried out for two dimers containing Cu or Pt, namely D-Cu, which is the anionic part of DEHKACO2, $[Cu_2I_4]^{2-}$ and N-Pt that obtained from NUKCAY, $PtI_2N_2H_6$. Attempts to calculate the interaction energy of conformation for the other complexes failed, therefore no NBO and AIM calculations were carried out. NBO analysis of D-Cu and N-Pt revealed that there is no electron transfer between iodine atoms in the $I \cdots I$ moiety in both the gas phase as well as in the solvent model. This confirms that the two fragments in the dimers are connected via dispersion interactions only. No minimum energy conformations were obtained in the gas phase, which was attributed to the presence of strong repulsive electrostatic forces acting between the two complexes in the dimers for the BCPs corresponding to the $I \cdots I$ interaction, hence no AIM parameters for the $I \cdots I$ interactions could be identified. However, when the dimers were placed in a solvent, stable conformations were obtained, with the AIM parameters depending on the surrounding environment (i.e., dielectric constant of the solvent). In general, an increase in the dielectric constant resulted in a significant increase in the calculated values of AIM parameters (i.e., ρ_b, $L(\rho_b)$, and H_b). However, the AIM analysis shows that neither Cu nor Pt is efficient in strengthening the $I \cdots I$ interaction compared to that found for dimers of $I_3^- \cdots I_3^-$.

7.2 Recommendations for future work

As mentioned in Chapter 2, various levels of theory are available which can be used to perform different computational chemistry calculations. In the current study, DFT methods were used to achieve the computational calculations, which were used to study dimers of various transition metal-iodide complexes. However, it was shown in Chapter 5 that DFT

methods used were unable to yield optimized structures of dimers of complexes of metals such as Bi, Hg, Ag or Ga even in a solvent model. The use of a different theory such as MP2 or different DFT functionals could be applied to study the $I \cdots I$ interactions in dimers containing the abovementioned metals. If successful optimization is achieved, AIM and NBO analysis should be used to confirm the nature and properties of these interactions. The CSD analysis also showed that other metals such as Cd, Pb, Au, Sb, As and Sn could have $I \cdots I$ interactions. The optimization should also be performed on dimers of complexes containing these metals to investigate the nature and strength of these interactions.

The CSD analysis and computational calculations should be also used to investigate the $I \cdots I$ interactions in dimers of $I–M–I \cdots I–M–I$, where the transition metal M is replaced by one of the alkali or alkaline earth metals. This could result in a different donor-acceptor type of interaction with iodine, which may lead to different $I \cdots I$ conformations. The focus should be on finding a stronger $I \cdots I$ interactions, which correspond to shorter interaction distances.

Digital Supplementary Information

The attached CD contains all the CSD searches, Gaussian output files, and NBO and AIM output files generated in this study.

CSD Results

Each metal-iodide complex has an excel file named $(I\text{-}M\text{-}I)_2$ which includes all parameters obtained by CSD analysis (e.g., DIST., ANG. and TOR.) with descriptions and notes when necessary. Note: there are some metals such as Ni, Sc, Tc, Y and V that do not have CSD results.

Gaussian output files

The output files for the optimization of the single structure (I–M–I) as well as the dimer form (I–M–I···I–M–I) for the selected metal-iodide complexes in the gas phase and solvents (water, ethanol or chloroform) are included. For the single form, the output files for complexes containing the following metal are included: Cu, Pt, Ag, Bi, Hg, Ga or Pd. Similarly, the output files for dimers of complexes containing these metals are included except those that contain Ag. Single point energy calculation of the dimers was performed for the complexes containing the following metals only: Cu, Pt or Pd.

NBO and AIM output files

NBO and AIM calculations were performed for dimers of complexes containing Cu or Pt in the gas phase and various solvents, namely water, ethanol and chloroform.